

# PART II: TECHNOLOGY

## Chapter 11

### Forming Techniques

11.1.	General Introduction	237
11.1.1	Friction and Lubrication	237
11.1.1.1	Friction During Plastic Deformation	238
11.1.1.2	Friction Measurement	239
11.1.1.3	Lubrication	241
11.1.2	TMP Furnaces	244
Literature		246
11.2.	Rolling	246
11.2.1	Introduction	246
11.2.2	Rolling Equipment	248
11.2.2.1	Plate, Sheet and Foil	248
11.2.2.2	Bars, Rods and Profiles	250
11.2.3	Mechanics	251
11.2.4	Typical Rolling Schedules	258
11.2.4.1	Steel	258
11.2.4.2	Aluminium	260
Literature		262
11.3.	Extrusion	262
11.3.1	Introduction	262
11.3.2	Deformation Conditions	264
11.3.3	Steels and High Melting Temperature Alloys	266
11.3.4	Aluminium Alloys	267
Literature		269
11.4.	Wire Drawing	269
11.4.1	Introduction	269
11.4.2	Wire Drawing Machines	270
11.4.3	Wire Drawing Dies	271
11.4.3.1	Geometry	271
11.4.3.2	Die Materials	272
11.4.3.3	Lubricants	272
11.4.4	The Drawing Force	273
11.4.5	Some Important Metallurgical Factors	275

11.4.6	Drawing of Metal Fibres	278
Literature		279
11.5.	Forging	279
11.5.1	Introduction	279
11.5.2	Forging Equipment	280
11.5.3	Forging Dies	282
11.5.4	Friction and Lubrication in Forging	284
11.5.5	Forging Optimization	284
11.5.6	Forgability	287
Literature		289
11.6.	Pilgering	289
11.6.1	Introduction	289
11.6.2	Pilgering Equipment and Process	291
11.6.2.1	Roll/die Design	292
11.6.2.2	Other Mill Details	293
11.6.2.2.1	Mandrel Design	293
11.6.2.2.2	Loading and Feed Mechanisms	293
11.6.2.2.3	Rolling Drive	294
11.6.2.2.4	Synchronization and Turning	294
11.6.2.3	Lubrication	294
11.6.3	Optimization in Pilgering.	295
11.6.4	Materials Aspects	296
Literature		297
11.7.	Sheet Metal Forming	297
11.7.1	Introduction	297
11.7.2	Plastic Anisotropy	298
11.7.2.1	Crystallographic Background	299
11.7.2.2	The $\bar{R}$ and $\Delta R$ Factors	299
11.7.3	Forming Limit Diagrams	301
11.7.3.1	Determination and Practical Use	301
11.7.3.2	Parameters that Affect the FLD	303
11.7.4	Stretch Forming	304
11.7.5	Deep Drawing	306
11.7.5.1	Stress and Strain	306
11.7.5.2	Redrawing and Ironing	309
11.7.5.3	Deep Drawing and Texture	310
11.7.6	Bending and Folding	311
11.7.6.1	Stress and Strain	311
11.7.6.2	Spring Back and Residual Stress	313

11.7.7	Other Techniques	314
11.7.7.1	Spinning	314
11.7.7.2	Incremental Forming	315
11.7.7.3	High Strain Rate Forming	316
11.7.7.4	Peen Forming	317
Literature		317
11.8.	Hydroforming	317
11.8.1	Introduction	317
11.8.2	Sheet Hydroforming	318
11.8.3	Tube Hydroforming	318
11.8.4	Important Parameters	320
11.8.4.1	Friction and Lubrication	320
11.8.4.2	Material Parameters	321
Literature		322
11.9.	Hipping	322
11.9.1	Introduction	322
11.9.2	Densification Mechanisms	322
11.9.3	Hipping Equipment	325
11.9.4	Typical Applications	326
11.9.4.1	Densification of Castings	326
11.9.4.2	Densification of Powder Metal Products	326
11.9.4.3	Cladding	327
Literature		327
11.10.	Superplastic Forming	327
11.10.1	Technology	327
11.10.2	Thinning	329
11.10.3	Cavitation	330
Literature		332



# Chapter 11

## Forming Techniques

### 11.1. GENERAL INTRODUCTION

The first section (Chapters 1–10) of this book dealt with the metallurgical issues involved in thermo-mechanical processing (TMP). Of an equal<sup>1</sup> importance are the issues pertaining to production technology – the subject of this second section. Many of these issues are domains of mechanical/production engineers, but the basics should also be mastered by materials engineers.

This chapter about forming techniques, deals with techniques ranging from rolling to forging, from sheet metal forming to superplastic forming. The individual sub-chapters attempt to bring out details on the machines, die-tool design, process optimization, etc. All such issues are covered based on their relevance to the respective forming techniques. This general introduction, on the other hand, tries to outline two issues – ‘friction and lubrication’ and ‘TMP furnaces’. The former, though extremely relevant to any forming technology, has not been specifically covered in the subsequent sub-chapters. The ‘TMP furnaces’ is not a forming technique, but was considered as a necessary input in the present section on TMP technology.

#### 11.1.1 Friction and lubrication

The resistance that is encountered when two bodies are rubbed against each other is called *friction*. Friction is an important factor in metal forming. It dissipates energy and hence increases the force needed to deform a material. It generates heat, which complicates the control of the deformation temperature. It can affect the material flow during deformation and leads to inhomogeneous deformation. Last but not least it can degrade the quality and appearance of the surface. For all these reasons, it will be necessary in almost all forming operations to reduce the friction by adequate *lubrication*.

The first ‘recorded’ recognition of friction came from Leonardo da Vinci (Schey [1970]). The subject was rediscovered by Amontons (Amontons [1699], Schey [1970], Möller and Boor [1996]). Friction coefficient was postulated by Amontons and Coulomb (Coulomb [1785], Schey [1970], Möller and Boor [1996]) as

<sup>1</sup> Perhaps, of larger interest to actual production are the technological issues. For example, forging was the earliest forming techniques and still remains an attractive one in terms of metallurgical properties of the product, but dominance of other forming techniques (e.g. rolling and extrusion) is based purely on technological considerations and on cost economics.

proportional to the normal force and independent of contact area and relative speed of the moving surfaces. Subsequent theoretical developments, in particular in the 19th century (Schey [1970]) and Hardy's theories (Hardy [1936]) on boundary lubrication, formulate today's understanding of friction in metal-working processes. The present section makes an attempt in bringing out issues relevant to friction and lubrication in metal forming – issues discussed under three brief sub-sections on friction during plastic deformation, friction measurement and lubrication.

**11.1.1.1 Friction during plastic deformation.** The friction between a die and a workpiece is an important factor in a shaping process. Nevertheless, this factor is often neglected (or first neglected and then 'corrected') for the sake of simplicity. The possible impact of friction on the forces in a simple metal-forming operation can be illustrated with the following example.

Consider the uniaxial compression of a flat disc. It is assumed that no barreling occurs and that the vertical compression stresses are homogeneously distributed over the disc. It is also assumed that the (Coulomb) friction coefficient  $\mu$  is constant and that  $p$  represents the stress perpendicular to the surface. During compression, the disc will expand sideways (radial direction) and this will generate a shear stress  $\tau$  towards the centre of the disc. One can write:

$$\mu = \frac{\tau}{p} \quad (11.1)$$

As a consequence of shear stress  $\tau$ , a lateral compressive stress will be generated. It is possible to show that the pressure distribution over the surface of the disc is

$$p = \sigma_y \exp \left[ 2\mu \left( \frac{r-a}{h} \right) \right] \quad (11.2)$$

where  $r$ ,  $a$  and  $\sigma_y$  represent respectively the radius of the disc, distance from the centre and flow stress. A derivation of expression (11.2) can be found in several handbooks – example Dieter [1976]. The pressure distribution is illustrated in Figure 11.1. On the edge of the disc, the compressive stress has a minimum and is equal to the flow stress of the material. Because friction hinders the flow of the material away from the centre, the compressive stress increases towards the centre. This characteristic distribution is often called a *friction hill*.

The average compressive stress ( $p_{av}$ ) can be calculated by integrating Eq. (11.2):

$$p_{av} \int_0^r \frac{\sigma_y}{r} \exp \left[ 2\mu \frac{r-a}{h} \right] da \sim \sigma_y \left[ 1 + \frac{\mu r}{h} \right] \quad (11.3)$$

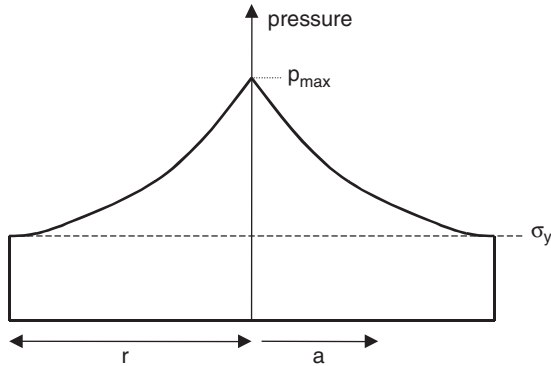


**Figure 11.1.** Distribution of the compressive stress during uniaxial compression of a flat disc.

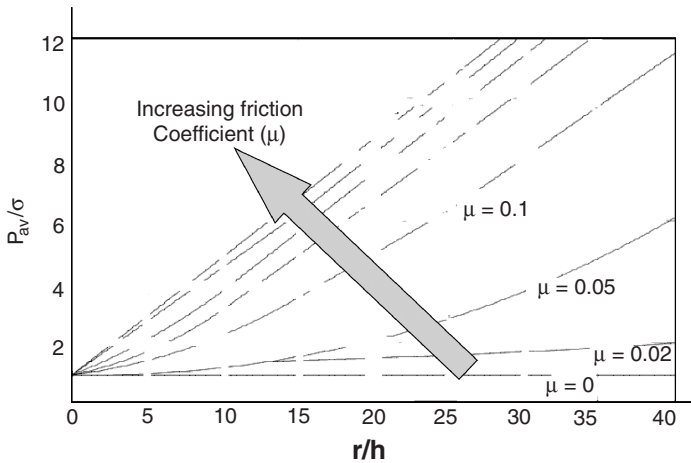


**Figure 11.2.** Effects of friction during compression tests.  $P_{av}/\sigma$  (average compressive stress/flow stress) vs. radius/height ratio ( $r/h$  – of the specimen undergoing compression) as a function of friction coefficient  $\mu$ . After Dieter [1976].

Figure 11.2. tries to highlight the importance of friction in ‘metal forming’. As shown in the figure, even at low friction coefficients ( $\mu < 0.02$ ) the forming/compression pressures can be 2–4 times larger than the flow stress of the material. Friction being more relevant for flat discs (or high  $r/h$ ).

**11.1.1.2 Friction measurement.** The friction coefficient must, in most cases, be determined by experiments. In principle, this could be done during a production process; but because of practical limitations and the risk of damage to production

equipment, the friction coefficient is normally determined in lab-scale tests. The results of such tests may never be exactly representative of the production line, but are quite suitable in comparing the influence of materials and lubricants on friction. One of the most popular tests is the so-called ‘ring compression test’ (Kalpakjian [1995]) (see Figure 11.3).

A flat ring is compressed between two flat plates and expands outwards. Without friction, the inner and outer diameter of the ring would expand proportionally. With increasing friction between the ring and the plates, the decreasing height is less and less compensated by the outward expansion of the outer diameter and more and more by a lesser expansion of the inner diameter. With very high friction, the inner diameter can even expand inwards (see Figure 11.3).

For a standard ring with a ratio of outer diameter to inner diameter to height of 6/3/2, calibration curves have been determined (see Figure 11.3b) (Kalpakjian [1995]). With such chart, it is possible to estimate the friction coefficient directly from the results of a ring compression test. For example, if the height is reduced by 40% and the inner diameter becomes 10% smaller, the friction coefficient of

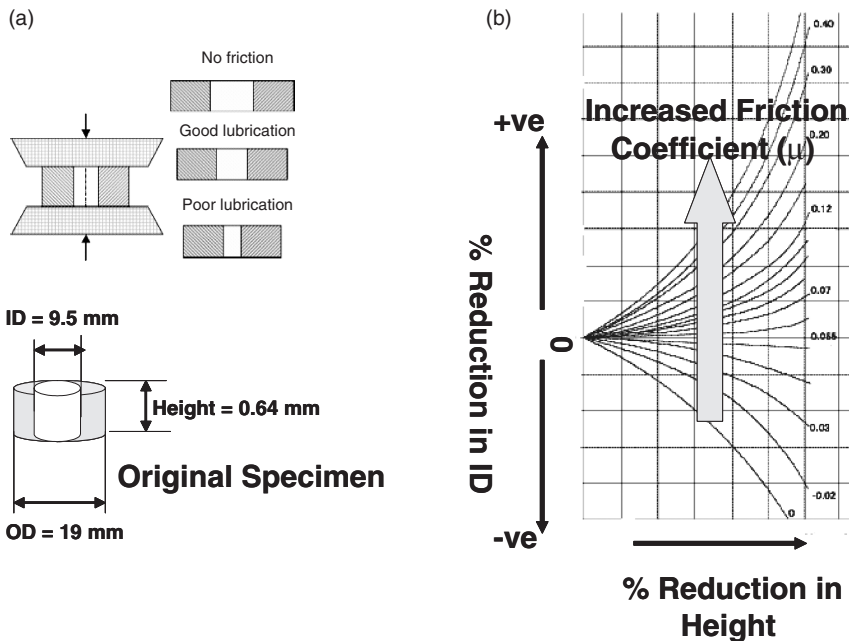


**Figure 11.3.** (a) Illustrations of ‘ring compression test’. (b) Friction coefficient from the data of the ring compression tests. After Kalpakjian [1995].

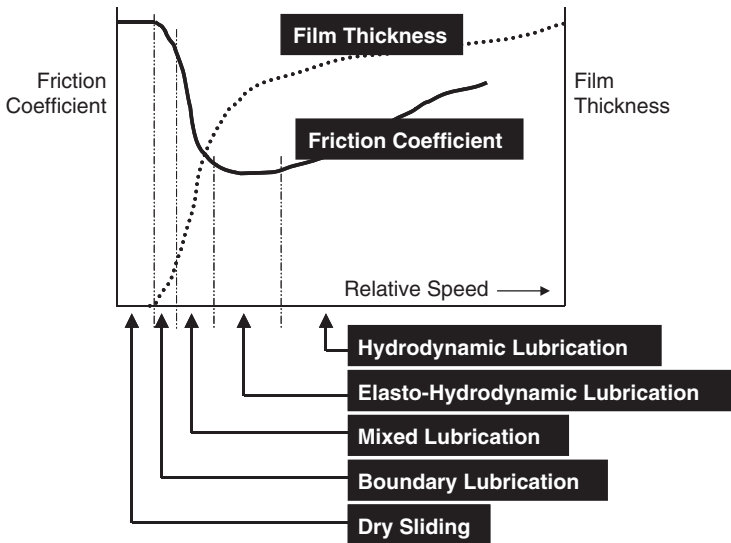


**Figure 11.4.** Stribeck curve – schematic diagram representing different frictional regimes in forming operations. After Möller [1996].

the tested system (material for the ring, material for the platens and lubricant) is equal to 0.1.

**11.1.1.3 Lubrication.** Friction accounts for 10–20% of the force in typical metal-forming operation (Blazynski [1976]). To counter frictional effects, including tribological effects, appropriate use of lubrication is required (Möller and Boor [1996]). Though no historical record of ‘intentional’ lubricant use exist in primitive metal forming (as in the archaeological evidences of hammering operations in the Middle East (Singer [1954])), unintentional usage like use of greasy fingers and hammering on asphalt, however, did possibly exist (Schey [1970]). Subsequent societies used lubricants as a common tool and except for two isolated developments in the present century,<sup>2</sup> basic ingredients of today’s lubricants were known for some time.

Figure 11.4, the so-called ‘Stribeck curve’ or ‘Reynolds–Sommerfield’ curve (Möller and Boor [1996]), offers a glimpse at different lubrication regimes. Such

<sup>2</sup> Phosphate conversion lubrication for severe cold deformation (as in drawing and extrusion) in Germany and glass pad lubrication for hot extrusion in France (Schey [1970], Möller and Boor [1996]).

regimes are outlined based on relative speed of the forming operation and film thickness/friction coefficient.

- *Dry sliding*: Direct contact of the workpiece and die-tool surfaces – surface damage and even material removal.
- *Boundary lubrication*: Lubricants form surface layers, absorbed or chemically modified layers, and fill surface imperfections. The layers may undergo a dynamic process of ‘rubbing off’ and ‘re-generation’.
- *Mixed lubrication*: Small quantity of lubricant is allowed to form light shearing layers by physical or chemical reaction. This avoids direct contact and reduces friction and wear.
- *Fluid lubrication*: Complete separation of contact surfaces by thick fluid/lubricant layers, friction is due to the shear resistance offered by the lubricant. Based on thickness/stability of lubricant layer, these are sub-divided as elasto-hydrodynamic and hydrodynamic. Other than friction/tribology, the lubricant also plays an important role in heat transfer. For example, the selection of a mineral oil would not only depend of the viscosity and thermal stability of the oil, but also on its thermal conductivity and specific heat.

Table 11.1 provides a summary of common lubricants used in metal forming. The most important liquid lubricants are:

- *Oil*: Most oils stick well to metals and have excellent lubrication properties, but have a rather low thermal conductivity and specific heat. For this reason, oil is less suitable when frictional heat has to be conducted away. Moreover, it is difficult to remove oil from the surface after the deformation process.
- *Emulsions*: An emulsion is a ‘composite’ of two immiscible liquids, e.g. water with oil; due to the presence of water, most emulsions have reasonable cooling properties; emulsions are frequently used in high-speed machining (also in specific forming operations) of metals.
- *Foams and greases*: Most foams are reaction products of specific salts; they form a protective layer between two metal surfaces and prevent a direct contact between them. Grease is a viscous lubricant that frequently used in all types of machinery, but it has a rather limited use in manufacturing.

The most useful solid lubricants are:

- *Graphite*: In the presence of air or moisture, graphite has a low friction coefficient and is well suited as a lubricant – even at high temperatures. In vacuum or on inert gas atmosphere, however, graphite can not be used.

**Table 11.1.** A summary of common lubricants used in metal forming.

Type of lubricant	Details
Solid	Graphite {0.1–0.2; +450°C}, moly-di-sulphide (MoS <sub>2</sub> ) {0.04–0.09; +400°C} and polymer (PTTE) {0.04–0.09; +250°C}. Respective friction coefficients and operating temperatures are mentioned within ‘{ }’
Semi-solid	<i>Greases</i> : Thickened mineral oils and synthetic oils with soaps (containing different metal ions – Na, Ca, Li, Al). Adhesive/tacky: bitumen is the predominant substance
Mixed or partial lubrication	For mixed lubrication – as in Figure 11.4. Depending on relative stability of the boundary layer mild or strong anti-wear additives are used <i>Mild</i> : Saturated/unsaturated fatty acids and primary/secondary alcohols <i>Strong</i> : Compounds of chlorine, sulphur or phosphorous
Fluid	From liquefied gasses to different types oils and water. Most common are hydrocarbon-based mineral oils (80–85 wt% C and 10–15 wt% H) and synthetic lubricants. The former can be classified as paraffins, naphthalenes and aromatics; while a range of esters, polyglycols, silicone oils, etc. are possible as synthetic fluid lubricants. Different additives are also used for improved performance and life

- *Molybdenum disulphide*: Molybdenum disulphide (MoS<sub>2</sub>) is somewhat similar to graphite, but is only useful at high temperature – example, MoS<sub>2</sub> mixed with oil is frequently used in warm-forming operations.
- *Glass*: Glass becomes viscous at high temperature and is suitable as lubricant; it has a low thermal conductivity and forms a thermal barrier between the work-piece and the tools; it is frequently used as lubricant in extrusion and in forging.
- *Metallic films and polymeric films*: Polymers (e.g. teflon and polyethylene) and soft metals (e.g. lead, tin; and in some cases, copper) can be useful as lubricant – example, during drawing of high-carbon wire (to be used in auto tires) a thin layer of Cu is electrolytically deposited on the wire and is used as lubricant.

The delivery of the lubricants, especially the automated delivery, is also of enormous technological importance. For example, in a modern rolling mill, an important aspect of the lay out and operations is the appropriate lubrication delivery. It involves lubrication reservoir, pumps, filters, gauges and controls, heating/cooling, automation and quality checks. The quality checks would typically involve checks for density, colour, flash point, aniline point, carbonization tendency, neutralization properties and saponification values (Möller and Boor [1996]). A more

**Table 11.2.** Broad classifications of industrial furnaces used in TMP.

Classification	Types	Remarks
Heat source	Electric Fuel-fired	The nature of electric power, e.g. resistance, induction, etc.; and the nature of fuel would decide the furnace design
Sub-classification of electric	Resistance Induction Microwave	Resistance heating is most common. Induction and microwave heating in TMP furnaces are still topics for R&D
Sub-classification of fuel-fired	Direct fired Indirect fired	Combustions products are circulated over work piece in direct fired, while in indirect fired the workpiece is protected. Examples of the latter include muffle (workpiece is enclosed in a muffle and then heated) and radiant tube (enclosing flame and combustion products)
Job type	Soaking pit Slot-forge	Furnaces are also classified based on its application. For example, soaking pits are ingot heating furnaces. Similarly, slot-forge, wire, carburizing, etc. are named for specific operations
Material handling	Batch Continuous	Batch: 'in-and-out' furnaces Continuous: material is moved while being heated

detailed description on lubricants in TMP can be found in Singer [1954], Schey [1970], Miller [1993] and Möller and Boor [1996].

### **11.1.2 TMP furnaces<sup>3</sup>**

As shown in Table 11.2, furnaces can be classified using different indices. Of all the classifications shown in the table, the batch and continuous furnaces (and annealing practices) are particularly relevant to the TMP – the latter being more applicable for 'steady-state' operations. As shown in Figure 11.5, a range of batch furnace designs are possible - designs based on specific applications/loading. The schematic of a 'multi-zone' fuel-fired continuous furnace, typical application – steel reheat, is given in Figure 11.6. Table 11.3 outlines the basic information on several types of continuous furnaces. The classifications on batch/continuous furnaces is not exhaustive, for further details on industrial furnaces the reader may refer Trink [2004].

<sup>3</sup> The annealing practices related to TMP does not end with furnaces and furnace design. Of an equal importance are atmosphere and environment control, heat transfer, heating, cooling, etc. In any of these, several issues of large technological importance exist. For example, cooling would involve cooling/quenching media (controlled water jets to oil or polymer quenching), control and optimization of cooling – including automation, de-scaling during cooling, etc.

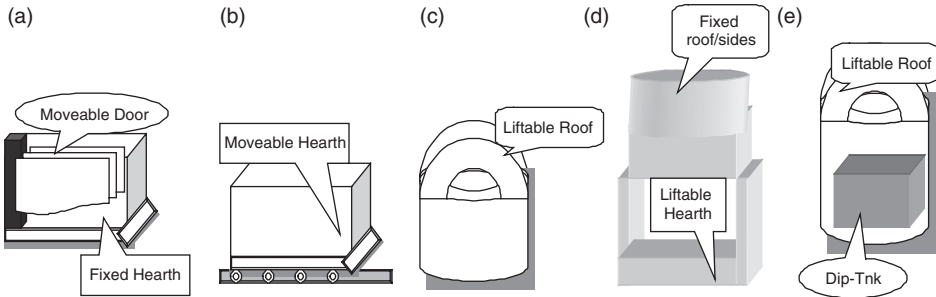


**Figure 11.5.** Schematics of different types of batch annealing furnaces. (a) Fixed hearth – this can be box or slot type. (b) Car or rollable hearth –hearth on steel wheels and rails for heavy loads (examples: car type, car bottom, lorry hearth, etc.). The furnace doors can be fixed to the car; or guillotine doors, to seal front/back ends, can be used. (c) Bell – fixed hearth with liftable roof/sides. (d) Elevator – liftable hearth, fixed roof/sides. (e) Dip-tank – for example, salt/lead-bath. The batch furnace types are not restricted to the five types mentioned in this figure, but can vary widely based on loading/applications.

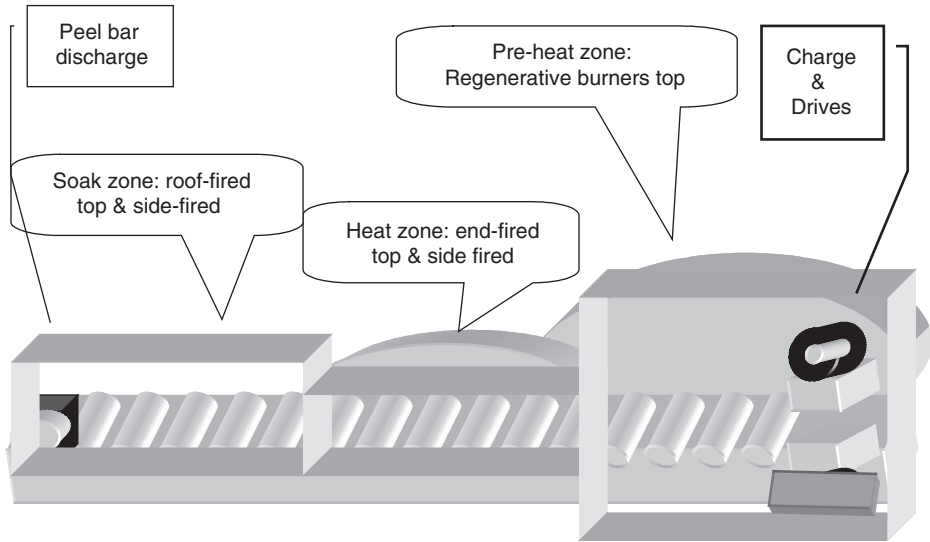


**Figure 11.6.** Schematic of a ‘multi-zone’ fuel-fired continuous furnace.

**Table 11.3.** Several types of continuous furnaces, furnaces typically used in TMP.

Furnace type	Details
Tunnel	A tunnel furnace, as in Figure 11.7, typically has different heating zones and conveyerized material movement. The latter may range from conveyors to rollers, typically kept within the furnace to preserve heat and to prevent belt/roller failures by repeated heating/cooling. Heating may range from electric to fuel fired. Several design innovations are possible – including heat circulating ‘plug-fans’, radiant tube, etc.
Shuttle car-hearth	Hybrids between batch and continuous. Example: A box-type furnace with doors at both ends with two rolling hearths for quick loading/unloading
Saw-tooth walking beam	Saw-tooth walking beams provide rollover action for round objects (example: pipes). Cold material is picked up by the saw-tooth and at every step of the walking beam, the material rolls down – exposing different parts to heating. The furnace typically employs top and bottom firing
Rotary hearth	Donut or oval shaped – the charged material rotates through different zones and gets heated and then discharged. The major design issue is to obtain reduced fuel rates. Water seals may limit, but does not eliminate, ‘air infiltration’ – the major cause for energy inefficiency
Fluidized bed	Shaft furnace containing a thick bed of inert balls/pebbles – bubbled streams of combustion gasses rise through grate or perforated plate from a combustion chamber below. Rapid heat transfer and uniform heating of complex shapes are the typical advantages

## LITERATURE

- Kalpakkian S., “Manufacturing engineering and technology”, Addison-Wesley (1995).  
 Möller U.J. and Boor U., “Lubricants in Operation” (Translated and Published from German), Ipswich Book Company, Suffolk, UK (1996).  
 Schey J.S., “Metal Deformation Processes: Friction and Lubrication”, Marcel Dekker Inc., New York (1970).  
 Trink W., Mawhinney M.H., Shannon R.A., Reed R.J. and Garvey J.R., “Industrial Furnaces”, John Wiley & Sons, Hoboken, NJ (2004).

## 11.2. ROLLING

### 11.2.1 Introduction

Rolling has been used for about 500 years to form flat sections and sheet metal. In fact, it was probably first developed in the mid-16th century for the production of gold and silver strip of near-constant dimensions, to be used for coining and minting (and still is employed for this). It basically involves pushing a metal work-piece into the gap between two rotating rolls, which then simultaneously draw the

workpiece into the rolls and compress it to reduce the thickness and increase the length. For large components this often requires significant power input, which was initially supplied by water mills, then steam power, before the advent of modern, electrically driven and highly automated rolling mills.

From an economic point of view, rolling is the most important metal working and shaping technique; it can be used to roll large ingots from half a meter thickness down to a few microns in the case of Al foil (of total length up to a hundred kilometres). Thus, 30 ton ingots are rolled down in a succession of rolls, often starting at high temperatures and finishing near room temperature. Using appropriately shaped rolls, hot rolling is also widely employed to form long profiles of more complex sections such as I beams and rails (known as ‘shape rolling’ as opposed to flat rolling). A very wide variety of forms, widths and thicknesses can therefore be manufactured, with high productivities, from semi-finished slabs through car-body sheet to packaging foil. Modern rolling mills are extremely efficient units capable of processing over a million tons of metal per year.

Rolling is carried out in a sequence of rolling passes during which the compressive strain can vary from a few percent to 50%. Since the deformation is only applied on the part of the workpiece between the rolls, i.e. a relatively small volume, the loads are reduced to moderate values even for very large ingots; this is of course the practical origin of the process. A reversible rolling mill is often used for the first stages of hot rolling of large sections such as ingots and slabs to reduce their thickness as rapidly as possible and avoid cooling down. Further reductions are achieved in a series of one-way mills known as ‘stands’. Cold rolling of sheet is also usually carried out at high strain rates between roll stands; but for thin foil, reversible rolls are used with coilers at each end.

Both hot and cold rolling can lead to major improvements of the material properties by refining the microstructure. As-cast ingots are often characterized by large grain sizes, significant porosity and coarse 2nd phase particles. During hot rolling, porosity can be closed up, grain size reduced by recrystallization and coarse particles broken up leading to stronger, tougher alloys. Cold rolling can also be used to increase strength by work hardening; the latter is often sufficient to limit the amount of achievable rolling strains so that intermediate softening operations by annealing are necessary to continue rolling. If the property improvements by hot and cold working have been known for centuries, their microstructural origin have only been really understood over the last 50 years and the detailed process – structure–property relations, through TMP are the current object of intense research and development. Rolling lends itself to TMP because of the large number of variables during the process: temperature, strain and strain rate per pass and interpass periods, all of which need to be tailored to a specific alloy composition.

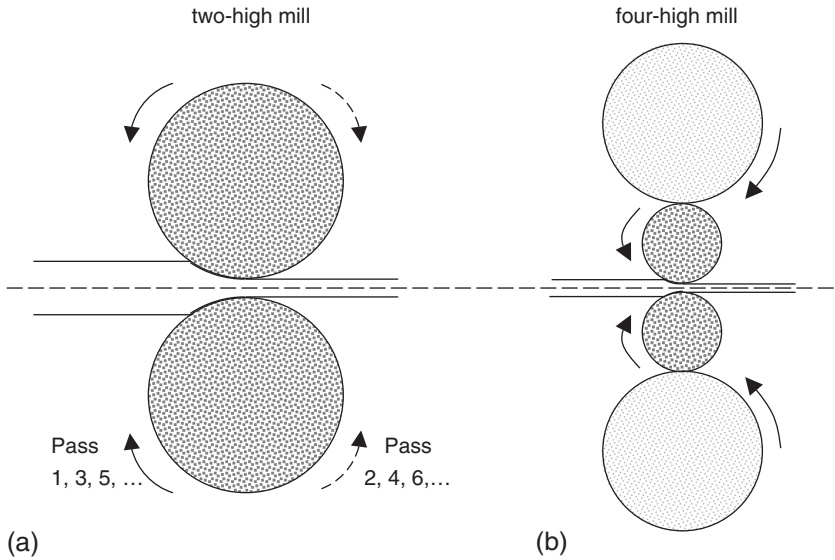


Figure 11.7. Schematic of a 2-high mill (a) and a 4-high mill (b).

## 11.2.2 Rolling equipment

**11.2.2.1 Plate, sheet and foil.** The first, and still a very common, type of rolling equipment is the two-high mill. Figure 11.7a illustrates a schematic two-high reversible mill in which the direction of rotation of the rolls is reversed after each pass to enable the workpiece to be passed successively backwards and forwards. This type of reversing mill with large diameter rolls is often used for the first stages of hot rolling ingots in the primary rolling mill (breakdown rolling in the blooming, slabbing or cogging mill). Typically, the ingot is reversibly hot rolled down from 500 to 30 mm (total average strain of 2.8) in a series of 10–20 passes.

Higher strains per pass are carried out during subsequent rolling operations down to sheet or foil using smaller diameter rolls to reduce the required power. However, smaller diameter rolls are less rigid than the large ones and therefore tend to bend significantly around the workpiece, producing camber in the strip particularly during cold rolling of hard metals. This is reduced, or eliminated, by using larger diameter *back up* rolls which support the smaller *work rolls*. Figure 11.7b shows a schematic of a four-high mill. The principle has been extended to the development of cluster mills, Figure 11.8, in which each roll is supported by two backing rolls. A Sendzimer mill is an example of such a cluster mill used to roll very thin sheet or foil.

High rates of production can be achieved in a continuous mill using a series of rolling mills often denoted tandem mills. Each set of rolls is placed in a stand and

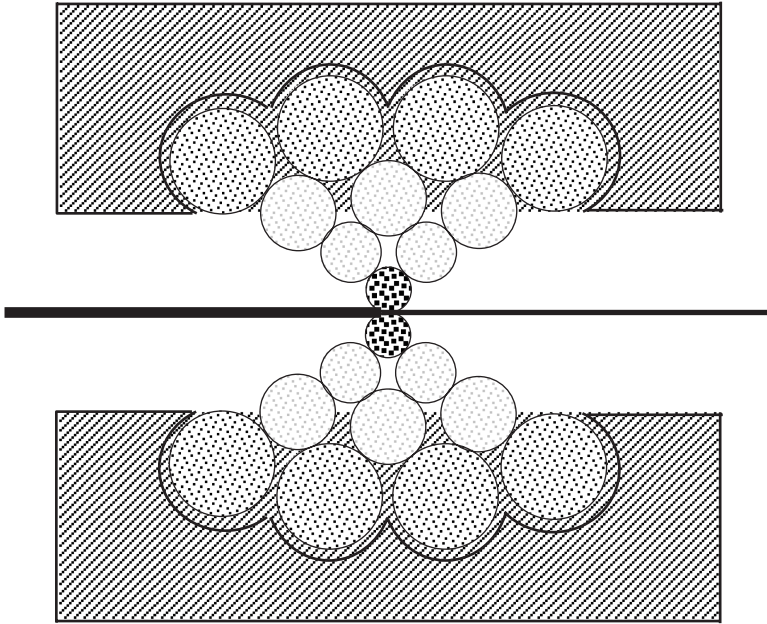


**Figure 11.8.** The Sendzimir mill, as an example of a cluster mill.

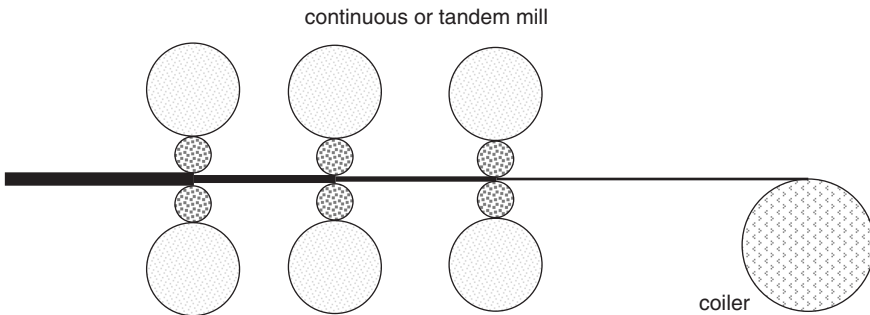


**Figure 11.9.** Schematic of a continuous mill.

since the input and output speeds of the strip at each stand are different, the strip between them moves at different (usually rapidly increasing) velocities. The rolling speeds of each stand are therefore synchronized so that the output speed of stand  $n$  equals the input speed of stand  $n+1$ , i.e. successive stands work in tandem. The final output sheet is usually coiled and both the coiler and the uncoiler can be adjusted to provide a back or a front tension. Continuous 4-high tandem mills are used for rolling

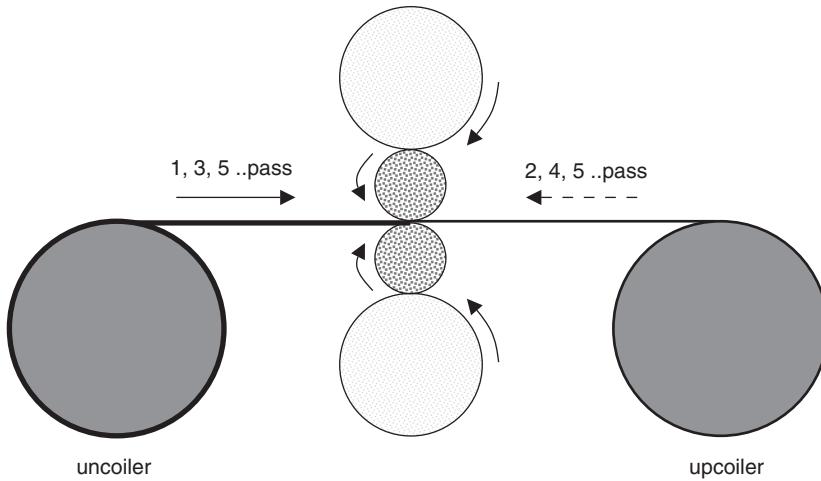


**Figure 11.10.** Illustration of a single-stand reversible cold rolling mill.

strip of typical thickness 30 mm down to a few mm in 3–5 stands; this can be done hot or cold (Figure 11.9). In the latter case, the production rates are very high but so are the capital costs and the product is very standardized (e.g. car-body sheet).

More flexible cold rolling is performed in 4-high single stand reversing mills with coilers at both ends (and which can also provide front and back tension) (see Figure 11.10).

A special type of mill for large reductions is the planetary mill which is made up of two large backing rolls surrounded by several small planetary rolls (Figure 11.11). Each of the latter gives a roughly constant reduction to the slab before it meets the next set of rolls. Thus, during a single pass (at high temperatures), the slab undergoes a large number of reductions so that it is, in effect, rolled down to strip in one pass.

**11.2.2.2 Bars, rods and profiles.** Long products such as beams, rails and wire rods are manufactured by rolling them through a series of work rolls of specific shapes, typically grooved rolls. The workpiece starts as an initial round or square bloom or billet which is then repeatedly passed through the calibrated work rolls, usually by reversible rolling. The pass geometry is generally established by empirical trials but some numerical methods are being developed.

During shape rolling, in contrast to flat rolling, the cross-section of the metal is reduced in two directions. In one pass, the metal is compressed in one direction and then rotated  $90^\circ$  for the following pass so that more ‘equiaxed’ sections can be achieved. Thus, a square billet is reduced to bar by alternate passes through oval and square-shaped grooves. The area of contact therefore changes continuously during

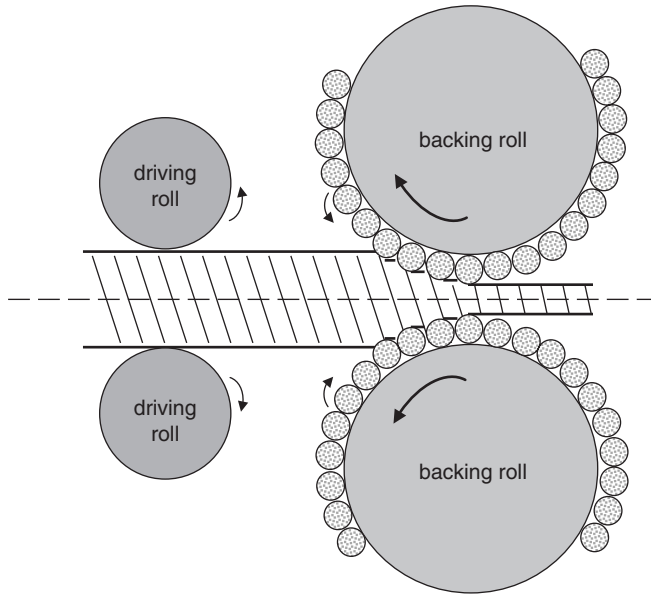


**Figure 11.11.** Schematic of a planetary mill.

the rolling process. The total reduction per pass is expressed in terms of the change in cross-sectional area, since there are both thickness reductions and width increase.

Shape rolling involves significant amounts of lateral spreading, which is difficult to control so the more complex shapes require very experienced designers.

### 11.2.3 Mechanics

Figure 11.12 illustrates the basic geometry of rolling (a) and the forces exerted during a flat rolling pass (b) under plane strain conditions (constant width  $w$ ). A workpiece of initial thickness  $h_0$  is passed between rolls of diameter  $R$  at an initial velocity  $v_0$  and exits at thickness  $h_f$  and velocity  $v_f$ . The surface velocity of the rolls is  $v_c$ . At the first point of contact, the metal advances more slowly than the rolls but, by volume conservation during a thickness reduction  $\Delta h$ , it exits more quickly; only at the neutral (or no-slip) point  $N$ , defined here by the angle  $\Psi$ , are the surface roll and workpiece velocities identical.

The total reduction and total true strain in one pass are defined as:

$$r = \frac{h_0 - h_f}{h_0} \quad \text{and} \quad \bar{\varepsilon} = \ln \left( \frac{h_0}{h_f} \right) \quad (11.4)$$

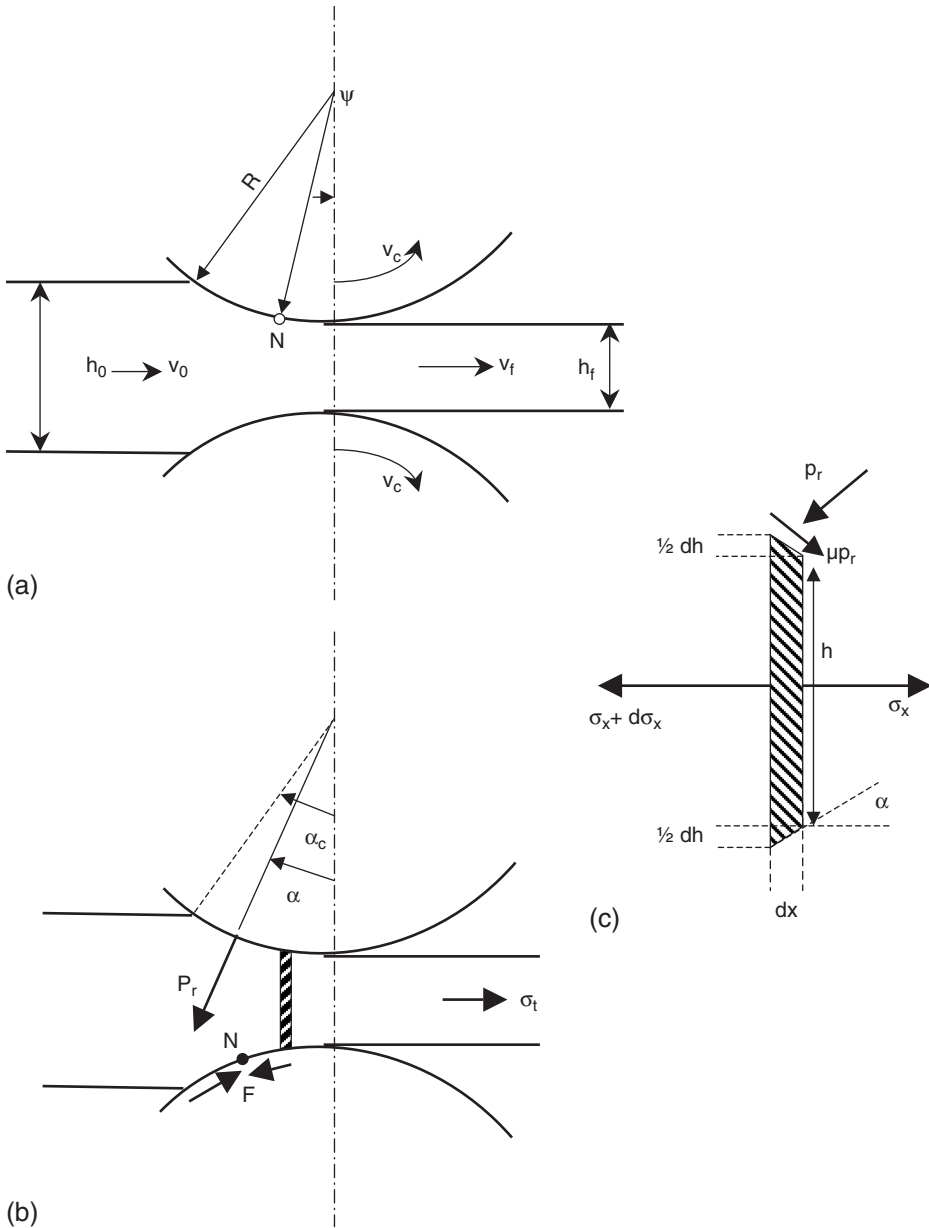


**Figure 11.12.** Basic geometry of flat rolling.

To feed the workpiece into the rolls, there has to be some friction between the two. The frictional force acting on the roll surfaces before the neutral point,  $N$ , pulls the strip between the rolls, while the friction force acting between the neutral point and the exit opposes the strip movement out of the rolls.

For the workpiece to enter the rolls, the horizontal component of the frictional force  $F$ , which acts towards the roll gap, has to be equal to or greater than the same component of the radial force  $P_r$  exerted by the rolls to compress the workpiece. The limiting condition at the entrance is expressed in the following way for the angle of contact  $\alpha_c$  (half the total included angle for plane strain compression).

$$F \cos \alpha_c = P_r \sin \alpha_c \quad (11.5)$$

Also since the frictional force  $F$  is related to the radial force  $P_r$  by the friction coefficient  $\mu$ :  $F = \mu P_r$ . Combining these two equations gives for the lowest possible value of  $\mu$ :

$$\mu = \tan \alpha_c \quad (11.6)$$

The workpiece will not be drawn into the rolls if the coefficient of friction is less than the tangent of the contact angle. The thicker the slab, the greater the friction coefficient required and if  $\mu = 0$  rolling cannot occur.

The exact values of the friction coefficients during rolling are difficult to establish with precision since they are considered to vary along the contact arc of the rolls. However, for most analyses, a constant value is assumed; typically  $\mu$  varies from 0.05 to 0.1 for cold rolling with lubrication to 0.2 or even above for hot rolling.

The vertical component of  $P_r$  is known as the rolling load  $P$  required to compress the metal. The specific roll pressure  $p$  is this force divided by the contact area, i.e. the product of the width and the projected length of arc of contact:

$$p \approx \left( \frac{P}{w[R(\Delta h)]} \right)^{1/2} \quad (11.7)$$

By simple geometry the draft  $\Delta h$  is related to the angle  $\alpha_c$  by the length of the arc of contact  $l_c = (R\Delta h)^{1/2}$  and the roll diameter  $R$ :

$$\tan \alpha = \frac{(R\Delta h)^{1/2}}{(R - \Delta h)/2} \approx \left( \frac{\Delta h}{R} \right)^{1/2}$$

But from Eq. (11.6)

$\mu \geq \tan \alpha_c$  so

$$(\Delta h)_{\max} = \mu^2 \cdot R \quad (11.8)$$

This determines the maximum reduction that can be achieved in one pass for a given set of rolls.

The minimum exit thickness ( $h_{\min}$ ) that can be obtained in a strip has been estimated by Stone [1953]; it depends on the average equivalent flow stress of the material  $\bar{\sigma}$  (averaged between the entrance and exit values), the friction coefficient  $\mu$  and the elastic properties of the rolls (Young's modulus  $E_r$  and Poisson's ratio  $\nu_r$ ):

$$h_{\min} = \frac{A\mu R}{E_r} (1 - \nu_r^2) (\bar{\sigma} - \sigma_t) \quad (11.9)$$

$A$  is a coefficient that takes values of 7 to 8 and  $\sigma_t$  is the tensile stress (if any) applied to the workpiece during rolling. In practice, it is possible to obtain thinner strip than expected from this relation by pressing the rolls together.

A rigorous calculation of the rolling force  $P$  (also known as 'the roll separation force') is not very easy to do. In a first very crude approximation, the effects of inhomogeneous deformation and of friction can be neglected and flat rolling is considered as simple plane-strain compression. The rolling force can then be calculated from Eq. (11.7) with the contact pressure  $p$  equal to the (plane strain) flow stress of the material:

$$P = \left( \frac{2}{\sqrt{3}} \right) \sigma_y w [R(\Delta h)]^{1/2} \quad (11.10)$$

A rough compensation for neglecting friction and inhomogeneous deformation consists in replacing the factor  $(2/\sqrt{3}) = 1.155$  by a factor 1.5, leading to the following 'rule of thumb' for the estimation of the rolling force:

$$P = 1.5 \sigma_y w [R(\Delta h)]^{1/2} \quad (11.11)$$

In reality, the roll pressure varies significantly along the arc of contact and a typical distribution is shown in Figure 11.13. The pressure goes through a maximum close to the neutral point and the general form of the curve is known as the 'friction hill'. The total area under this curve is proportional to the rolling load. The area under the dotted line represents the force required to deform the metal in plane

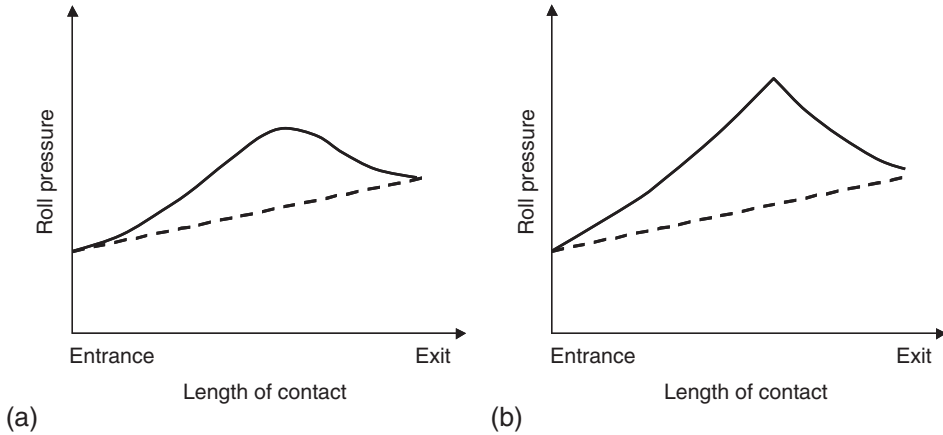


**Figure 11.13.** Schematic variation of roll pressure along the arc of contact (a) experimental and (b) calculated according to Eqs. (11.13)–(11.15).

strain compression. The area above this line is related to the force required to overcome the friction between roll and workpiece, hence the name of friction hill.

The height of the friction hill depends upon the value of the friction coefficient, but both the peak height and position can be shifted by the application of front or back tensions to the workpiece. A back tension will significantly reduce the rolling load and shift the peak towards the exit side so this is often applied industrially.

A more realistic roll pressure analysis follows from the standard theory of plastic working (see, e.g. Dieter [1988], Rowe [1977], Mielnik [1991]). The horizontal components of forces acting on an element of metal situated in the roll gap at a position described by the angle  $\alpha$  (see Figure 11.12) are:

- $(\sigma_x + d\sigma_x)(h + dh) - h\sigma$ : due to longitudinal stress.
- $2(p_r \sin \alpha)(dx/\cos \alpha)$ : due to radial pressure on both rolls.
- $2\mu(p_r \cos \alpha)(dx/\cos \alpha)$ : due to friction against both rolls.

The force balance gives:

$$hd\sigma_x + \sigma_x dh + 2\mu p_r dx \pm 2\mu p_r dx = 0 \quad (11.12)$$

where, as before,  $p_r$  is the radial pressure,  $h$  is the current thickness and  $\sigma_x$  is the horizontal component of stress in the metal. The  $\pm$  sign accounts for the change in sign of the frictional force at the neutral point. Equation (11.12) is often known as the ‘von Kármán’ [1925] equation, who first proposed it.

Rigorous solutions to this equation require numerical techniques, but an approximate analytical solution is given following Bland and Ford [1948] by taking the small angle approximations  $\sin \alpha = \alpha$  (in rad),  $\cos \alpha = 1$  and  $Pr = P$  and assuming that the variation in flow stress is small compared with the variation in roll pressure so that one obtains:

$$\text{on the entrance side } P = \frac{2\sigma_0 h}{\sqrt{3}h_0} \cdot \exp[\mu(H_0 - H)] \quad (11.13)$$

$$\text{and on the exit side } P = \frac{2\sigma_0 \cdot h}{\sqrt{3} \cdot h_f} \cdot \exp[\mu H] \quad (11.14)$$

$$\text{where the quantity } H = 2\sqrt{\frac{R}{h_f}} \cdot \tan^{-1}\left(\sqrt{\frac{R}{h_f}} \cdot \alpha\right) \quad (11.15)$$

If front tension ( $\sigma_f$ ) and back tensions  $\sigma_t$  are applied to the strip, then these pressure are reduced by respective factors of  $(1 - (\sigma_f/\sigma_0))$  and  $(1 - (\sigma_t/\sigma_0))$ .

These equations implicitly assume plane strain compression, homogeneous deformation and relatively low-friction coefficients; they apply essentially to the case of cold rolling strip, except for the case of very light reductions as in skin pass rolling, where the deformation takes place in the surface regions. It should also be noted that due to the high loads, the radius of curvature of the rolls  $R$  is not necessarily constant; in fact, they tend to flatten significantly by elastic deformation and Hitchcock [1935] has given an estimate of the larger  $R$  value ( $R'$ ) to be used in Eq. (11.11).

$$R' = R \left[ 1 + \frac{CP}{(h_0 - h_f)w} \right] \quad (11.16)$$

with  $C$  the elastic constant of the roll ( $C \sim 0.022 \text{ mm}^2/\text{kN}$ ).

The mechanics of hot rolling is more complicated because of the higher frictions, the superimposed shear components in the surface regions for thicker slabs and the strain rate sensitivity of the flow stress. An early analysis of the roll stresses by Ekelund [1927] for this case gives:

$$\frac{P}{w} = \left\{ \sigma_0 + \frac{2V\eta\sqrt{\Delta h/R}}{h_0 + h_f} \right\} \cdot \sqrt{R\Delta h} \left\{ 1 + \frac{1.6\mu\sqrt{R\Delta h} - 1.2\Delta h}{h_0 + h_f} \right\} \quad (11.17)$$

where  $\sigma_0$  is the 'static' yield stress,  $V$  the peripheral speed of the rolls and  $\eta$  the material viscosity.

During hot rolling, the near-surface regions undergo additional (redundant) shears since the friction coefficient is significantly higher than for cold rolling and also because of the higher thickness to contact length ratio. There is often significant lateral spread.

The frictional forces lead to near-surface shears, whose sign changes at the neutral point. If  $x$  is along RD and  $z = \text{ND}$ , then from Figure 11.12b the displacement gradient component of the shear deformation  $de_{xz} = du_x/dz$  induced, by the friction stresses, is initially positive (in the upper half of the sheet), goes to zero at the neutral point then becomes negative afterwards. If the neutral point is near the middle of the arc of contact, then this shear component will roughly balance out to an accumulated friction-induced shear near zero. However, the geometrical shape change of the metal induced by what is the equivalent of a converging channel is described by the  $de_{zx} = du_z/dx$  component of the displacement gradient. For the same material element, this  $de_{zx}$  component is clearly negative at first, decreases in amplitude during the pass and can also change sign but not necessarily at the neutral point. Consequently, the conventional shear strain  $d\epsilon_{xz}$ , which is half the sum of both components does not always give an adequate description of the true material deformation.

There is a rule of thumb for estimating the relative importance of these two types of shear from the ratio of the contact length  $l_c$  to average sheet thickness  $\frac{1}{2}(h_0 - h)$ :

- $l_c/\frac{1}{2}(h_0 - h) > 5$  means that the friction-induced effects at the surface, along the contact length, dominate; a thin sheet rolled with large diameter rolls undergoes very superficial surface shears  $de_{xz}$  (as in a skin pass).
- $l_c/\frac{1}{2}(h_0 - h) < 0.5$  means that the shape change effect dominates and leads to large shear components inside the metal. This occurs during hot rolling, particularly when large draughts are applied to thick band. At  $\frac{1}{4}$  thickness, there are strong shear effects  $de_{zx}$ , particularly during reversible rolling.

When  $0.5 < l_c/\frac{1}{2}(h_0 - h) < 5$ , the deformation is supposed to be homogeneous but homogeneous is clearly a relative term when applied to rolling deformation.

Hosford and Caddell [1983] also define a  $\Delta$ -factor (thickness (or diameter)/contact length). The application to wire drawing is described in Chapter 11.4.

$$\text{For flat rolling, the } \Delta\text{-factor gives: } \Delta = \left[ \frac{2-r}{2} \right] \left[ \frac{h_0}{rR} \right]^{0.5} \quad (11.18)$$

In principle, one wants  $\Delta < 1-2$ ; for  $\Delta > 5$ , most of the deformation is concentrated on the surface (thick specimen; small rolls);  $\Delta$  can also be high for very small reductions.

The strain rate in rolling is related to the geometry of the mill and to the surface speed  $v$  of the rolls. If slipping friction between sheet and rolls is assumed, an approximate estimation of the mean strain rate in rolling can be obtained from Mielnik [1991]:

$$\dot{\epsilon} = \frac{v}{h_0} \sqrt{\frac{h_0 - h_f}{R}} \quad (11.19)$$

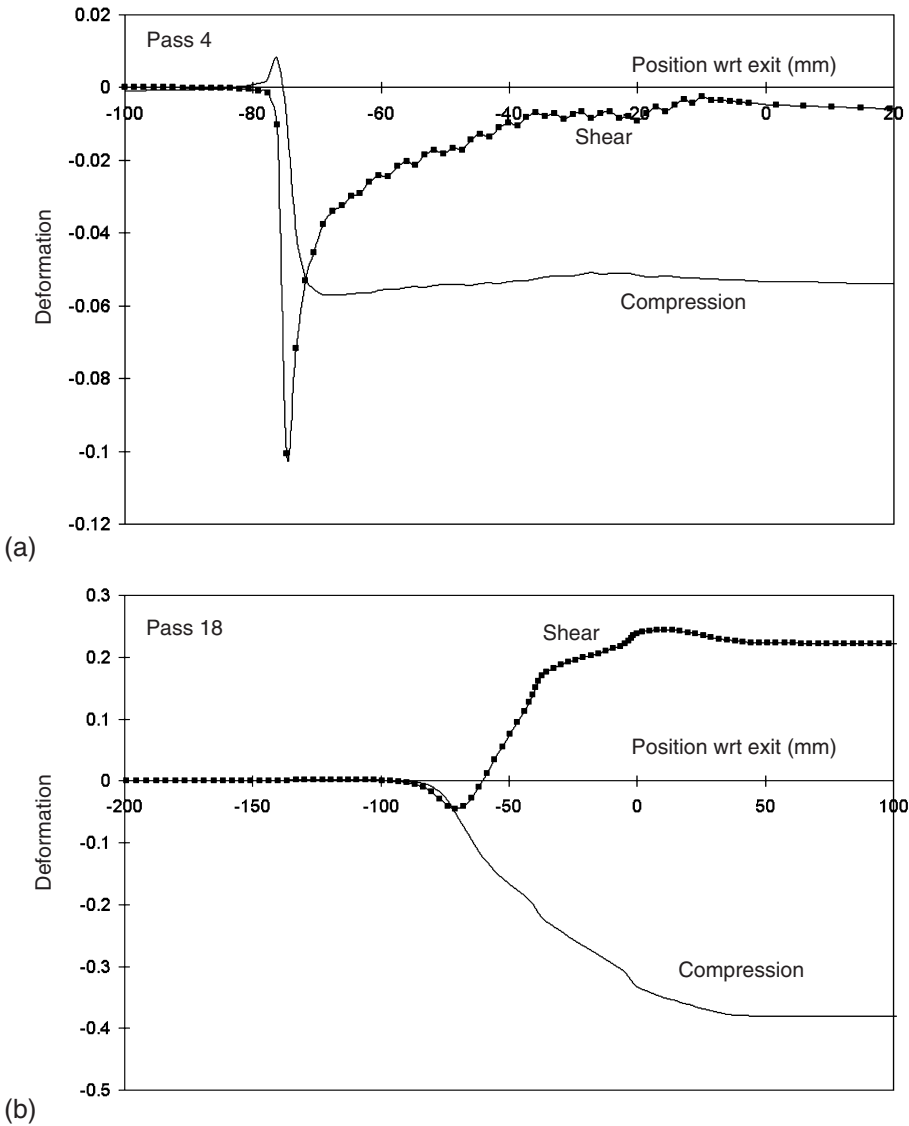
There is a general tendency to use finite element methods (FEMs) for the detailed analysis of hot rolling mechanics to derive both the roll forces and the local deformation modes of the material. Figure 11.14 indicates how the shear and compression strains of an aluminium alloy vary through the roll gap during two passes of breakdown rolling near the start of rolling (pass 4) and towards the end (pass 18).

In Figure 11.14a, the initial (small) negative  $\epsilon_{xz}$  shear is reversed during the pass and reduced to almost zero, whereas during pass 18, Figure 11.14b the same, larger shear becomes positive and is retained at the exit.

### 11.2.4 Typical rolling schedules

**11.2.4.1 Steel.** Most steels are now produced by continuous casting with typical cross-sections of 0.2–0.3 m (thickness) and up to 2 or 3 m in width. In some cases, the as-cast steel is rolled hot directly after casting and solidification but usually it is cooled down and sectioned into slabs. The slabs are then reheated to temperatures around 1200°C then hot rolled down to thicknesses of the order of 50–30 mm in a roughing or slabbing mill before going into the finishing mill for reductions down to a few mm. Strain rates in the roughing mill are of the order of 10/s and then increase up to 100/s during finishing. Note that these conditions are only given as an indication. Individual mills can have quite different rolling schedules as a function of equipment, alloy composition and final application (see Chapter 15). The final sheet gauge is obtained by cold rolling down to thicknesses of about 1 mm for applications such as car-body sheet. In this case, the cold-rolled sheet is then annealed at temperatures of about 700°C to provide a ‘soft’ recrystallized sheet suitable for deep drawing.

In the case of plain carbon steels, the initial roughing starts at temperatures around 1150°C and ends at about 1000°C before the finishing in the temperature range 1000–910°C. For these steels, the final cooling after finishing is particularly important since the cooling rate controls the phase transformations that occur (e.g. austenite to perlite or bainite, etc.) and therefore the final properties. For special products such as the high-strength low alloys (HSLA) or multiphase steels, etc. the

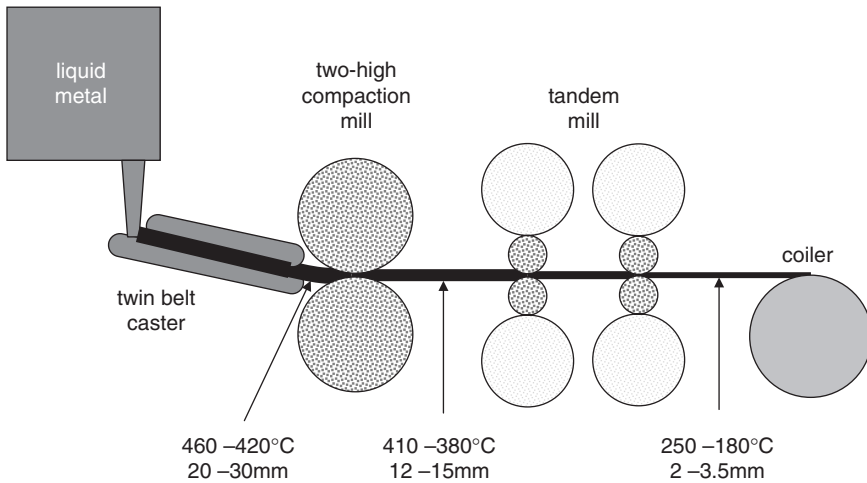


**Figure 11.14.** The cumulated shear (dotted) and compression (continuous) strain components through the roll gap of a breakdown mill, near the surface for two passes (strain rate and temperature fields calculated by finite element methods for an AA 3104 (Al-1Mn-1Mg) alloy in the stationary regime (Perocheau [1999])).



**Table 11.4.** Some typical rolling conditions for Al alloys.

	Reversible	Tandem	Cold rolling
Start temperature (°C)	500–600	400–500	20
Finish Temperature (°C)	400–500	250–350	100
$N^\circ$ passes	9–25	2–5	2–10
Initial thickness (mm)	400–600	45–15	2–6
Final thickness (mm)	45–15	2–9	0.01–1
Strain per pass	0.1–0.5	0.7	0.3–0.7
Total strain	3.5	3	<5
Strain rates (s)	1–10	10–100	>50
Inter-stand times (s)	10–300	<3	

**Figure 11.16.** Schematic continuous strip casting line.

Cold rolling is usually carried out in a reversible 4-high cold mill between two coilers. When correctly set-up this equipment can be used to roll down the ‘softer’ alloys to a thickness of 15–20  $\mu\text{m}$ . To obtain very thin packaging foil of about 6  $\mu\text{m}$  thickness, the foils are then doubled up and re-rolled. Intermediate annealing is frequently necessary to achieve large cold rolling reductions. It is also worth noting that modern, high speed, cold rolling of medium strength alloys such as the 3xxx and 5xxx series for canning sheet (Chapter 14.1) generates a substantial temperature increase so that the output sheet can attain 120–150°C (or  $0.45T_m$ ).

An increasing proportion of the less strongly alloyed sheet products are now produced by continuous strip casting methods. As shown in Figure 11.16, the hot

metal is poured between rotating cylinders to produce ‘thick’ sheet (10–20 mm) which is then immediately rolled in a tandem mill.

## LITERATURE

- Backofen W.A., “Deformation Processing”, Addison-Wesley, Reading, MA (1972).  
Ginzburg V.B., “Steel Rolling Technology”, Marcel Dekker, New York (ISBN 0-8247-8124-4), (1989).  
Roberts W.L., “Cold Rolling of Steel”, Marcel Dekker, New York (ISBN 0-8247-6780-2), (1978).  
Rowe G.W., “Principles of Metal Working”, 2nd edition, Edward Arnold, London (1977).  
Singh R.V., “Aluminum Rolling, Process, Principles and Applications” TMS Warrendale, PA (2000).  
Totten G.E., Funatani K. and Xie L., “Handbook of Metallurgical Process Design” Marcel Dekker, ISBN 0-8247-4106-4, 2004 in particular, chapter 3 “Design of Microstructures and Properties of Steel by Hot and Cold Rolling” by R. Colás, R. Petrov and Y. Houbert and chapter 4 “Design of Aluminum Rolling Processes for Foil, Sheet and Plate” by J. Driver and O. Engler.

## 11.3. EXTRUSION

### 11.3.1 Introduction

Extrusion is a process in which a billet of metal is first placed into a chamber with a die at one end and a ram on the other. The billet is then pushed through the relatively narrow die to form long profiles of constant section determined by the die geometry (rather like squeezing toothpaste out of a tube) (see Figure 11.17).

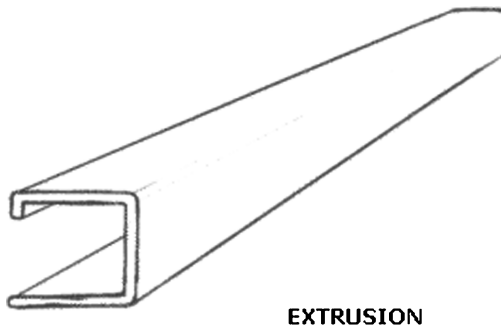


**Figure 11.17.** Example of an extrusion profile.

The process is usually carried out at high temperatures, of the order of  $0.5-0.75T_m$  to reduce both the applied loads and wear on the dies, but on softer metals can be performed at room temperature. The loads are imposed by mechanical presses or hydraulic rams through a mandrel onto the metal billet, which is restrained by the chamber designed to withstand the large radial stresses generated during extrusion; Figure 11.18 is a schematic of the direct extrusion process. According to the die geometry, a very large variety of cross-sections can be produced varying from round or rectangular bars, through L, I or T shapes etc. to tubes and complex sections.

A second type of extrusion – known as ‘indirect or back extrusion’ – uses a hollow ram containing the die, while the other end of the billet is completely blocked off. As the ram is pushed into the billet, the metal is extruded out in the opposite direction through the die (back out along the hollow ram). This has the advantage that there is no relative movement between the container wall and the billet so that the friction forces and the required power level are smaller. However, the use of a hollow ram limits the loads that can be applied.

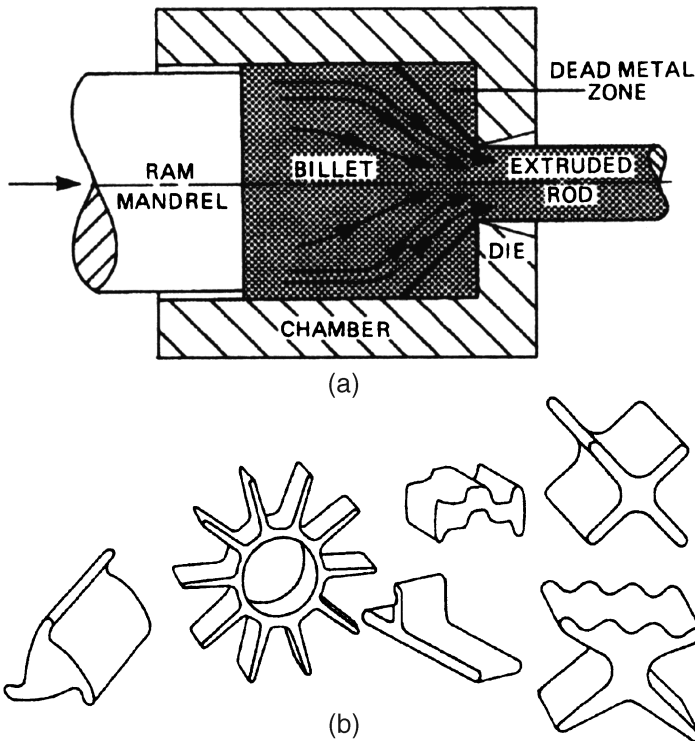


**Figure 11.18.** (a) Direct extrusion process and (b) some typical profiles – (Avitzur [1983]).

A variant of this is impact extrusion, which is used to produce short lengths of hollow shapes, e.g. toothpaste tubes, from solid rods or disks. A high-speed mechanical press pushes the ram into the disk placed above a female die so that the wall of the can or tube is then punched out between the ram and the die.

In general, extrusion tooling is inexpensive; lead times for custom shapes or prototypes are relatively brief and many alloys can be readily formed into complex shapes. Consequently, extrusion has developed significantly over the last two or three decades to become the second most important plastic forming operation, after rolling.

### 11.3.2 Deformation conditions

The overall deformation is often described by the extrusion ratio, i.e. the ratio of the billet cross-sectional area to the final cross-section area after extrusion:  $R_{\text{ext}} = A_0/A_f$  and the average strain approximated by  $\ln R_{\text{ext}}$ . By conservation of volume, the velocity of the extruded product is the ram velocity  $x R_{\text{ext}}$ . Given that at high temperatures, the material flows at constant stress the extrusion force is related to the natural logarithm of the extrusion ratio:

$$P = k A_0 \ln R_{\text{ext}} \quad (11.20)$$

where the extrusion constant  $k$  includes the effects of material flow stress, friction and inhomogeneous deformation. For the extrusion of bars, an average strain rate can be calculated using:

$$\dot{\epsilon}^{\circ} = 6VD_0^2 \text{tg}\alpha \frac{\ln R_{\text{ext}}}{(D_0^3 - D_e^3)} \quad (11.21)$$

with  $D_0$  the diameter of the billet,  $D_e$  the diameter of the bar,  $V$  the speed of the plunger, and  $2\alpha$  the die angle.

Because of the relatively complex shapes formed during extrusion, the plastic strains vary substantially with position in the workpiece. They are usually close to uniaxial elongation in the centre of round bars and near plane strain compression for flat sections, but with large shear components near the surface where the metal flows past the chamber walls and the die edges. There is often a dead metal zone in the corner of the exit side of the chamber. Lubrication conditions can therefore be critical for some metals.

In fact, two metals, Cu and Mg, are particularly easy to extrude since their oxides are softer than the metal at high temperatures. The oxide layer formed during heating the billet acts as a natural lubricant.

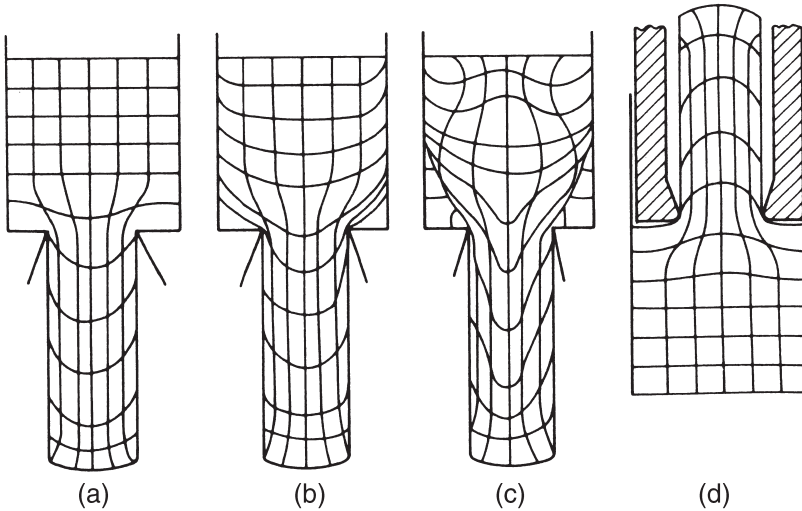


**Figure 11.19.** Some typical deformation patterns during direct (a–c) and indirect extrusion (d) with a square die: (a) good lubrication, (b) average lubrication, (c) poor lubrication and (d) indirect extrusion. From Schey [1968].

Figure 11.19 shows some typical deformation patterns in extrusion: (a) for the case of relatively homogeneous deformation with a well-lubricated billet or indirect extrusion as in Figure 11.19d. Figure 11.19c illustrates the deformation for a high-friction condition, where the material flow is concentrated near the centre in association with internal shearing near the surface.

The die geometry is important for facilitating material flow without excessive friction and heterogeneous deformation. Well-lubricated billets are extruded using die fronts with conical entrances of semidie angle, typically  $45\text{--}60^\circ$ , to reduce the extrusion pressure. However, some metals such as aluminium form a dead zone and then shear internally about it to form their own die angle; in these cases, the die entrance face is flat.

A simple method of estimating the die pressure  $P_d$  is to use the analysis of extrusion through a conical die of semidie angle  $\alpha$ . Assuming Coulomb sliding friction (but no redundant deformation) Hoffman and Sachs [1953] gives a solution analogous to that of wire drawing through a die:

$$P_d = \sigma_0 \left[ \frac{1+B}{B} \right] \left[ 1 - R_{\text{ext}}^B \right] \quad (11.22)$$

where  $B = \mu \cot \alpha$ .

Slip line theory (without friction) yields solutions of the form:

$$P_d = \sigma_0(a + b \ln R_{\text{ext}}) \quad (11.23)$$

with  $a$  and  $b$  taking values of order unity.

More detailed analyses of the die pressures can be found in Dieter [1988].

The ram speed has to be controlled to ensure defect-free products. Some metals such as highly alloyed aluminium and copper are susceptible to hot shortness so the ram speed is reduced to low values ( $<1$  m/min) to avoid excessive frictional heating during the process. Hot shortness leads to periodic transverse cracking along the product, denoted fir-tree cracking. For other materials, such as the refractory metals extruded at very high temperatures, heat transfer from the billet to the tools is a problem and the extrusion has to be carried out as rapidly as possible (ram speeds of up to 30 m/min).

Extrusion develops compressive and shear forces in the stock but usually no tensile stresses so that high deformations are possible with only one extrusion operation. The tolerances can be small, particularly for cold extruded products.

### 11.3.3 Steels and high melting temperature alloys

Up to the invention of the Ugine–Sejournet process (Séjournet and Delcroix [1955, 1966]), the extrusion of steel was severely hampered by lubrication problems. Without a suitable lubricant the very high frictional forces developed during extrusion led to severe wear of the dies so that reproducible extrusions were very difficult to obtain. Séjournet [1955] devised a method of lubrication based on the use of molten glass in which both the chamber walls and the die surfaces are lubricated. The hot steel billet is rolled in a powder of glass which melts and forms a thin, viscous, film coating before introduction into the chamber. The front end of the billet is also placed in contact with a glass pad, located just before die orifice, whose surface gradually melts during the extrusion to provide a continuous supply of lubricant between the die and the extruded product. This process has been extended to practically all metals and alloys that are extruded in or above the steel hot working range. Figure 11.20 illustrates the strain rate distribution in a partially extruded steel billet.

Steels such as carbon steels and stainless steels are hot extruded in the typical temperature ranges 900–1200°C, i.e. in the hot working austenite range, and therefore undergo the same deformation–transformation reactions as during hot rolling. The potential for TMP is not so great since only one deformation step is performed but, even given this limitation, TMP has perhaps not yet been sufficiently developed for the extrusion process. For example, Lesuer *et al.* [1999] has shown that the properties of hypereutectoid carbon steels can be significantly improved by hot extrusion.

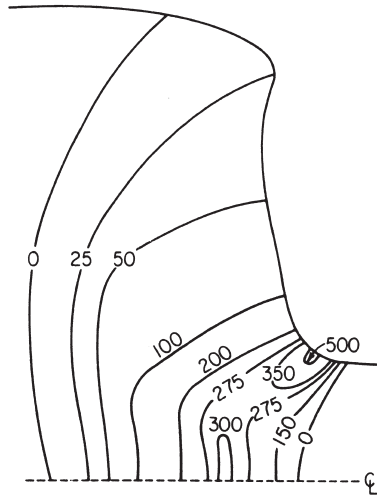


**Figure 11.20.** The strain rate distribution in a partially extruded steel billet ( $R = 16.5$ , ram speed = 12.6 m/min,  $T = 1440$  K (Childs [1974])). Permission obtained from Maney.

Carbon steel envelopes are also used to extrude and consolidate powder metallurgy products.

There is a general tendency to develop cold extrusion of steels since the product has higher strength through work hardening, better surface finish and improved tolerances. Here again frictional effects are very important; cold extrusion of steel only became possible, thanks to the introduction of phosphate lubrication. The steel surface is coated with a spongy phosphate coat that absorbs the lubricating liquid, often a soap solution, to substantially reduce friction and wear during extrusion. The literature on cold forming, including cold extrusion, has been reviewed by Watkins [1973].

### 11.3.4 Aluminium alloys

Aluminium extrusions are usually carried out in the temperature range 450–500°C but some of the softer alloys can be extruded at temperatures down to 400 or even 350°C. The extruding rate depends upon the alloy and the complexity of the die shape; to first order, they can be simply classed according to the velocity of the ram used to push the billet. For example, ram velocities are in the range 0.5–2 m/min for hard 7xxx alloys, 10–80 m/min for the intermediate 6xxx alloys and 20–100 m/min for commercially pure aluminium as used for electrical conductors.

The corresponding average strain rates vary over two orders of magnitude from 0.1–50/s, i.e. the same range as hot rolling operations. The nominal

strains defined as  $\ln l/l_0$  are of the order of 1–4 and sometimes higher for very soft metals. These are much higher than the strains encountered in a single rolling pass.

As noted above, the real strains and strain rates vary widely through the section of the extruded profile because of the geometrical complexity inherent to the process. Also aluminium extrusion is carried out without lubrication so the immediate surface ‘sticks’ to the container surface enhancing the surface shear deformations. Thus, in a relatively simple case of plane strain extrusion, the centre part undergoes a deformation close to PS compression but the outer sections deform in a mixture of compression and shear as they are forced to flow round the dead zone and into the die orifice. Even for a simple case of axisymmetric extrusion of a round bar (just involving a change of cross-section area) the off-centre particle paths can be quite complicated. Some finite element calculations of this case are given in Figure 11.21.

As for the case of hot rolling, there is also a significant increase in temperature – of the order of 20–50° – in the high deformation zone of the die during the extrusion process.

There has been a very strong effort over the last two decades to improve the technology of extrusion, essentially by improving die shapes to facilitate metal flow. Scientific studies of extrusion microstructures began with the classic work of McQueen *et al.* [1967] relating the subgrain sizes to the Zener–Hollomon parameter during extrusion of Al alloys.

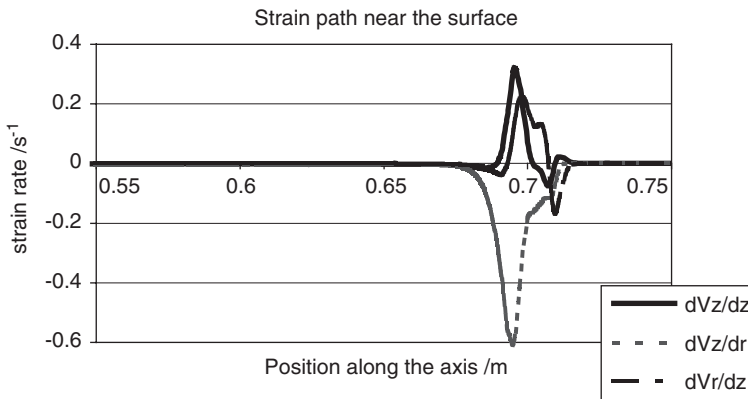


**Figure 11.21.** Velocity gradient components calculated for slow, axisymmetrical extrusion of a round bar of a hard 7xxx Al alloy at a point near the surface (90%).  $dV_z/dz$  is the (elongation) strain rate along the extrusion direction  $z$  and the other two represent the shear components.

From Courtesy of D. Piot, Ecole des Mines de Saint-Etienne.

## LITERATURE

Pearson C.E. and Parkins R.N. "The Extrusion of Metals" Chapman Hall, London (1961).

Storen S. and Moe P.T. 'Extrusion', in "Handbook of Metallurgical Process Design", G. Totten, K. Funatani and L. Xie (eds), Chapter 6, Marcel Dekker, New York (2004), pp. 137–204.

## 11.4. WIRE DRAWING

## 11.4.1 Introduction

In a conventional wire drawing process, the diameter of a rod or wire is reduced by pulling it through a conical die (Figure 11.22a). In industrial production lines, a large reduction is obtained by pulling the wire or rod through a series of consecutive dies. In some cases, an intermediate annealing treatment may be necessary. For most metals, drawing is carried out at ambient temperature, although the temperature inside the die can rise considerably due to heating associated with deformation and friction. Some materials (e.g. tungsten wire for incandescent lamp filaments) are drawn at high temperature.

Wire drawing is not limited to wires with a cylindrical shape; rectangular or more complex cross-sections can also be produced with appropriate dies. A possible alternative for the classical die, is the so-called 'Turk's head' (Figure 11.22b). This consists of four rolls, which can be adjusted to different positions for different products. Flat wires can easily be drawn, but the rolls can be shaped to draw other profiles.

Drawing can also be used to reduce the diameter of tubes (Figure 11.22c). The wall thickness can be reduced in the same operation, using a mandrel.

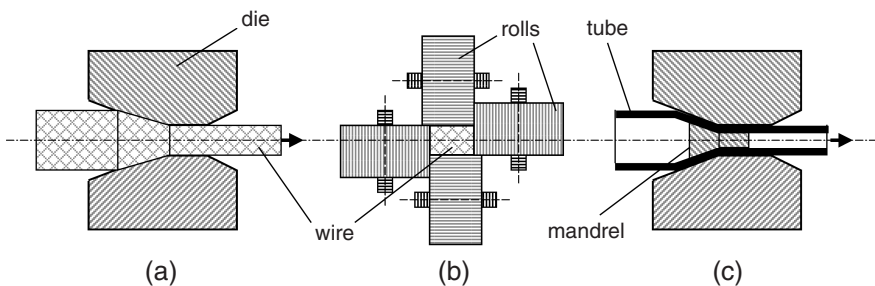


**Figure 11.22.** Illustration of some drawing operations: (a) conventional wire drawing with circular cross-section; (b) wire drawing with rectangular cross-section, using a so-called 'Turk's head'; (c) tube drawing using a floating mandrel.

### 11.4.2 Wire drawing machines

Tubes and straight rods with diameters above 20 mm are usually drawn with draw benches (Figure 11.23). These machines contain a single die and the pulling force is provided by a drawing trolley. The drawing speed is relatively low (0.1–1 m/s), and the length of the tube or the rod is limited (typically less than 30 m). Longer rods and wires are drawn by a rotating drum, called a ‘bull block’ or ‘capstan’. Many design variations are available. Single-die machines (Figure 11.23) are relatively simple and are used for breakdown or finishing operations. In most wire drawing plants, several die/capstan combinations are mounted in series to form a continuous wire drawing machine (Figure 11.24). Since the wire diameter  $D$  is reduced in each pass, the wire speed  $v$  increases after each die. In principle, the following continuity relation must be satisfied:

$$D_{n-1}^2 v_{n-1} = D_n^2 v_n = D_{n+1}^2 v_{n+1} \quad (11.24)$$

with  $n-1$ ,  $n$  and  $n+1$  successive drawing passes. In reality, because of wear in the drawing dies, the diameter of the wire after each pass is not constant in time.

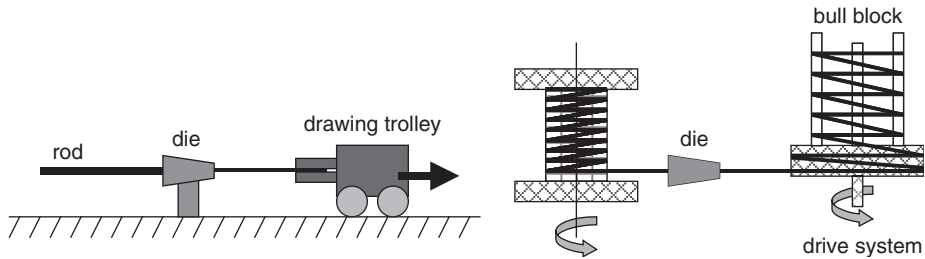


Figure 11.23. Draw bench (left) and single pass drawing equipment (right).

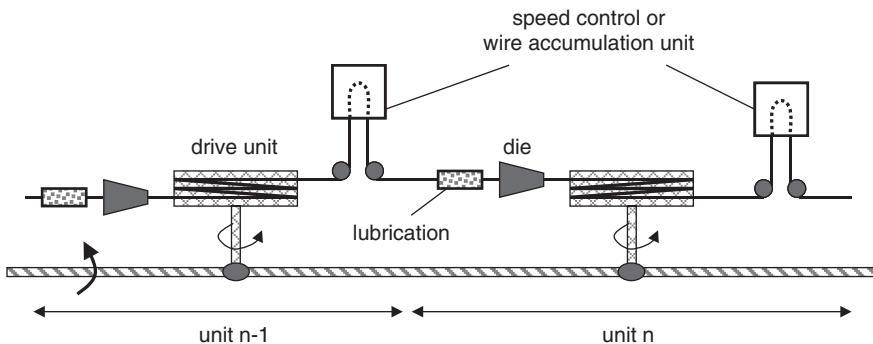


Figure 11.24. Continuous wire drawing machine of the “non-slip-type”.

Suppose that the diameter after pass ‘ $n$ ’ (Figure 11.24) increases to a value  $D'_n > D_n$ . When the rotation speed of drum ‘ $n$ ’ is kept constant, more material per unit time leaves the die ‘ $n$ ’ and hence the speed  $v_{n-1}$  of the wire in unit ‘ $n-1$ ’ will increase. This would cause a so-called ‘negative slip’ on drum ‘ $n-1$ ’: the speed of the wire becomes higher than the circumferential speed of the drum and this generates an extra tension in the wire. This situation cannot be tolerated because of an increased risk of wire breaks. In some installations, each drum is powered by an independent dc-motor and the speed of each motor is adapted to the actual speed of the wire by a tension arm, located between the drums. In other machines, several drums are driven by one single motor and the rotation speed of drum ‘ $n-1$ ’ cannot be changed independently from the others. In that case an ‘accumulation unit’ is placed after each drum. These accumulation units can temporarily provide the required extra volume of wire. When unit ‘ $n-1$ ’ is exhausted, all following drums are disconnected from the central shaft and the accumulator ‘ $n-1$ ’ is replenished. In these ‘non-slip-type’ machines, a dry lubricant is used. Continuous wire drawing machines for fine wires are usually of the ‘slip-type’ and operate with a wet lubricant. The rotation speed of the drums is initially regulated in such a way that the circumferential speed is higher than the speed of the wire. This ‘positive slip’ only causes some wear on the drum and it can absorb an increase in wire speed. When the speed of the wire becomes equal to the speed of the drum, the die in the following unit must be replaced.

### 11.4.3 Wire drawing dies

**11.4.3.1 Geometry.** A schematic of a classical wire drawing die is shown in Figure 11.25. The core of the die is made from a wear-resistant material and fits into a steel frame. The entrance angle  $\beta$  permits the lubricant to enter the die and

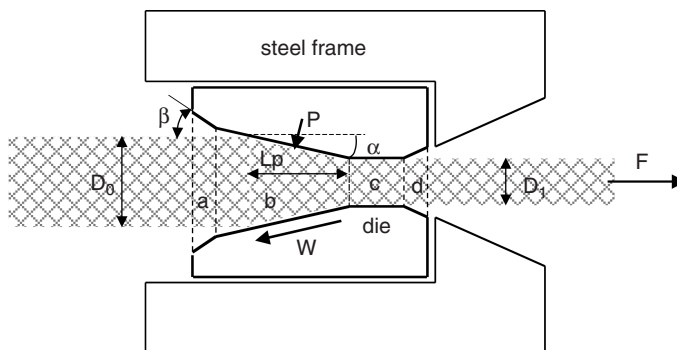


Figure 11.25. Geometry of a drawing die.

adhere to the wire. The deformation takes place in zone b. The deformation zone is characterized by two important parameters: the length  $L_p$  and the semi die angle  $\alpha$ . In most dies, the latter takes values from  $4^\circ$  to  $12^\circ$ . A shorter die reduces the friction, but increases the redundant deformation<sup>4</sup> (see Section 11.4.4). In this zone, the drawing force  $F$  is balanced by the horizontal components of the friction force  $W$  and the compressive force  $P = F \sin \alpha$ . In zone c, called the bearing surface, the final sizing of the exit diameter is performed. Finally, zone d is the exit zone.

The reduction  $r$  and the true strain  $\varepsilon$  in wire drawing are defined as:

$$r = \frac{D_0^2 - D_1^2}{D_0^2} = 1 - \left(\frac{D_1}{D_0}\right)^2 = 1 - \left(\frac{1}{\exp(\varepsilon)}\right) \quad (11.25)$$

$$\varepsilon = \ln \left(\frac{D_0}{D_1}\right)^2 = \ln \left[\frac{1}{1-r}\right] \quad (11.26)$$

The semi die angle  $\alpha$  and the reduction  $r$  can be combined in one parameter  $\Delta$ , which will be used to express the degree of redundant deformation (Hosford and Caddell [1983]):

$$\Delta = \frac{D_g}{L_p} = \sin \alpha \frac{[1 + (1-r)^{0.5}]^2}{r} \quad (11.27)$$

with  $D_g$  the mean wire diameter in the deformation zone and  $\alpha$  expressed in degrees.

**11.4.3.2 Die materials.** The inner core of a drawing die is fabricated from a wear-resistant material, usually cemented tungsten carbide or, for fine wires, from diamond. Hardened tool steel (HRC around 60) is only used for small series. Dies made from diamond are very expensive, but can outperform the cemented tungsten carbide dies by a factor of 10–200. When a die is worn out, it can be reworked and used again for thicker wires.

**11.4.3.3 Lubricants.** Friction between wire and die is not required in a drawing process. It causes wear of the die, possible damage to the wire surface and an increase in drawing force and temperature. Proper lubricants have to be used to minimize friction and in some cases to cool the wire.

<sup>4</sup>Internal distortion of the metal, not contributing to the dimensional change of the wire.

In dry drawing, the surface of the wire is coated with dry soap powder by passing the wire through a box filled with the lubricant and the wire is cooled, while it resides on the bull blocks or by cooling the die holder with water. High-strength materials are often coated with a softer material that acts as a lubricant, e.g. steel with brass.

In wet drawing, the die is completely immersed in oil or in an emulsion. In this case, the lubricant also serves as cooling medium. In general, the friction coefficient in wire drawing ranges from 0.01 to 0.1.

#### 11.4.4 The drawing force

Although wire drawing seems to be a rather simple deformation, a precise calculation of the drawing force is not an easy task. In the simplest approach, factors such as friction, redundant deformation and work hardening are neglected. If the effective strain is considered to be a pure uniaxial elongation [ $\varepsilon = \ln(D_0/D_1)^2$ ] and the material as ideal plastic (with constant flow stress  $\sigma_f$ ), the drawing force  $F$  can be estimated from:

$$F = \sigma_f \ln\left(\frac{D_0}{D_1}\right)^2 \frac{\pi D_1^2}{4} \quad \text{or} \quad \sigma_F = \sigma_f \ln\left(\frac{D_0}{D_1}\right)^2 = \sigma_f \varepsilon \quad (11.28)$$

This simple approximation predicts that for  $\varepsilon > 1$  ( $r > 63\%$ ) the tensile stress in the wire ( $\sigma_F$ ) would exceed the flow stress of the material which would lead to fracture.

Several attempts have been done to incorporate the influence of friction and redundant deformation. Two of the more elegant formulas have been proposed by Siebel *et al.* [1947] and by Hoffman and Sachs [1953].

The formula of Siebel starts from Eq. (11.28) and simply adds a friction and a redundant deformation term:

$$\sigma_F = \sigma_f \left[ \varepsilon + \left(\frac{\mu}{\alpha}\right)\varepsilon + \left(\frac{2}{3}\right)\alpha \right] \quad \text{with } \alpha \text{ in radials} \quad (11.29)$$

The formula of Hoffman and Sachs adds a friction term, and a ‘correction coefficient’  $\Phi$  which, according to Hosford and Caddell [1983] can be expressed as a function of the  $\Delta$ -factor (Formula 11.4):

$$\sigma_F = \Phi \sigma_f \varepsilon (1 + \mu \cot g\alpha) \quad \text{with } \Phi = \frac{\Delta}{6} + 1 \quad \text{and } \alpha \text{ in degrees} \quad (11.30)$$

In most cases, the drawing force can be estimated with these formulas with an accuracy of about 20%. Several other approaches have been proposed in the literature. The reader is referred to overviews of Wistreich [1958], Wright [1976] and Avitzur [1983].

Both formulae illustrate the influence of the semi die angle  $\alpha$ . A larger  $\alpha$  (shorter die) decreases the friction, but increases the redundant work. An optimal value for  $\alpha$ , minimizing the drawing force, can be calculated but in practice other criteria like die wear, cost and standardization may determine the choice of the angle  $\alpha$ .

The redundant deformation is a function of  $\alpha$  and the reduction, and hence of  $\Delta$ . For a complete homogeneous deformation,  $\Delta$  should in principle not exceed the value of one. But in many wire drawing operations  $\Delta$ -values up to 2 or 3 are tolerated.

Equations (11.29) and (11.30) can be adapted to take into account the strain hardening. The constant value of the flow stress ( $\sigma_f$ ) should be replaced by some appropriate hardening law, e.g.  $\sigma = k\epsilon^n$  or others (cf. Chapter 4).

In many wire drawing lines, the wire is not only subjected to a forward pulling force, but also to a 'back pull' or 'back tension', exerted by downstream capstans. The main effect of a back tension is to increase the drawing force and the risk of fracture, but with a decrease in die pressure and with possible reduction in friction (Wright [1999]).

#### Illustrative problem

*A pearlitic wire should be drawn from 5 mm till 2.6 mm diameter, using a wire drawing machine with a maximal pulling force of 15.5 kN. The desired reduction scheme is: 5 mm  $\rightarrow$  4 mm  $\rightarrow$  3 mm  $\rightarrow$  2.6 mm. Three types of dies are available with  $\alpha = 4^\circ$ ,  $\alpha = 8^\circ$  and  $\alpha = 16^\circ$ . The friction coefficient is always 0.05. Calculate for each pass and each die angle the pulling force. Choose for each pass the best (available) die and discuss your answer.*

The pulling force is the product of the pulling stress and the wire cross-section after the die. The pulling stress can be estimated using Eqs. (11.29) or (11.30). Since pearlite shows a large work hardening during drawing (cf. next paragraph), an appropriate work hardening law should be used to estimate the actual material flow stress after each die. The results are shown in Table 11.5. In the first drawing pass, the die with a semi die angle of  $4^\circ$  leads to a pulling force that exceeds the capacity of the drawing machine. The dies with angles of  $8^\circ$  and  $16^\circ$  can both be used, but the die of  $8^\circ$  leads to a more homogeneous deformation (lower  $\Delta$ -factor) and a slightly lower pulling force.

In the second pass, the pulling force is lower, but another problem occurs for the die of  $4^\circ$ : although the flow stress of the wire has considerably increased, the pulling stress in the wire is higher than the flow stress, which would lead to deformation and fracture of the wire after the second die. The two other dies can in principle be

**Table 11.5.** Calculation of the pulling force during wire drawing.

		Equations						Limitations		
(11.29): $\sigma_F = \sigma_f [\varepsilon + (\mu/\alpha)\varepsilon + (2/3)\alpha]$ with $\alpha$ in radians								Pulling force < 15.5 kN		
(11.30): $\sigma_F = \Phi\sigma_f\varepsilon(1 + \mu \cot g\alpha)$ with $\Phi = \Delta/6 + 1$ and $\alpha$ in degrees								$\sigma_F < \sigma_f$		
(11.27): $\Delta = \sin \alpha [1 + (1-r)^{0.5}]^2/r$								$\Delta < 2$ to 3		
Pearlite: $\sigma_f = 72 + 1304 \exp(\varepsilon/4)$ (MPa)										
		5→4 mm			4→3 mm			3→2.6 mm		
$\alpha$ (°)		4	8	16	4	8	16	4	8	16
$r$ (%)			36.0			43.8			24.9	
$\varepsilon$			0.446			0.575			0.286	
$\Delta$		0.63	1.25	2.48	0.49	0.97	1.93	0.98	1.95	3.86
$\phi$		1.10	1.21	1.41	1.08	1.16	1.32	1.16	1.32	1.64
$\sigma_F$ (11.29) (MPa)		1243	1070	1090	1815	1535	1518	1011	906	985
$\sigma_F$ (11.30) (MPa)		1294	1119	1133	1873	1592	1568	1073	967	1038
$\sigma$ flow (MPa)			1529			1755			1880	
Pulling force (kN) (11.29)		15.6	13.4	13.7	12.8	10.8	10.7	5.4	4.8	5.2
Pulling force (kN) (11.30)		16.3	14.1	14.2	13.2	11.3	11.1	5.7	5.1	5.5

used, but the die of 16° could be preferred because it requires the lowest pulling stress, although it gives a somewhat less homogeneous deformation compared to the 8° die. In reality, most production lines operate with a pulling stress of maximum 60–70% of the flow stress of the material, so an adaptation of the proposed pass schedule is advisable. In the third pass, the pulling stresses and forces are lower, because of the smaller reduction, but the homogeneity of the deformation in the 16° die is questionable. In this step, a die of 4° seems to be the best choice.

#### 11.4.5 Some important metallurgical factors

During wire drawing of fcc metals, classical strain hardening of the wire takes place. This hardening is related to the substructural developments, as discussed in Chapter 4. But during drawing of bcc materials, such as low-carbon steel, some unexpected hardening behaviour can be observed. After a parabolic transition, the stress increases linearly with strain (Langford and Cohen [1969]). Strange enough, this behaviour is not observed during a torsion test carried out on the same material (Gil Sevillano *et al.* [1980]).

During wire drawing, grains should elongate in the drawing direction and contract in all directions perpendicular to the wire axis. In reality this is observed in fcc materials, but in bcc materials, such as low-carbon and pearlitic steel, tungsten and niobium, a peculiar effect occurs (Peck and Thomas [1961], Hosford [1964]).

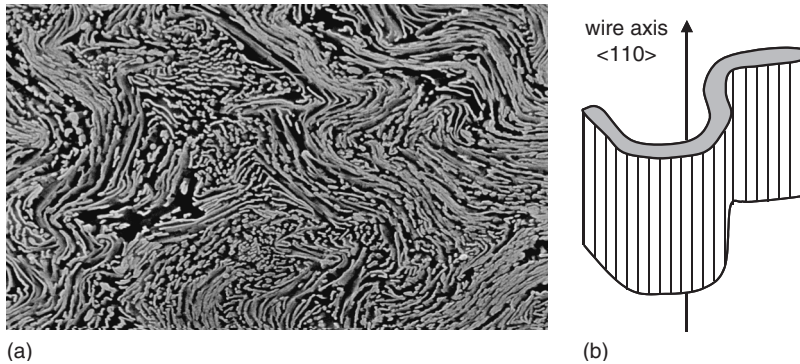


**Figure 11.26.** Illustration of the curling effect in pearlitic steel (a) view parallel with the wire axis; (b) scheme of a cementite lamella after wire drawing.

The grains do not only elongate in the direction of the wire axis, but also get a kind of folding, visualized in Figure 11.26. This is called the *curling effect*. In order to fold the grains over each other, some extra dislocations have to be generated. These geometrically necessary dislocations (GNBs, see Chapter 4) all have the same sign and are not annihilated. As a result, the mean cell size never reaches an equilibrium as in the case of Cu or Al, but continuously decreases and the flow stress linearly increases. In a torsion test, this curling effect does not occur and hence the flow stress and cell size reach an equilibrium after a certain strain.

The curling effect is a direct consequence of the crystallographic texture of bcc metals after wire drawing. In cold-drawn wires of bcc materials, many grains have an  $\langle 110 \rangle$  direction more or less parallel with the wire axis. This is called ‘a  $\langle 110 \rangle$  fibre texture’ (cf. Chapter 8). To understand the curling effect, let us first consider a single crystal with a  $[011]$  direction parallel with the wire axis (Figure 11.27). The dominant slip directions are  $[111]$  and  $[-111]$  and also  $[-1-11]$  and  $[1-11]$ . Only the first two contribute to an elongation in the  $z$ -direction. They also provoke a contraction along the  $[100]$  axis but no length change along  $[0-11]$  (plane strain). In order to realize an axisymmetric deformation (as imposed by the drawing die), the  $[-1-11]$  and  $[1-11]$  slip directions should also be activated and generate a contraction along  $[0-11]$  and an elongation along  $[100]$ . It can however be shown (Hosford [1964]) that a plane strain deformation requires less stress than an axisymmetric deformation.

This means that in the real wire with a strong  $\langle 110 \rangle$  texture, every grain will show a strong tendency to undergo a plane strain deformation, with the contraction axis perpendicular to the wire axis. Of course, in this way, the cohesion between the grains would be lost; and moreover, the die forces a global (macroscopic)

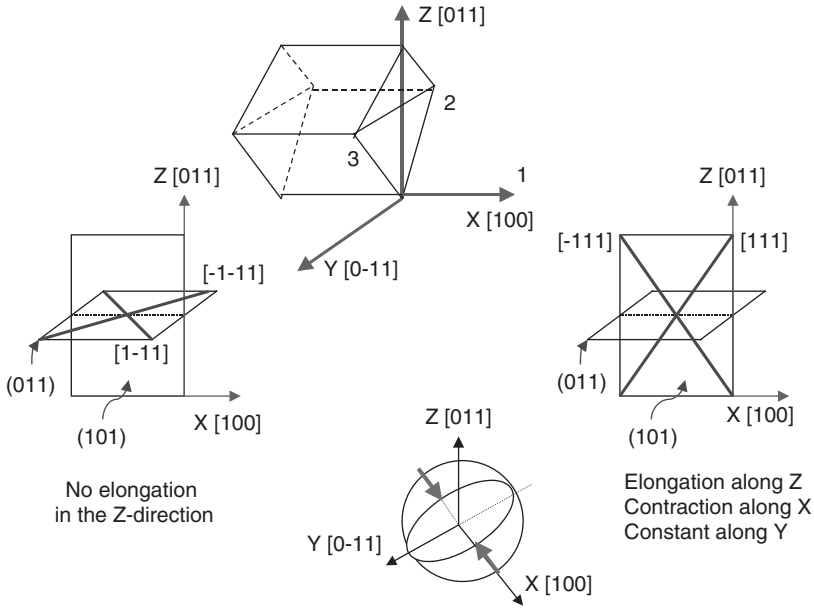


**Figure 11.27.** Illustration of the  $\langle 111 \rangle$  slip directions in a bcc lattice with the  $[011]$  direction parallel to the wire axis.

axisymmetric deformation. To comply with that, the grains have to curl over each other as seen in Figure 11.26.

In pearlitic steel, but also in other lamellar or fibrous materials like Fe–Al (Wahl and Wassermann [1970]), an exponentially increasing flow curve is recorded during wire drawing. During drawing of pearlitic steel, the ferrite and cementite lamellae are gradually re-oriented and get more and more parallel with the wire axis (a ‘morphological texture’). Owing to the reduction of the wire diameter, the cementite lamellae are pushed together and the distance between them diminishes (Chapter 15.5). In fine pearlite, the spacing between two lamellae is smaller than the ‘natural’ size of the cells in the substructure. With further deformation, the mean cell size ‘ $d$ ’ will artificially be reduced with increased deformation, because the spacing between the lamellae is reduced. To a first approximation, it can be assumed that the reduction in cell size is proportional to the macroscopic reduction in diameter ‘ $D$ ’:

$$\varepsilon = \ln \left( \frac{D_0^2}{D^2} \right) = \ln \left( \frac{d_0^2}{d^2} \right) \quad (11.31)$$

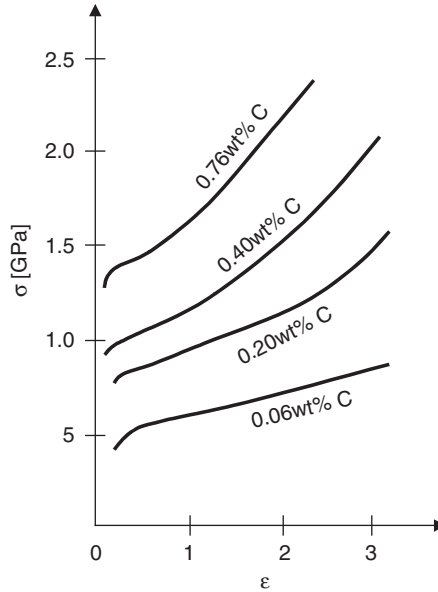


**Figure 11.28.** Stress strain curves during wire drawing of steel. After Gil Sevillano *et al.* [1980].

Substitution in the Hall–Petch relation  $\sigma = \sigma_0 + kd^{-0.5}$  gives:

$$\sigma = \sigma_0 + k' \exp\left(\frac{\varepsilon}{4}\right) \quad (11.32)$$

This expression is in good agreement with an empirical relation (Gil Sevillano [1974]):

$$\sigma = 72 + 1304 \exp\left(\frac{\varepsilon}{4}\right) (\text{MPa}) \quad (11.33)$$

Figure 11.28 shows some stress–strain curves for steel with different carbon contents during wire drawing. The upper curve shows the exponential hardening obtained during wire drawing of lamellar pearlite. The lower curve illustrates the linear strengthening of low-carbon steel. The other curves can be described by a rule of mixture.

#### 11.4.6 Drawing of metal fibres

Ultrafine wires ( $< 50 \mu\text{m}$ ) and fibres have interesting applications such as filters, anti-static textiles, magnetic shielding, medical products, bonding wires in

microelectronics, etc. Metal fibres can be produced in many ways such as conventional drawing, bundle drawing, shaving and melt spinning.

Most ductile metals can be drawn into ultrafine wire by pulling them through thinner and thinner dies. In most cases, drawing conditions have to be selected with care: low drawing speeds, low per pass reductions and diamond dies with low approach angles are recommended. Unfortunately, production costs are very high and increase exponentially as the diameter decreases.

An alternative technique to produce fine fibres is the so-called 'bundle drawing'. Instead of drawing a single wire, several (in some cases up to a few thousand) are bundled, tightly packed into a tube and drawn simultaneously. The challenge is to separate the individual wires with a suitable material prior to bundling. This separating material must be easily removable after drawing, e.g. by leaching. Stainless steel fibres can be drawn to a diameter of  $1\ \mu\text{m}$  with this method. Most metals can be drawn up to  $8\text{--}12\ \mu\text{m}$  in diameter and even brittle superconductor alloys like NbTi and Nb<sub>3</sub>Sn are processed in this way (ASM Handbook [1988]).

Another alternative is 'coil shaving'. The material is first rolled into foil, which is coiled. A sort of big razor blade cuts thin slices of material from the side of the coil. A fibre with rectangular cross-section, one dimension being the thickness of the foil (typically  $25\text{--}100\ \mu\text{m}$ ) is obtained.

Ribbons of glassy metals, typically  $20\text{--}60\ \mu\text{m}$  thick, can be obtained by melt spinning. A jet of molten metal is poured onto a cool, fast rotating wheel. The solidification is very fast and amorphous or semi-crystalline materials can be obtained.

## LITERATURE

Altan T., Oh S. and Gegel H.L., "Metal Forming: Fundamentals and Applications", ASM, Ohio (1983).

## 11.5. FORGING

### 11.5.1 Introduction

Forging is the oldest of the metal forming processes. Archaeological evidence of forging or simple hammering of native gold, silver and copper dates back to 8000–5000 BC (Singer *et al.* [1954], ASM [1988]). The succeeding Bronze Age reduced, albeit temporarily, the dependence on forging; as cast bronze tools and weapons dominated. The beginning of the iron age around 800 BC, however, brought the importance of forging to new heights (Schey [1970]). The blacksmith's trade became an art of strategic importance. The subject evolved slowly over centuries – cold forging of roman coins (Singer *et al.* [1954]), forging of

Damascus sword (Naujoks and Fabel [1953]), introduction of tilt hammers around 13th century (ASM [1988]) to interchangeable forging dies for rifle parts in 18th century (Schey [1970]). Today, the technology of forging has come a long way – from being a blacksmith’s art to the relative maturity of being called a technology. In the subsequent sub-sections, different aspects of today’s forging technology are discussed.

Table 11.6 provides a broad classification of the forging processes for bulk metallic materials. A more detailed classification can be obtained in forging handbooks (Altan *et al.* [1973], Metalforming [1982], ASM [1988]). Such detailed classifications are, however, based on minor modifications in process/equipment/die-tool/applicability. It is also to be noted that the forging of finished components often involves several steps of forming or TMP (Metalforming [1982]) as shown in Figure 11.29.

### 11.5.2 Forging equipment

As shown in Table 11.7, the basic forging equipment can be classified as hammers and presses. The table provides only a ‘snap shot’ of forging equipment, leaving

**Table 11.6.** Broad classification of forging processes for bulk metallic materials. The specialized forging techniques like radial forging, isothermal forging, etc. (ASM [1988]) are covered in the broad categories. Techniques like roll forging fall in the preview of both forging and rolling. The processes may involve cold or hot deformation (in special cases with isothermal condition) with intricacies in die and equipment design. The brief schematics of the processes are given in Figure 11.30.

Forging process	Brief description	Applicability
Open-die forging	Flat or curved dies, respectively attached to hammer or press and anvil	Large jobs, limited quantity, difficult to forge material
Closed-die forging	The metal is shaped between the cavities of the two dies – the finished product carries the ‘impression’ of die shape or cavity. Excess material is released through a ‘flash’	More productive than open die forging and capable of making complicated shapes Forgability of the material and die design are important
Rotary swaging	Reduction in cross-sectional area by repeated radial blows from two or more dies	Tube manufacturing
Rotary forging	Two die process, deformation being localized to a small part of the workpiece in a continuous manner	Substitute for conventional forging, typically applied to symmetric parts

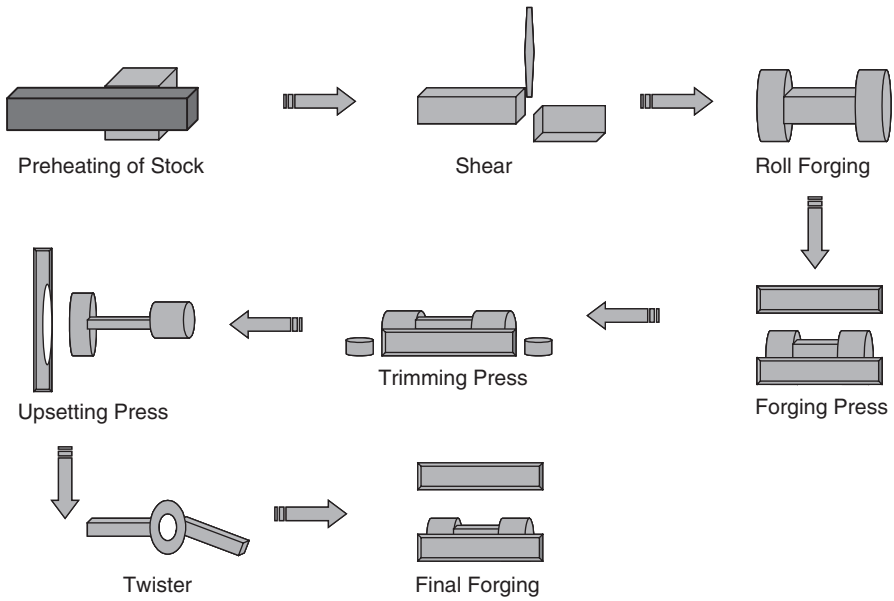


**Figure 11.29.** Schematic of the different stages involved in the forging of a crankshaft – intermediate annealing is common. This is a simplified picture of the actual process.

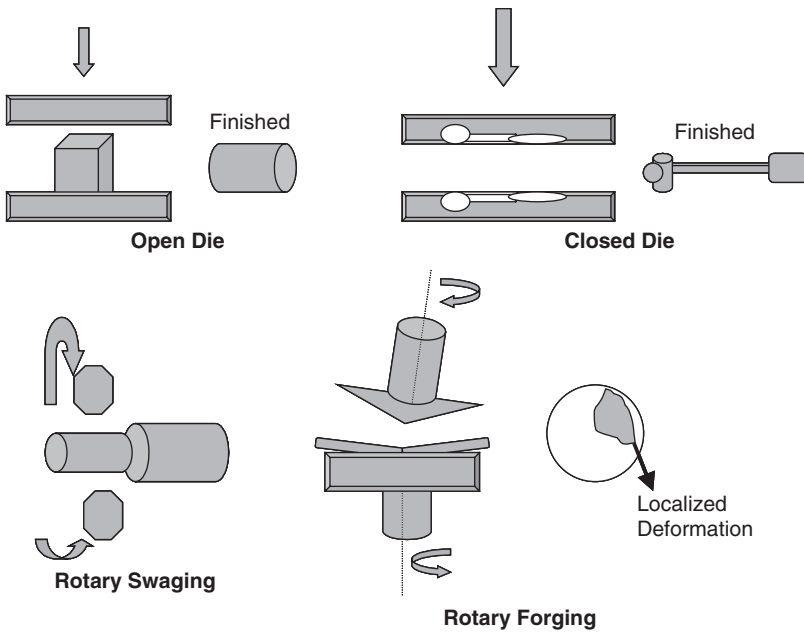


**Figure 11.30.** Schematics of the forging processes, as in Table 11.6.

**Table 11.7.** Classification of forging equipment.

Forging equipment		Description	Remarks
Hammers	Gravity drop	The lifted hammer is allowed to fall under gravity. Lift mechanisms may differ, but the energy of the blow is largely restricted by the hammer weight	‘Energy restricted’ Typically, available range of ram weight, blow energy, impact speed and number of blows per unit time are <i>lower</i> in gravity drop
	Power drop	The hammer blow is accelerated by air/steam/hydraulic pressure	
Presses	Mechanical	Rotational motion of eccentric shaft is translated to linear motion by appropriate mechanism(s)	‘Stroke restricted’ Better than hammers in all aspects except for cost and the fact that the energy cannot be varied – and hence are not suited for preliminary forging operations
	Screw	Rotational motion of flywheel is translated to linear motion by threaded screw	‘Energy restricted’ More energy per stroke than mechanical presses, but normally the full force is restricted near the centre of the workpiece
	Hydraulic	Direct or accumulator driven	‘Force restricted’ Other than high cost, these are typically of slower action. But there are serious advantages in terms of control/optimization of operation and die/tool design

aside detailed information on design, performance and applicability (Naujoks and Fabel [1953], Altan *et al.* [1973], Metalforming [1982], ASM [1988]). For example, high energy rate forging equipments are high-speed hammers with interesting design innovations, while painstaking design aspects are involved in forging presses (Altan *et al.* [1973], ASM [1988], Ishinaga [1997]).

### 11.5.3 Forging dies

Dies used in open die forging are restricted to flat dies, swage dies and V dies – the latter two respectively have a semi-circular and V shape cut at the centre of the dies (both upper and lower) to avoid bulging (and for faster operations with easier material flow, though die changes are essential for different sizes). Change-over from open die to closed die forging is required based on die-forging dimensions.

Thumb rules are often cited (Metalforming [1982], Ghosh and Malik [1985]) as first step towards forging die design:

- $L < 3d$  for open die forging
- $D < 1.5d$  and  $l < d$  for closed die forging

$L$  and  $l$  and  $D$  and  $d$ , for open and closed die forging, are shown in Figure 11.31. It is to be noted that  $L$  and  $l$  have similar implications – respectively representing unsupported length in open and in closed die forging. Actual die design involves considerations of many more parameters, especially valid for closed die forging (dies may have single or multiple cavities and die design often calls for multistage dies), to meet both production and materials aspects. For example, closed die design is expected to provide sufficient friction so that enough pressure is built up to fill all the cavities. The gutter and flash, are often an integral part of such design – excess material leaves the die through the gutter and gets ‘collected’ in the flash (see Figure 11.31b). Table 11.8 outlines some of the standard terminologies associated with die design of closed die forging; for more details, the reader may refer standard forging handbooks (Altan *et al.* [1973], Metalforming [1982], ASM [1988], Lapovok [1998], Doege and Bohnsack [2000], Groenbaek and Birker [2000]).

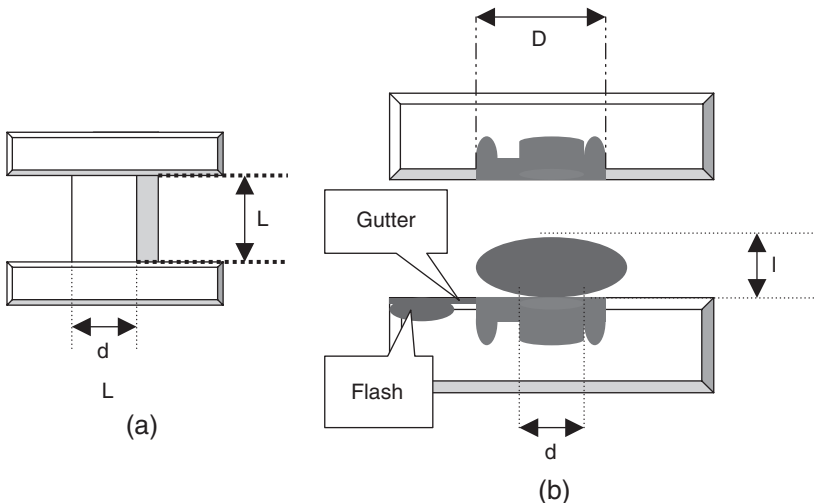


**Figure 11.31.** Schematics of (a) open and (b) closed die forging. Relative values of  $L$  &  $l$  and  $D$  &  $d$  provide the basic outline for die design. Closed die forging also needs considerations of several other aspects – e.g. gutter-flash, parting line, draft, etc.

**Table 11.8.** Standard terminologies associated with closed die forging dies and die design.

Nomenclature	Brief description
Fullers, edgers, rollers, flatteners, benders, splitters, blockers, finishers	Respectively to reduce cross-section area, to redistribute for heavier sections, to round the stock, to flatten, to bend, to make fork-type forgings, to prepare for finishers and to provide final overall shapes
Parting/flash line	Plane dividing upper and lower die
Flash land and gutter	Excess material flows through gutter to flash land
Webs and ribs	Thin sections parallel and perpendicular to parting line
Fillet and corner radii	May limit metal flow and increase stresses on the die surface
Draft	Draft or taper is used for easy removal of the forgings
Die insert	Used for economy and dimensional tolerance – plug and full types
Locks	For non-flat parting line, locations for dies to mesh/lock
Mismatch	Mismatch between dies can be a serious problem, but optimum die mismatch can also be used to produce non-symmetrical parts (e.g. crank shafts)

#### 11.5.4 Friction and lubrication in forging

Even in the simplest form of forging, pressure–temperature–velocity combinations change continuously – making formulation of any generalized velocity–stress–strain–friction distributions rather difficult. In open die upsetting, one of the simplest forms of forging, friction may change from sliding to sticking (or a combinations of the two), depending on the forging parameters and material aspects (Schey [1970]). For closed die forging, the frictional behaviour is more complicated and analytical solutions may exist only for the simplest geometries (Schey [1970], Boisse *et al.* [2003]). Though the exact historical time frame for lubricant use in forging cannot be pin-pointed (Schey [1970]); the use of appropriate lubricants – as in Table 11.9 – for frictional and other considerations – as in Table 11.10 – is common in today’s forging technology.

#### 11.5.5 Forging optimization

Forging force can be calculated as  $\sigma AC$ , where  $\sigma$ , A and C are respectively stress, cross-sectional and correction factor. C typically varies between 4 and 9 for closed die forging, dependent on the complexity of the workpiece. It is also difficult to find a value for  $\sigma$ , as strain, strain rate, strain path and temperature distribution can be very inhomogeneous and only an approximate ‘mean’ value can be used or a point-to-point bookkeeping must be done – which, in turn, requires the use of FEM.

**Table 11.9.** Lubricants used in cold and hot Forging (Schey [1970], Möller [1996]).

Cold	Mineral oils, animal oils, vegetable fats, soaps, waxes, graphite in water/oil, etc.
Hot	For high-temperature forging graphite in a suitable medium is recommended (Möller [1996]). Below 400°C, molybdenum-di-sulphide has better frictional response. Also used are sawdust, mica, grease, asbestos, glasses, organic polymers, phosphates, oxides, bromides, fluorides, carbonates, etc. (Schey [1970])

**Table 11.10.** Factors, and their implications, determining the use of lubricants in forging.

Factors	Implications
Frictional issues	To reduce sliding friction between die and forging, to reduce the forging load and provide a better die filling (however, high friction in flash gutter is needed for die filling). Lubricants act as a parting agent by reducing sticking friction and local welding and providing better die life and good surface quality of the product
Insulating properties	To reduce heat loss from workpiece and to minimize temperature fluctuations on the die surface – better forgability
Balanced gas pressure	Primarily used for quick release of forging from die cavity, but can also be used to ‘calibrate’ lubricant wettability.
Surface wettability	Uniform surface wettability – lack of lubricant may lead to sticking, while excess of lubricant may cause partial die filling
Non-abrasive	To prevent die surface wear
Residues	May accumulate and lead to forging defects and environmental issues

Typically the optimization of forging parameters, including estimation of forging loads, are obtained by:

- *Analytical solutions:* The complexities of the forging processes may vary enormously – from the simple open die upsettings to the complex precision forgings offering near net shapes (ASM [1988]). Straight analytical approach to forging optimizations are possible only for the *simplest* of the cases. For example, the maximum blow force of a open die forging hammer ( $p_{MAX}$ ) can be approximated by Li *et al.* [1997] as:

$$p_{MAX} \Rightarrow \sqrt{\frac{C_1 M_1 (M_1 + M_2)}{(M_2 + 2M_1)}} (v_1^2 - v_x^2) \quad (11.34)$$

where  $M_1$  and  $M_2$  are the respective masses of ram and anvil,  $v_1$  and  $v_x$  are the blow velocity (ram velocity at the moment of ‘contact’) of the ram / hammer and

the downward velocity of ram and anvil, respectively and  $C_1$  is stiffness-related (given as  $2K_0rE/(1-\nu^2)$ ;  $r$  = maximum radius of the workpiece,  $E$  and  $\nu$  are the respective elastic modulus and Poisson's ratio for the die material and  $K_0$  is a constant).

- *Constitutive equations*: Use of constitutive equations in forging optimization is common (ASM [1988]), but these are typically applicable for simpler forgings.
- *Physical modelling*: Easily deformable materials like plasticine and wax (and even aluminium (ASM [1988])) are used (Vazquez and Altan [2000]) to 'approximate' material flow, friction conditions, etc. and are often used as an effective optimization tool. Such simulations are easy and inexpensive. In the case of aluminium, grids can be made to study the deformation behaviour quite effectively).
- *Computer modelling*: Use of computer modelling (both finite element and finite volume based) in forging optimization is a reality of today's technology – a list of developers of such commercial optimization/simulation codes is given in Table 11.11 (more details on semi-commercial and academic packages can be obtained elsewhere (ASM [1988], Bramley and Mynors [2000])). Such programs, though not magic boxes to solve all forging related problems (Like any other computer program, forging optimizations depend totally on the input data, material database and the physics (empirical/constitutive/analytical relationships) behind the codes.), are now used routinely.
- *Deformation modelling*: Actual forging parameters can be simulated in a deformation or forging simulator – a topic discussed in more detail in Chapter 13. The material behaviour can be optimized through forgability tests or deformation maps (the basics of deformation maps are covered in Chapter 6).

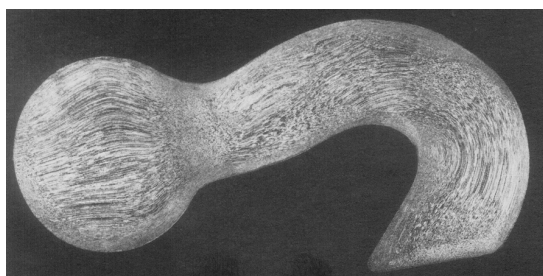
**Table 11.11.** List of major developers for forging simulation/optimization packages.

Primary code	Developer
Caps – Finel	CPM Gesellschaft für Computeranwendung Prozeß- und Materialtechnik mbH, Kaiserstr.100, D-52134 Herzogenrath; <a href="http://www.schraubenverband.de">http://www.schraubenverband.de</a>
Deform	Scientific forming technologies corporation, 5038 Reed Road, Columbus, Ohio 46220-2514, USA; <a href="http://www.deform.com">http://www.deform.com</a>
Forge 2/3	Transvalor S.A., Parc de Haute Technologie, Sophia Antipolis 694, av. du Dr. Maurice Donat 06255 Mougins Cedex, France; <a href="http://www.transvalor.com">http://www.transvalor.com</a>
MARC Superform	MSC Software Corporation, 2 MacArthur Place, Santa Ana, CA 92707, USA; <a href="http://www.marc.com">http://www.marc.com</a>
Qform	Quantor Ltd., PO Box 39, 117049 Moscow, Russia; <a href="http://www.quantor.com">http://www.quantor.com</a>

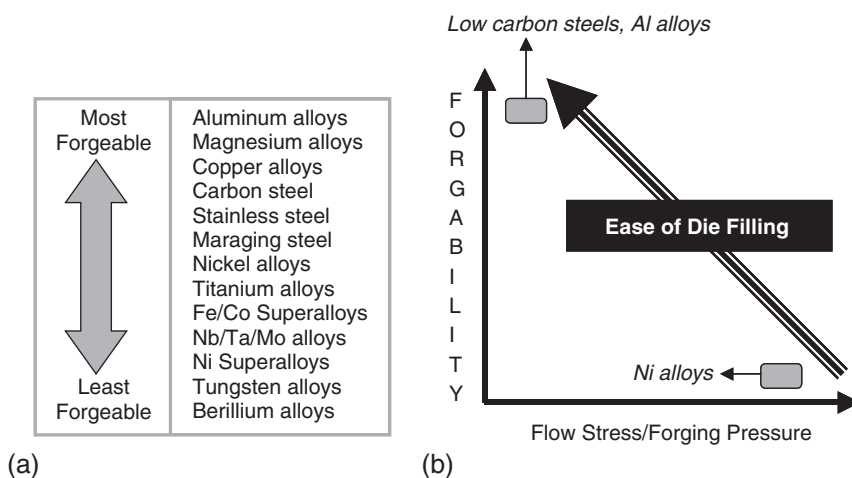
### 11.5.6 Forgability

Figure 11.32 shows the flow lines typical of forgings. The ease of development of such flow lines, representing plastic flow during forging, naturally depends on material and forging parameters. Together they determine the forgability of a material. The main forging parameters are the stress–strain relations, changes in strain path, temperature, strain rate, friction and other constraints. To evaluate the material under specific deformation parameters, tests are conducted which may involve simple forgability tests or more complex tests and elaborate deformation maps.

General forgability of different metals and their alloys is classed in Figure 11.33a. For closed die forging, however, the ease of die filling depends on a combination of



**Figure 11.32.** Macroetched structure of a hot forged hook – etchant hot aqueous 50% HCl. Courtesy of ASM [1988] (copyright (2007) with permission from ASM).



**Figure 11.33.** (a) Relative forgability for different metals and alloys. This information can be directly used for open die forgings. (b) Ease of die filling as a function of relative forgability and flow stress/forging pressure – applicable to closed die forging.

inherent forgability and flow stress/forging pressure (see Figure 11.33b). Table 11.12 and Figure 11.34 summarize the common forgability tests. After the tests, specimen observations (on cracking, metallography, etc.) are typically used to establish forgability. More complex tests are also designed to study flow localizations and complex forging practices.

**Table 11.12.** Common forgability tests. These and more complex tests are typically used to establish crack initiation through flow localization, forgability at a given forging condition and also to study structural changes. Schematics of the forgability tests/specimen geometries are given in Figure 11.34.

Forgability test	Brief description
Upsetting	Similar to a compression test. Simplest, but non-isothermal upsetting can be effective to characterize flow localizations through die chilling
Wedge forming	Wedge-shaped 'representative' sample tested between parallel/flat dies – to establish forgability at different reductions and forging conditions
Side pressing	Compressing a cylindrical bar perpendicular to the axis of the cylinder; normally performed between flat/parallel dies for un-constrained deformation – but minor modifications in die design can be used to test constrained deformation. Effective to study surface related cracking
Notched bar	Bars with notches perpendicular to loading direction – notches are used to initiate cracking through stress concentration (approaching actual forging practices). Effective in differentiating forgabilities, which otherwise may indicate marginal differences
Truncated cone	Indentation of a cylindrical specimen by a conical tool – effective in studying initiation of surface/sub-surface cracking and to optimize cold forgability against surface flaws

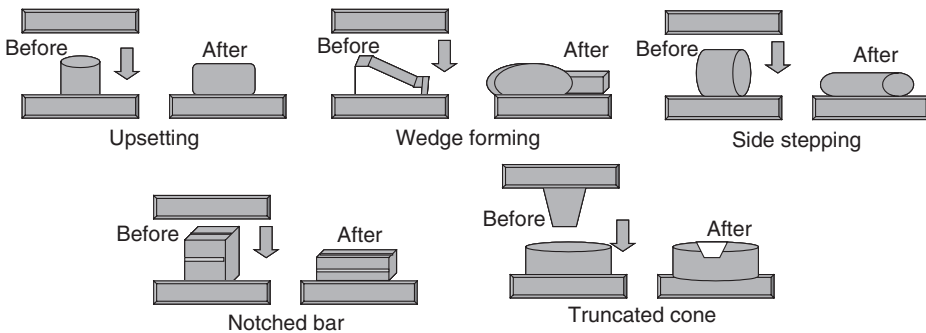


**Figure 11.34.** Schematic of the specimens in common forgability tests. The specimen dimensions are often standardized based on industrial standards and also on the structural heterogeneity present before the forgability tests. More details on the tests are given in Table 11.12.

## LITERATURE

- Altan T., Boulger F.W., Becker J.R., Akgerman N. and Henning H.J., “Forging Equipment, Materials and Practices”, Metals and Ceramics Information Centre – Department of Defence Information Analysis Centre, USA (1973).
- Metals Handbook “Forming and Forging”, 9th Edition vol. 14, ASM, Ohio, USA (1988).
- Schey J.S., “Metal Deformation Processes: Friction and Lubrication”, MerceL Dekker Inc., New York (1970).

## 11.6. PILGERING

## 11.6.1 Introduction

Tubes and pipes do find wide ranging applications in the present technological society (Chapters 15.3. and 16.1. – pipe-line steel and Zr clads in nuclear reactors). Other than the welded tubes (any comparison of seamless vs. welded tube standards (e.g. DIN 2448 vs. DIN 2558) would clearly show that welded tubes are preferred for small wall thicknesses and large outside diameters), seamless tubes can also be ‘formed’. Seamless ‘tube-forming’ typically avail several technologies – pierce and pilger rolling, plug rolling, tube extrusion, pierce and draw, assel rolling, etc. In addition to these primary processes, ‘forming’ the final tube may also require, both from dimensional tolerances and appropriate structure–property correlation, downstream processes like cold drawing and cold pilgering. Intermediate operations like de-scaling (before and after hot forming, typically using water jets), pickling (before cold working), calibration (to provide a small taper before the piercing operation), elongation (1 to 2 times increase in original length along with correction for concentricity), reeling (to loosen the hollows from the mandrel by using hyperbolically profiled rollers), etc. are also used as and if required.

This chapter does not attempt to overview all the processes of seamless tube manufacturing, but rather *concentrates on the topic of pilgering*. It all started

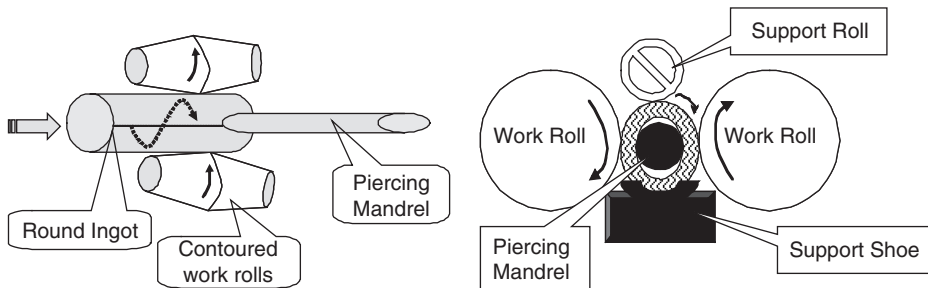


Figure 11.35. Schematics of pierce rolling at two cross-sections.

(Source: <http://www.mannesmann-archiv.de/englisch/faq>) with innovations by the Mannesmann brothers at the end of 19th century. ‘Pierce rolling’, was patented in 1886 (see Figure 11.35). A pierce rolling mill consists of two contoured (i.e. two halves of the rolls are at shallow angles – as shown in Figure 11.35) work rolls, driven at the same direction. These work rolls are typically placed at an angle of 3–6° around the hot billet. The roll gap is closed respectively from top and bottom by a support roll (non-driven) and support shoe. At the centre of the roll gap, the piercing point is held by the mandrel via an external thrust block. Typically, the hot billet is thrust and bitten by the tapered inlet section of the rolls. The helical movement of the rolls leads to a certain degree of ‘locking’ of the billet, while spiral motion of the billet over the piercing mandrel produces the thick-walled hollow shell – mother tubes or hollows.

For further processing of the mother tubes or hollows, Max Mannesmann subsequently (early 1890) developed the pilgering or pilger rolling process. In this process, discussed in more details later, a pair of grooved rolls and a moving plug or mandrel are used to reduce both the wall thickness and the diameter of the mother tubes. The repeated back and forth movement of the tube, during the rolling passes, was related to the dance (three steps forward and one back) of the ‘pilger’ (German for pilgrims) during Echternach dancing procession. The process was thus named as ‘pilger rolling’ or ‘pilgering’. The Mannesmann’s pilgering was a hot working process. Subsequent developments in North America by Neubert during late 1920 (Randall and Prieur [1967]), formed much of the basis of the present cold pilgering process. The reasons that pilgering is often employed over more conventional cold drawing are summarized in Table 11.13. As described in the table, typical

**Table 11.13.** Comparison between cold drawing and cold pilgering.

The issue	Cold drawing	Cold pilgering
The process	Hot-formed hollows are pointed, pickled and surface treated for cold drawing. The process involves drawing the hollows through reducing dies, usually supported by a plug or mandrel	Hot-formed hollows are pickled and then cold pilgered. The process involves repeated rolling through grooved conical shaped rolls and over a moving mandrel
After drawing/pilgering, finished tubes are subjected to cutting, degreasing, heat treatment (if required) and straightening operations		
The product	Close-dimensional tolerances are possible, but maximum reductions, reduction in wall thickness, are often limited	Close-dimensional tolerances, very high reductions and reductions in both wall thickness and tube diameter are possible. Superior surface finish and better metal lurgical control are possible

advantages involve reduced processing stages, superior product quality and excellent formability (i.e. high reductions are possible without intermediate annealing).

### 11.6.2 Pilgering equipment and process

Figure 11.36a provides a schematic of the basic equipment of cold pilgering. A pilger stand has typically two rolls (the rolls are referred sometimes as dies – a reference linked to the forging action associated with the pilgering process) with a tapered

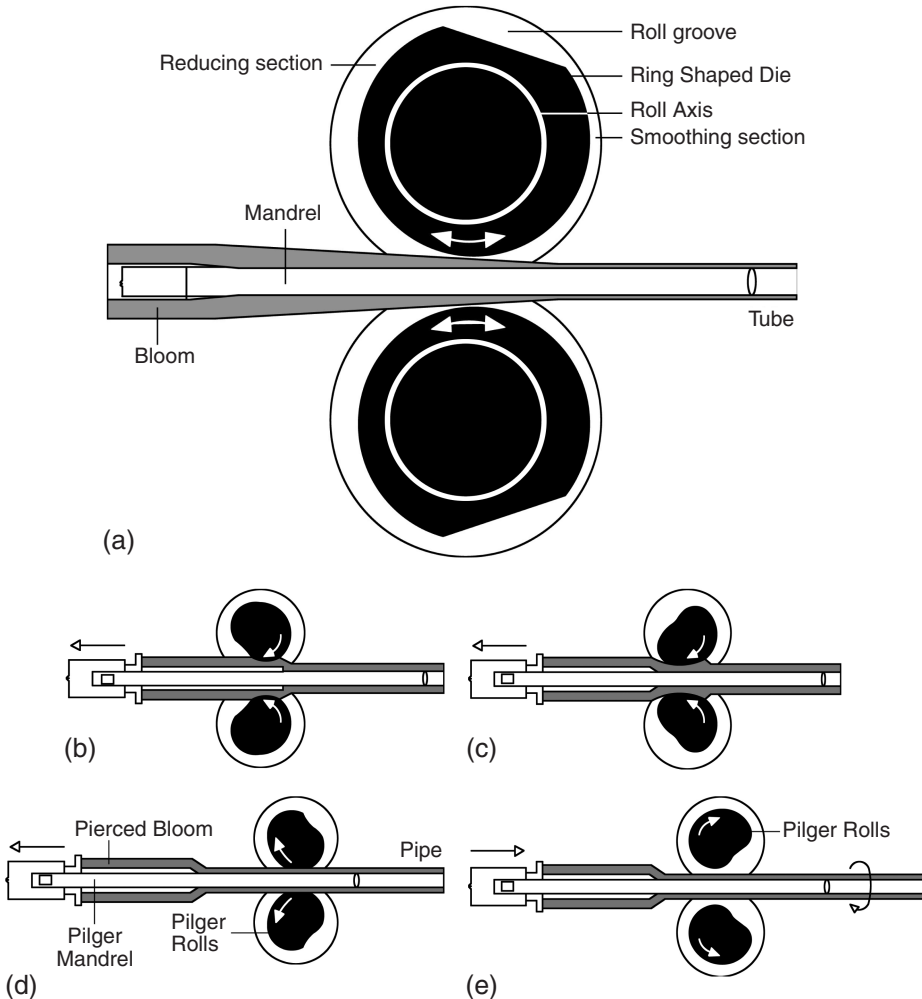


**Figure 11.36.** (a) Schematic of pilgering equipment. (b)–(e) different stages of pilgering. (b) start of rolling or the 'bite', (c) forging or pilgering, (d) polishing, (e) advancing or feed. After <http://mannesmann-dmv.de/en/products-services/production/cold-pilgering-and-cold-drawing/>

groove around their circumferences. Mother hollow or tubes are rolled *repeatedly* over an axisymmetric mandrel. Reduction of tube diameter can be obtained through a tapered mandrel, while grooved rolls enforce reduction in wall thickness. The basic pilgering operation is explained schematically in Figures 11.36b–e. Mother hollow or tube is first pushed over the lubricated mandrel and then:

- *Figure 11.36b*: Start of rolling – hollow-mandrel assembly is ‘bitten’ by the grooved rolls.
- *Figure 11.36c*: Forging or pilgering – the grooved rolls forge out a small wave of material to the desired wall thickness.
- *Figure 11.36d*: Polishing – the soothing section of the gooved rolls, see Figure 11.36a, reels or polishes the forged wall.
- *Figure 11.36e*: Advancing or feed – roll and mandrel movements are reversed and a fresh section of the mother hollow is ‘bitten’.

After each stroke or pass, Figures 11.36b–d, the tube is rotated by 30–90°, advancing or feed – Figure 11.36e – and a new stroke, albeit in the reverse direction, starts. Appropriate advancing or feed is critical for maintaining concentricity. The synchronization of the mandrel stroke (typically 80–100 strokes are used in a cold pilgering operation) and the reversing roll movements are maintained by suitable mechanical arrangements. The usual pilgering mills are two-high single stand, though use of 4-high (or even higher) multi-stand mills do exist for specific applications.

**11.6.2.1 Roll/die design.** The critical aspect of roll/die design is the design of the groove (Randall and Prieur [1967], Roberts [1983], Montmitonnet *et al.* [1992]). As shown in Figure 11.37, the grooved rolls typically have 3 zones – forging/rolling (AB), polishing (BC) and idling (CA) (Roberts [1983]). Rolls bite the mother tube at the beginning of forging/rolling zone, point A of Figure 11.37, roll rotation and mandrel movement pushing the tube forward. The forging/rolling zone is followed by a polishing zone. The generalized strain patterns in the forging/pilgering and polishing zones are given in Table 11.14. After reaching the end of the polishing zone (point C in Figure 11.37) or reaching the end of a stroke, a suitable mechanical design (discussed latter in Section 11.6.2.2) reverses the motion of the rolls/mandrel bar and at the same time rotating the tube assembly. The advancing or feed also involves roll movement, albeit without any plastic deformation (see Figure 11.36e). This involves the idling zone – CA in Figure 11.37.

A successful pilgering stroke requires continuous decrease in groove diameter along the length of the contact area, AB and BC in Figure 11.37, while an increase in groove width is also necessary. The latter is called ‘side relief’ (the primary

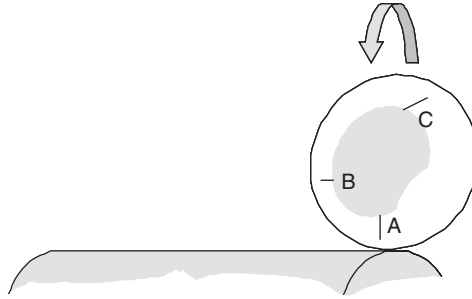


**Figure 11.37.** Schematic of a grooved roll. AB, BC and CA, respectively represent the die zones used for rolling/forging, for polishing and for idling.

**Table 11.14.** Generalized strain patterns during forging/pilgering and polishing.

Forging/pilgering	Polishing
$\varepsilon_r < 0$ , $\varepsilon_\theta < 0$ and $\varepsilon_z > 0$ $\varepsilon_r$ = radial, $\varepsilon_\theta$ = hoop and $\varepsilon_z$ = axial strain, respectively	$\varepsilon_r > 0$ , $\varepsilon_\theta < 0$ and $\varepsilon_z = 0$

basis for the ‘side relief’ is that the tube elongates straight forward and not down the taper – Randall and Prieur [1967]) and is a prime requisite for successful cold pilgering operation. Operating with insufficient ‘side relief’ may result in die pick-up, end spitting or tube shear marks, while excessive ‘side relief’ may cause tube splitting through excessive ovalizing, loss of dimensional tolerance and half moon tears through preferential elongation of the cross-section. For ‘side relief’ design, feed, elongation, die taper, die separation under load, tube springback, tube end ovalizing and groove wear are to be considered (Randall and Prieur [1967]).

**11.6.2.2 Other mill details.** Several other mechanisms/design aspects are equally vital to the overall pilgering operation. Some of these aspects are highlighted in the next few paragraphs.

**11.6.2.2.1 Mandrel design.** Mandrel is designed to keep the roll separating force within limits. Mandrel design varies from simplified straight taper mandrels to more complicated multi-tapered types, the last of the tapers being shallow enough to produce close tolerance tubes.

**11.6.2.2.2 Loading and feed mechanisms.** For loading a fresh tube in a high-speed pilgering mill, two alternatives are usually adopted: (I) fresh tube is fed by a

pusher tube into the mandrel bar, the mandrel bar having a suitable locking–unlocking mechanism and (II) loading of the fresh tube is through the sides of the mill so that the mandrel can be inspected totally from both sides after each pilgering run (Randall and Prieur [1967]). The design of the feed mechanism is also vital (Voith [1985]) and several possibilities, mechanical as well as hydraulic, exist (Randall and Prieur [1967]).

**11.6.2.2.3 Rolling drive.** A large roll groove in a small machine would have a tendency to pull the tube into the dies, while the reverse would increase the tendency of excessive slippage (Randall and Prieur [1967]). Use of appropriate rolling drive and drive parameters are vital for the pilgering operations (Pavlovskii [1984]).

**11.6.2.2.4 Synchronization and turning.** Two of the most important design aspects of a pilger mill are ‘synchronization’ and ‘turning’. A pilgering mill operating at 150 strokes a minute is subjected to five reversals in a second (Randall and Prieur [1967]). Each reversal requires turning the tube, by 30–90°, and reversing the roll/mandrel movement – a pretty demanding situation in any machine design. Synchronization of the mandrel, rolls and the feed mechanism can be achieved (Randall and Prieur [1967]) through a fairly complicated array of crank drive, rack and pinion, gears and rotating cam. Appropriate pneumatic clutch and breaking arrangements are also required. Turning, on the other hand, is achieved efficiently (Randall and Prieur [1967]) through a turning cam, mounted on the drive shaft and rotating at the same speed. The turning cam is ‘timed’ to push a sliding shaft and a worm, the latter acting as a rack in activating a worm gear – the gear executing actual turning operation. Once the turning is finished, the worm returns to its starting position.

**11.6.2.3 Lubrication.** Pilgering lubricants are often similar to that of drawing (Möller and Boor [1996]). Lubrication is typically applied in the inner surface once and for all by injection a suitable emulsion (e.g. stabilized animal fats, chlorinated paraffins) before the mother tube is fed, while the external surface is continuously sprinkled with the same, albeit dilute, emulsion (Montmitonnet *et al.* [1992]). However, examples of continuous lubricant application in the inner surface (lubricant being pumped through a hollow mandrel) also exist (Randall and Prieur [1967]). Cold pilgering is typically in a ‘mixed’ (as in Figure 11.4) lubrication mode<sup>5</sup> giving ‘plateaux and valleys’ (Montmitonnet *et al.* [1992]). High concentration of ‘plateaux’ does create serious risks of surface defects. The

<sup>5</sup> For more details on lubrication mode, the reader may refer Section 11.1.1.3.

concentration of the ‘plateaux’, on the other hand, can be controlled by proper lubrication – controlling the lubricant delivery and filtering.

### 11.6.3 Optimization in pilgering

Pilgering optimization may range from relatively simple in-plant empirical modelling for increasing productivity/efficiency (Mfshchikov [1984], Plyatskovskii [1986]) to more complicated analytical and/or numerical modelling of the plastic deformation (Siebel *et al.* [1954], Roberts [1983], Furugen [1984], Masahiro [1985], Voith [1985], Montmitonnet *et al.* [1992], Huml [1994], Mulot [1996], Montmitonnet *et al.* [2002]). The earliest analytical model of cold pilgering (Siebel *et al.* [1954], Montmitonnet *et al.* [2002]) is based on an approach similar to the analytical solution of cold strip rolling. The model (Siebel *et al.* [1954]) estimates the vertical rolling force,  $F(z)$ , as:

$$F(z) = K(z)L_d(z)D(z) \quad (11.35)$$

where  $L_d$  is the projected contact length (in rolling, contact length =  $L = (R\Delta h)^{1/2}$ ,  $R$  and  $\Delta h$ , respectively being the roll diameter and reduction.),  $D$  is the external diameter of the tube ( $L_d D$  being the projected contact surface with one die/roll) and  $K$  is the average normal stress (depends on yield stress and on friction). Considering two different contact lengths, material in contact with both mandrel and die/roll and material in contact with only die/roll (Siebel *et al.* [1954], Mulot [1996], Montmitonnet *et al.* [2002]), the following analytical solutions for  $L_d$  and  $F(z)$  were proposed (Siebel *et al.* [1954]):

$$L_d = \left( 2Rm \left( \frac{S_0}{S} \right) \right)^{1/2} \cdot \{(\phi - \delta)^{1/2} + (\delta)^{1/2}\} \quad (11.36)$$

$$F(z) = \sigma_0 \left( \frac{1 + \mu L_d}{2t} \right) \cdot D \left\{ \frac{2Rm}{S_0/S} \right\}^{1/2} \left\{ \frac{(\phi - \delta) + ((\delta)^{1/2} + 2t)}{D} \right\} \quad (11.37)$$

where at a section  $z$ ,  $R$  is the die radius,  $m$  the feed length,  $S$  the cross-sectional area,  $\phi$  and  $\delta$  are mandrel and die/roll contact angle,  $t$  is the tube thickness and  $D$  is the tube diameter.  $S_0$ ,  $\sigma_0$  and  $m$  are the initial cross-sectional area, yield stress and friction coefficient, respectively.

Though simplified in approach, the 2D analytical model (Siebel *et al.* [1954]) shows serious discrepancies with experiential results (Yoshida [1975]). A 3D analytical model (Furugen [1984]) has subsequently been proposed and shows better predictive behaviour. The model has been used effectively for overall

stress analysis, though shear components are somewhat neglected even in this approach, and to correct die/mandrel geometry (Furugen [1984]). A complete picture of the stress distribution, and hence a complete approach to pilgering optimization seems possible only through FEM (Mulot [1996], Montmitonnet *et al.* [2002]). It is also to be noted that the FEM approach often uses existing commercial codes (Montmitonnet *et al.* [2002]). The capability and promises for overall pilgering optimization, especially for die/roll and mandrel design, of these codes are very un-equal and relatively simpler analytical approaches are still being used effectively for optimization during the pilgering process itself – from simple load calculations (Roberts [1983]) to relatively more complicated estimations of maximum feed at a given tolerance for relative ovality (Voith [1985]).

#### 11.6.4 Materials aspects

Because cold pilgering is more of a compression forming process, the malleability is a better measure of formability than ductility. This makes the usual high reductions a common feature for cold pilgering operations – reductions exceeding 50% are possible even in difficult to process materials like Hastelloy and Ti-6Al-4V, while reductions approaching 80% are common for more formable metals (Randall and Prieur [1967]). Cold pilgering has a large possible range of applications: from breakdown of hot-formed mother tubes to final finishing to close dimensional tolerances (less than 5% dimensional tolerance is typical), from forming of expensive material (and thus avoiding ‘point-loss’ usual in tube drawing operation) to forming of difficult to draw material (high strength material) and from forming bar/rod products with uniform mechanical properties across the cross-section to forming specific components (e.g. for aerospace and nuclear industry) with difficult shapes (tapering of inner/outer diameter and/or hexagonal/square shapes for inside channel).

The strains involved with the pilgering process are often generalized from the ‘ $Q$ -factor’, which is the ratio of reductions in tube wall and tube diameter (Jeffrey [1991], Kiran Kumar *et al.* [2003]). Though the strain history is complex triaxial, processing with large  $Q$  may bring it close to plane strain. Naturally the  $Q$  factor has strong effects on developments of mechanical anisotropy, by controlling the deformation texture development (Jeffrey [1991], Davies *et al.* [2002], Kiran Kumar *et al.* [2003]).

Though a process with better formability, the complex history of cold pilgering may lead to defects. Table 11.15 provides a typical listing of defects in cold-pilgered Zr tubes (for reactor cladding applications). This list was formulated by considering available plant data. As shown in the table, a larger percentage of defects in cold-pilgered tubes are on the inner surface – *about 45% of the overall defects being cracks on the inner surface*. Cracks typically develop through low cycle rolling contact fatigue at locations of microstructural heterogeneity. As indicated in the table, other than quality control of the hollows or the mother tubes and eliminating defects

**Table 11.15.** Listing of defects in cold-pilgered Zr tubes for reactor applications.

Location	Type	Source
Defects in the outer surface (about 40–45% of total defects)	<i>Pilgering defects:</i> Cracks	Rough surface (die/mandrel), improper lubrication (both cooling and filtering), wrong calculation of feed and ‘side relief’, non-uniform rotation during pilgering
	<i>Others:</i> Cracks, handling defects (e.g. grinding and burning defects)	<i>Cracks:</i> Owing to defects present in the mother tube (in solidification, hot forming or heat treatment) <i>Handling defects:</i> Owing to improper handling or defects in the accompanying operations (grinding, sand blasting, etc.)
Defects in the inner surface (about 50–55% of total defects)	<i>Pilgering defects:</i> Cracks/laminations and surface roughness	Use of low $Q$ -factor, wrong mandrel size and/or feed, improper lubrication (can affect surface roughness seriously and large surface roughness, especially high plateaux concentration, may lead to other defects as well (Montmitonnet [1992])
	<i>Others:</i> Cracks and porosity	Owing to defects present in the mother tube or created during accompanying operations

in the accompanying fabrication/TMP steps, control (control and usage of appropriate tooling and process variable are typically the decisive issues in the overall quality control scheme) of the tooling in pilgering (roll/die and mandrel) and process control (control of feed,  $Q$  factor and lubrication) are important steps in the overall quality assurance.

## LITERATURE

- Montmitonnet P., Loge R., Hamery M., Chastel Y., Doudoux J.L. and Aubin J.L., *J. Mater. Process Tech.*, 125–126 (2002), 814.  
 Randall S.N. and Prieur H., *Iron and Steel Engineers*, (August) (1967), 109.  
 Roberts W.L., “Hot rolling of steel”, Marcel Dekker, New York (1983), 419.

## 11.7. SHEET METAL FORMING

### 11.7.1 Introduction

Large quantities of thin sheets are produced at a relatively low cost by rolling mills. They are transformed into familiar products, such as beverage cans, car bodies, metal desks, domestic appliances, aircraft fuselages, etc., by sheet metal-forming processes. Many of these processes involve a rather complex deformation path. In most cases, the latter can be considered as a superposition of some ‘elementary’

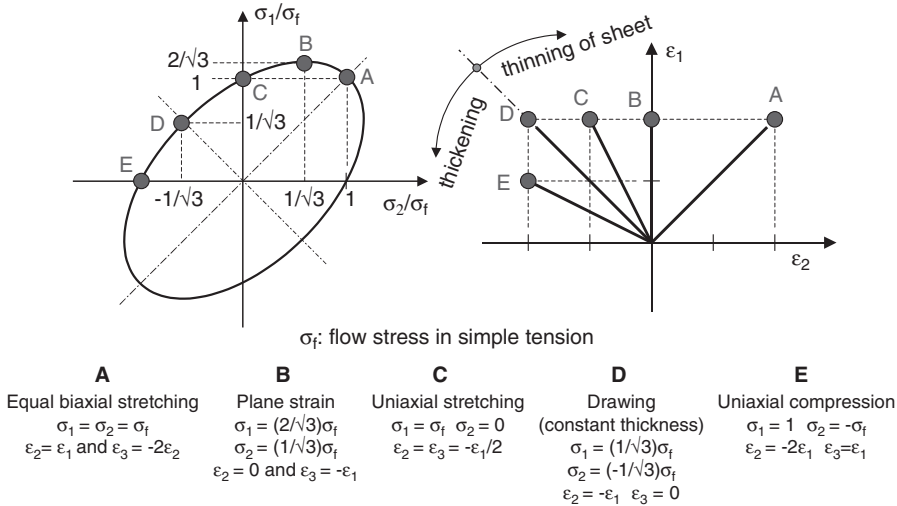


**Figure 11.38.** Stress and strain state of some plane stress conditions ( $\sigma_3 = 0$ ) in an isotropic material. For more information, the reader is referred to any introductory textbooks on plasticity.

processes like bending, stretching and deep drawing, which will be discussed in this chapter.

In most sheet metal-forming processes, the stress perpendicular to the sheet surface is small compared to the stresses in the plane. It is often assumed that this 'normal' stress can be neglected. When the normal stress is zero, the stress state is called 'plane stress'. Some possible plane stress situations and their associated strain state are illustrated in Figure 11.38.

An important feature of many sheet metal-forming operations is the so-called 'plastic anisotropy' of the sheet. This will be discussed in the next paragraph. After that, a paragraph is devoted to the concept of 'forming limit diagrams' (FLDs). An FLD indicates how much deformation a sheet can withstand before failure and is an important tool for many practical press-forming operations. Subsequently, the most important sheet metal-forming operations like stretching, deep drawing, bending and others will be analysed.

### 11.7.2 Plastic anisotropy

The term 'anisotropy' refers to a directionality of some particular material properties. These properties can be elastic (e.g. Young's modulus), plastic (strength, formability), electrical (conductivity), magnetic (hysteresis losses), etc. In the frame of this textbook, we will mainly concentrate on 'plastic anisotropy'. It will be shown in the next paragraph that the main cause of plastic anisotropy is the crystallographic texture of the material. This is in contrast with the directionality

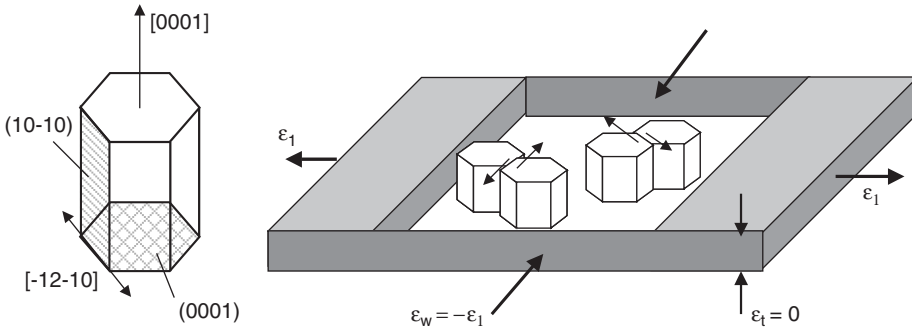


**Figure 11.39.** Slip systems in pure Ti. In uniaxial tension, the fibre texture prohibits thinning in the thickness direction. After Hosford and Caddell [1983].

in fracture behaviour, which results mainly from a morphological texture (elongated grains, alignment of precipitates, etc.).

**11.7.2.1 Crystallographic background.** As described in Chapter 10, the macroscopic deformation of a metal is the result of many microscopic shear deformations on particular crystallographic planes (for simplicity, we do not consider other deformation mechanisms like twinning, etc.). Take the example of pure Ti which has a hexagonal closed packed (hcp) structure up to 882°C. Deformation takes place by glide in the  $\langle 1-210 \rangle$  directions in the basal (0001) plane and prismatic  $\{10-10\}$  planes (Figure 11.39). In none of these cases, can any deformation in the [0001] direction occur. Suppose now that a Ti sheet has an ‘ideal’ fibre texture and consist of grains with the basal plane (0001) parallel with the sheet surface, but with a random distribution of crystallographic orientations around the [0001] axis (see Chapter 8 for more details on crystallographic textures). A uniaxial deformation in the sheet plane will be performed by glide on the prismatic  $\{10-10\}$  planes. The elongation of the sheet in the tensile direction ( $\epsilon_t$ ) will be compensated by a perpendicular contraction in the width of the sheet ( $\epsilon_w$ ), but the activated slip systems will not allow any contraction in the thickness direction ( $\epsilon_t$ ) (Figure 11.39). The difference in contraction between width and thickness is due to the material anisotropy (Chapter 3). On the other hand, because of the random distribution of crystallographic directions around the [0001] axis, the tensile properties will not vary with the angle between tensile axis and rolling direction: this is called ‘planar isotropy’.

**11.7.2.2 The  $\bar{R}$  and  $\Delta R$  factors.** In practical situations an ‘ideal’ texture as depicted in Figure 11.39 will never occur. In a real tensile test on a Ti sheet, some contraction in thickness would be observed. As briefly introduced in Chapter 3, the

ratio between plastic strain in the width over plastic strain in the thickness direction in a uniaxial tensile test is called the  $R$ -value:

$$R(\alpha) = \frac{\varepsilon_w^{\text{pl}}}{\varepsilon_t^{\text{pl}}} \quad (11.38)$$

with  $\alpha$  the angle between the rolling direction and the tensile axis. A large value of  $R$  means that the crystallographic orientations of the grains are such that the sheet has a large resistance against thinning. In practical circumstances, it is often difficult to measure the change in thickness during a tensile test. Because  $\varepsilon_t^{\text{pl}} = -(\varepsilon_w^{\text{pl}} + \varepsilon_l^{\text{pl}})$ , the  $R$ -value can also be calculated from width and length variations. In most cases the total (elastic + plastic) strains are measured, so a more practical definition of the  $R$ -value is:

$$R(\alpha) = \frac{-\varepsilon_w}{(\varepsilon_w + \varepsilon_l)} \quad (11.39)$$

To minimize the error introduced by neglecting the elastic strain, the  $R$ -value is usually measured between 10 and 15% length strain.

Since the  $R$ -value of most materials depends on the direction in the surface plane of the sheet (indicated by angle  $\alpha$  between tensile axis and rolling direction), a mean  $R$ -value ( $\bar{R}$ ) can be calculated. A rigorous definition would be:

$$\bar{R} = \frac{2}{\pi} \int_0^{\pi/2} R(\alpha) d\alpha \quad (11.40)$$

Because in most cubic materials a minimum or maximum of  $R$  is found at  $\alpha = 0^\circ$ ,  $45^\circ$  and  $90^\circ$ , the  $\bar{R}$ -value is often calculated based on only three sets of tensile tests with:

$$\bar{R} = \frac{(R_{0^\circ} + 2R_{45^\circ} + R_{90^\circ})}{4} \quad (11.41)$$

This mean  $R$ -value is called ‘the normal anisotropy’ and is an important technical parameter because it is related to the deep drawability of the sheet, as will be discussed in Section 11.7.5 and illustrated in the case study, Chapter 15.1 on ‘steel for car body applications’.

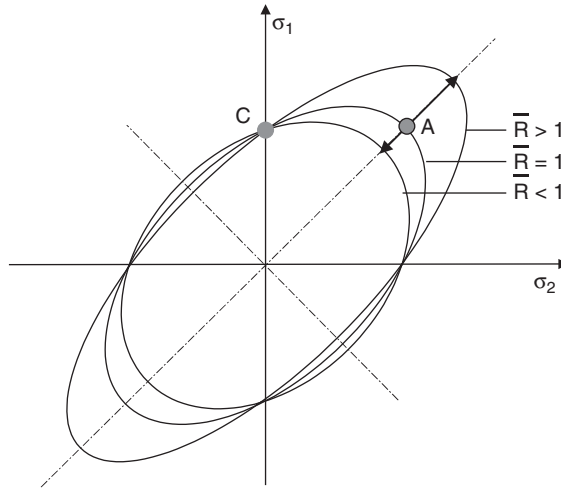


**Figure 11.40.** Influence of plastic anisotropy on the shape of the yield locus.

The planar anisotropy is also important from a technical point of view. The planar anisotropy reflects the variation of  $R(\alpha)$  in the plane of the sheet and can be defined as:

$$\Delta R = \frac{(R_{0^\circ} - 2R_{45^\circ} + R_{90^\circ})}{2} \quad (11.42)$$

It will be shown in Section 11.7.5 and illustrated in the case study on ‘Al beverage cans’ (Chapter 14.1) that  $\Delta R$  can be related to the earing behaviour during deep drawing.

It is obvious that plastic anisotropy will change the shape of the yield locus. This is illustrated in Figure 11.40. It is worth noting that the uniaxial yield stress (point C) is not affected by a change in mean  $R$ -value, but that the biaxial yield stress (point A) increases with increasing  $\bar{R}$ .

### 11.7.3 Forming limit diagrams

**11.7.3.1 Determination and practical use.** A forming limit diagram (or ‘FLD’), as schematically shown in Figure 11.41, indicates how much deformation a material can take before it fails.<sup>6</sup> For example, when a material is biaxially stretched along path ‘a’ till strain state ‘A’, no failure is predicted. Following strain path ‘b’ till point

<sup>6</sup> An FLD is also known as a ‘Keeler–Goodwin’ diagram, referring to the original work of Keeler [1965] and Goodwin [1968]. Reviews on FLDs have been given by Wagoner [1989] and Esche *et al.* [1996].

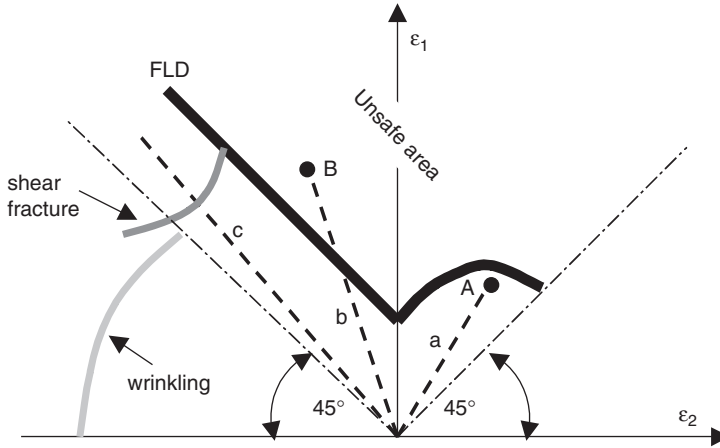


**Figure 11.41.** Schematic illustration of a forming limit diagram (the thick black line).

'B' will however cause failure as soon as the strain state reaches the forming limit curve. 'Failure' is considered here as the point where a local neck develops. The real 'fracture' of the material will occur immediately after the development of a local neck, at a slightly higher strain.

In the region where thickening of the sheet occurs (cf. Figure 11.38), the sheet will not fail by local necking, but wrinkling is likely to occur. This is not indicated in most FLDs. Along certain strain paths, e.g. path 'c', fracture (in this case a so-called 'shear fracture') can occur before the actual FLD is reached. Also this line is often not indicated in a simple FLD diagram.

An FLD is not only useful to predict the maximum strain one can apply in a particular stamping operation, but it can also be used to analyse a stamped part. Suppose one can measure or calculate the local strain state in every area of a stamped part. These strain states can then be plotted on an FLD and the most critical areas of the part, in the safe area but close to the FLD, can be identified and the shape of the part can be adapted if necessary. The calculation of local strain states is performed in most cases by finite element simulations. An experimental verification can be done in the following way: the sheet is covered with a grid pattern of circles using some electrochemical technique. These circles have typically a diameter of 2–5 mm. The sheet is then stamped and during deformation most circles are converted into ellipses. The large and small axes of all the ellipses are measured with a microscope or with some automatic optical system and from these dimensions the local strains  $\epsilon_1^i$  and  $\epsilon_2^i$  are calculated and plotted on the FLD. When certain points are close to the 'forming limit', it may be advisable to adapt in that location the shape of the part. Even when the actual prototype part has not

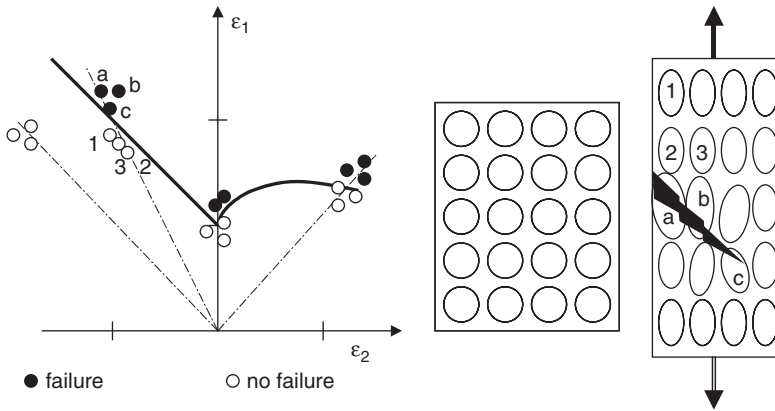


**Figure 11.42.** Experimental determination of an FLD diagram.

failed, a slight change of some of the production parameters (friction, deformation rate, sheet thickness, etc.) could bring the local deformation in the ‘unsafe’ region and several failures during a production run can be anticipated.

The experimental determination of an FLD is time-consuming and can be done in the following way. A number of test sheets are covered with a pattern of circles (or other markings). All the sheets are deformed till failure along a certain deformation path (uniaxial stretching, biaxial stretching, drawing, plane strain, etc.). The dimensions of the deformed circles are measured and the local deformation is calculated and plotted in a  $(\epsilon_1, \epsilon_2)$  diagram. Ellipses in the crack or in a necked region are indicated with full circles; other points are indicated with open circles (Figure 11.42). Based on this information, the forming limit curve can be determined. More information about the practical determination of FLDs can be found in ASM [1988].

**11.7.3.2 Parameters that affect the FLD.** Each material has its own FLD. But also the actual state of a material (cold deformed, recrystallized, etc.) will affect the position of the FLD. In the next paragraphs, the most important parameters that affect the FLD will shortly be discussed.

*The strain hardening coefficient ‘n’.* The general effect of an increase of the strain hardening coefficient ‘n’ is to shift the whole FLD upwards (Figure 11.43). In fact, it can be shown (see, e.g. Marciniak *et al.* [2002]) that the left-hand side of an FLD can roughly be described by:  $\epsilon_1 + \epsilon_2 = n$ . For  $\epsilon_2 = 0$  (plane strain)  $\epsilon_1 = n$ . For strongly cold-worked metals,  $n$  is close to zero. This means that the plane strain formability or uniaxial deformability will be close to zero, but that in equi-biaxial

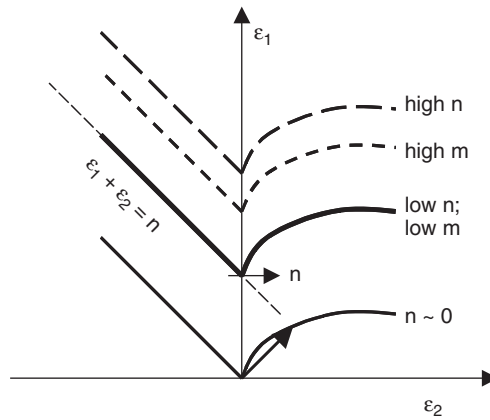


**Figure 11.43.** Influence of strain hardening ( $n$ ) and strain rate sensitivity ( $m$ ) on the forming limit diagram. For strongly cold deformed metals ( $n \sim 0$ ) some equi-biaxial stretching is still possible.

direction some stretching is still possible, as illustrated in Figure 11.43. Especially for biaxial stretching, the strain hardening has a large effect on formability.

*The strain rate sensitivity coefficient 'm'.* The development of a local neck can be delayed by a high strain rate sensitivity. Increasing ' $m$ ' shifts the FLD upwards and the intersection with the  $\epsilon_1$  axis is higher than  $n$ .

*The thickness of the sheet.* The sheet thickness has more or less the same effect as the strain rate sensitivity: increasing thickness shifts the FLD upwards.

*Strain path changes.* Nearly all experimental FLDs available in the literature have been determined for proportional loading, which means that  $\epsilon_1/\epsilon_2$  is constant. In many complex stampings this is not the case and changes in strain path during deformation occur. It has been shown in by Nakazima *et al.* [1968] that such strain path changes can have a drastic effect on the position of the FLD curve, as illustrated in Figure 11.44. It was shown that for a combination of equi-biaxial stretching, followed by uniaxial stretching (curve 'a') or plane strain deformation (curve 'c'), failure occurred before the 'proportional' FLD was reached. On the other hand, for a combination of uniaxial stretching followed by equi-biaxial stretching, a much larger deformation could be applied than anticipated from the conventional FLD. Since it is impossible to determine experimental FLDs for all possible strain path changes for all materials, efforts have been done to predict the influence of strain path changes with computer models (see, e.g. Hiwatashi *et al.* [1998]).

#### 11.7.4 Stretch forming

In stretch forming, the material is clamped along the edges and stretched over a punch. A simple case of stretch forming is an equi-biaxial stretch over a

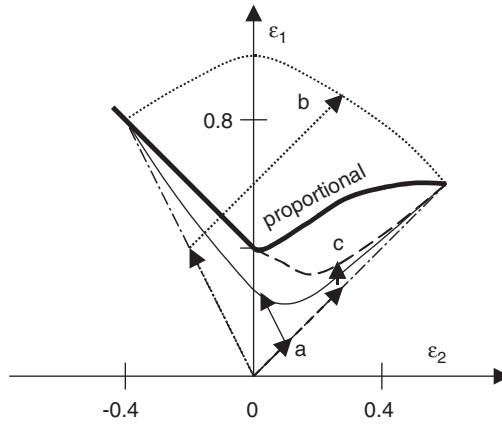


**Figure 11.44.** Influence of strain path changes on the position of the FLD. (a) equi-bi-axial stretching followed by uniaxial tension; (b) uniaxial tension followed by equi-bi-axial stretching; (c) equi-bi-axial stretching followed by plane strain deformation. Adapted from Nakazima *et al.* [1968].

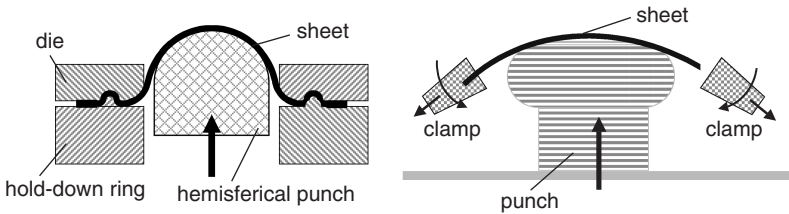


**Figure 11.45.** Equi-bi-axial stretching using a clamped sheet and a hemispherical punch (left) and a schematic of an industrial stretch-forming operation (right).

hemispherical punch as shown in Figure 11.45 (left). The edges of the sheet are clamped by some groove in the die (the so-called ‘draw-bead’). In many industrial stretch-forming operations, the situation is more complex. The sheet is often rectangular and is clamped along two sides only (Figure 11.45, right). In this case, the strain is close to plane strain. The middle section of the sheet is less stretched because of the friction between punch and sheet.

To avoid unstretched regions (without work hardening) uniaxial stretching with the clamps, before ‘draping’ the sheet over the punch can be a solution. In many cases, the clamps can not only exert a tensile force, but can also rotate in order to maintain the tensile force tangential to the sheet. Instead of using a simple punch, some presses make use of a male and female die (Figure 11.46). The forming operation is now very complex.

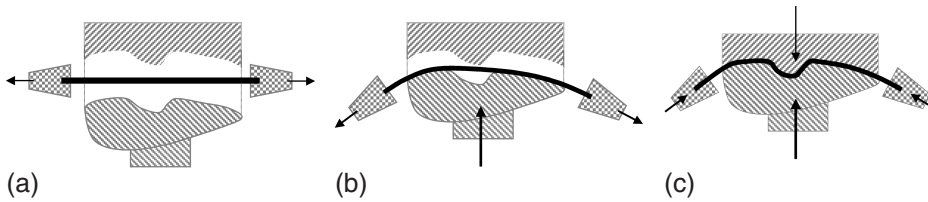


**Figure 11.46.** Complex stretch-forming operation using a male and a female die.

Many possible routes exist, but a standard stamping could be as follows:

- Uniaxial stretching of the sheet; because of the large width of the sheet, this will lead to a strain state close to plane strain.
- Draping of the sheet over the punch by an upward movement of the latter, the clamps maintain a tangential tensile force.
- Downwards movement of the upper die; the clamps move back inwards to feed new material in the opening between the two dies. The deformation is then a combination of stretching and deep drawing (see Section 11.7.5).
- The dies move back to their initial position, and the clamps release the pressed part.

Stretch forming is very useful to produce large parts with a large radius. It is frequently used in the aircraft and automotive industries. Another advantage is a limited springback.

### 11.7.5 Deep drawing

**11.7.5.1 Stress and strain.** During deep drawing, a sheet is pushed through an opening in a die. A blank holder prevents wrinkling of the sheet but, in contrast to stretching, the material from the flange can more or less without constraints be drawn towards and into the die opening. The most common example of deep drawing is the formation of a cylindrical cup (Figure 11.47). For a constant punch diameter  $D_p$ , the height of the cup wall will increase with increasing sheet or blank diameter ( $D_{bl}$ ). There is, however, a limit to the height that can be obtained in one drawing pass, without fracturing the cup wall. This limit is called the ‘limiting drawing ratio’ or LDR and is defined as:

$$\text{LDR} = \frac{D_{bl}^{\text{MAX}}}{D_p} \quad (11.43)$$

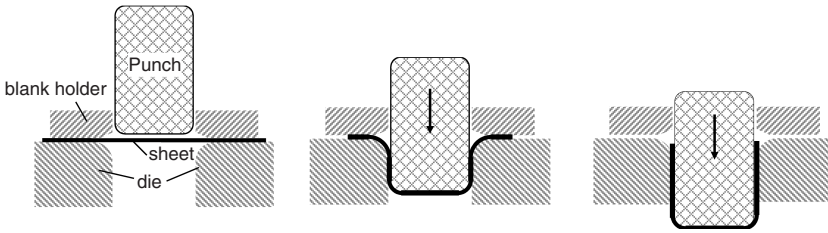


Figure 11.47. Deep drawing of a cylindrical cup from a circular blank.

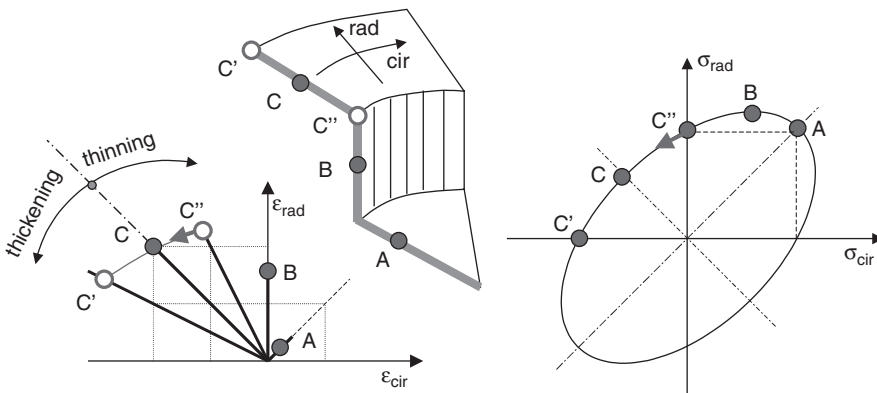


Figure 11.48. Stress and strain state in various points of the cup during deep drawing. Possible compressive stresses in flange and wall are not taken into account.

During deep drawing, four important zones can be identified: the flange, the transition between flange and cup wall, the cup wall and the bottom of the cup.

- The bottom of the cup, which is formed by the material under the punch, is equibiaxially stretched (point 'A' in Figure 11.48). In principle, the material will thin down; but in practice, the strain in the bottom is not so large and it is often assumed that the bottom of the cup has more or less the same thickness as the original sheet.
- The situation in the flange is more complicated. The material is drawn into the die hole by a radial tensile force. An imaginary circle on the flange will shrink during drawing, so the stress state is tensile in the radial and compressive in the circumferential directions. In an ideal case, the strain can be considered as 'ideal drawing' without change in thickness (point 'C' in Figure 11.48). In reality, the stress- and strain-state change in radial direction. At the outer surface,  $\sigma_{rad} = 0$  (point C' in Figure 11.48). This means that the edge of the flange will thicken.

At the edge of the die hole, using Tresca's yield criterion (Marciniak *et al.* [2002]), the stress state can be described by

$$\sigma_{\text{rad}} = \sigma_f \ln \left( \frac{D_{\text{bl}}}{D_p} \right) \quad \text{and} \quad \sigma_{\text{cir}} = -(\sigma_f - \sigma_{\text{rad}}) \quad (11.44)$$

with  $\sigma_f$  the flow stress. Since  $\sigma_{\text{rad}}$  cannot exceed  $\sigma_f$ , the limiting drawing ratio  $D_{\text{bl}}^{\text{MAX}}/D_p = e = 2.72$ . In that case,  $\sigma_{\text{cir}} = 0$  (point C'' in Figure 11.48). In reality, most deep-drawing materials have an LDR between 2 and 2.4, which keeps  $\sigma_{\text{rad}} < \sigma_f$  and  $\sigma_{\text{cir}} < 0$ . In any case, the strain state will be such that the material will thin down. In many cases, the blank holder – whose principle task is to prevent the flange from wrinkling – will prevent (or limit) the thickening of the blank. In that case, an additional stress  $\sigma_3$  perpendicular to the sheet will be present.

- The force exerted by the punch is transmitted to the deforming flange by the material in the cup wall. Hence this material is subjected to a tensile force. Because of the geometry of the cup and punch, no contraction in the circumferential direction is possible. This results in a plane strain deformation (an elongation of the cup wall compensated by a reduction in thickness), point B in Figure 11.48. The purpose of deep drawing is to concentrate the deformation in the flange and not in the cup wall. For this reason, the thinning of the wall must be kept to a strict minimum. As will be explained in the following paragraph, this is done by choosing materials with a large  $\bar{R}$ -value.

With the assumption that flange, wall and bottom of the cup retain the initial sheet thickness, the following expression for the height of the cup can be found:

$$h \sim \frac{D_p}{4} \left\{ \left( \frac{D_{\text{bl}}}{D_p} \right)^2 - 1 \right\} \quad (11.45)$$

For a material with a LDR = 2.25, the maximal cup height that can be drawn in one pass is equal to the cup diameter. It must be noted that the assumption of constant wall thickness is not completely correct. In reality, the wall will thin down close to the bottom part, while the top is thickened.

- The transition between flange and cup wall is done by bending and unbending. This will add some extra component to the total force needed for deep drawing, it will increase the work hardening and it will lead to an extra reduction in thickness.

The total force  $P$  that has to be exerted on a blank to draw a cup, depends on many factors. Besides the complicated stress state described above, the friction

between blank holder and flange and between cup wall and die must be considered, as well as the blank holder force and the force needed to bend the material. An approximate equation for the total punch force as function of the blank diameter  $D_{bl}$  at any stage of the process is (Dieter [1976]):

$$P = \left[ \pi D_p t (1.1 \sigma_f) \ln \left( \frac{D_{bl}}{D_p} \right) + \mu \left( \frac{2BD_p}{D_{bl}} \right) \cdot \exp \left( \frac{\mu \pi}{2} \right) + A \right] \quad (11.46)$$

where  $D_{bl}$  the blank diameter,  $D_p$  the punch diameter,  $t$  the thickness of the wall,  $\sigma_f$  the average flow stress,  $A$  the force to bend and unbend the material,  $B$  the blank holder force,  $\mu$  the friction coefficient. The first part of the equation gives the ideal force to draw a cup, the second term expresses the friction force under the blank holder and the exponential factor brings the friction between wall and die into account.

**11.7.5.2 Redrawing and ironing.** According to formula (11.45), the cup height that can be obtained in one single drawing pass is limited. To obtain deeper cups, two techniques are frequently used: redrawing and wall ironing. Both techniques are illustrated in Figure 11.49.

In redrawing, several consecutive drawing passes are applied. After each pass, the cup radius decreases and the cup height increases. When the cup is turned inside out after each pass, the process is called ‘reverse redrawing’. In wall ironing, the cup passes through a series of ring-shaped dies (Figure 11.49, right).

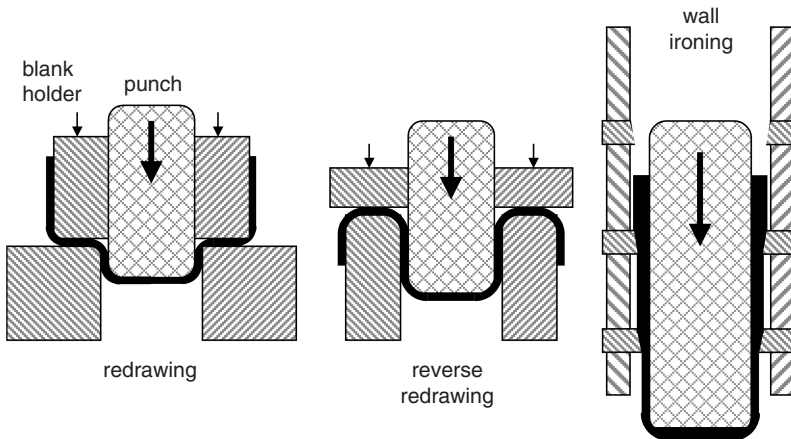


**Figure 11.49.** Redrawing, reverse redrawing and wall ironing to produce deeper cups.

The clearance between the punch and each die is less than the local sheet thickness, which increases the height and decreases the thickness of the cup wall.

**11.7.5.3 Deep drawing and texture.** In the previous paragraph, it has been shown that the deep drawability of a material can be expressed by the value of its LDR, which can be experimentally determined by drawing a series of blanks with increasing diameter till fracture occurs. Owing to the work of Held [1965] and many others, it became clear that the LDR is linearly related to the mean R-value ( $\bar{R}$ ) of the material.

This means that deep drawability can be estimated from tensile tests. On the other hand, initial work of Whiteley [1960] and Hultgren [1968] established for low-carbon steel sheet a linear correlation between  $\bar{R}$  and the texture. It is now common knowledge that in low-carbon steel, grains with a  $\{111\}$  plane parallel to the rolling plane will enhance the deep drawability of a sheet, while grains with a  $\{001\}$  plane parallel to the rolling plane are detrimental. Figure 11.50 illustrates the position of these ‘good’ and ‘bad’ crystallographic directions in Euler space. In the case study (Chapter 15.1) on ‘steel for car body applications’, it will be shown how a well-balanced TMP can optimize the texture and the deep drawability.

After drawing, the tops of the cups are not completely flat, but show minima and maxima (commonly called ‘ears’). This earing is a consequence of the planar anisotropy of the sheets and correlates well with the  $\Delta R$  value or the angular variation of  $R$  (Figure 11.51). In the directions of a low  $R$ -value, more thickening of the sheet will occur and the material is drawn faster into the die hole. Although earing manifests itself in the wall of the cup, it is a consequence of the deformation history of the flange. For  $\Delta R < 0$ , ears will occur at  $45^\circ$  with the rolling direction and for  $\Delta R > 0$  at  $0^\circ$  and  $90^\circ$ . For fcc materials, it has been established that cube-oriented grains stimulate the  $0^\circ/90^\circ$  ears, while orientations belonging to the  $\beta$ -fibre give rise to  $45^\circ$  ears. It will be shown in the case study on ‘aluminium

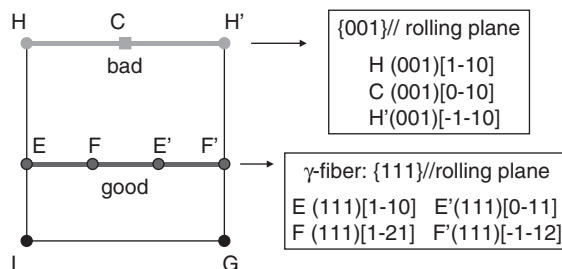


**Figure 11.50.**  $\varphi_2 = 45^\circ$  section of Euler space (Chapter 8), with crystallographic orientations that are ‘good’ and ‘bad’ for the deep drawability of a low-carbon steel sheet.

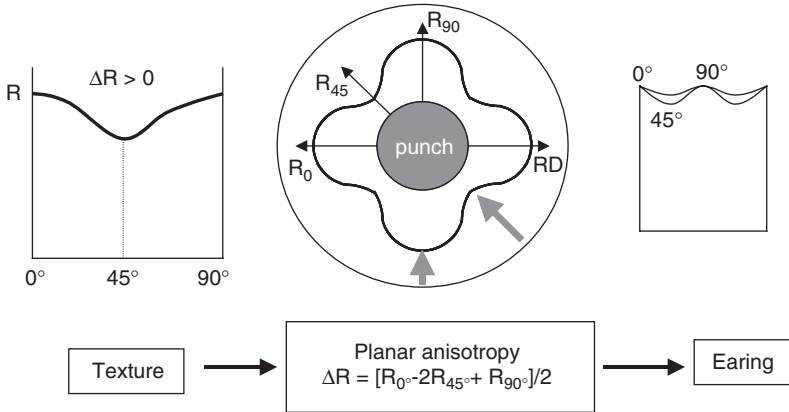


Figure 11.51. Influence of R-value directionality on material flow during cup drawing and resulting earing profile.

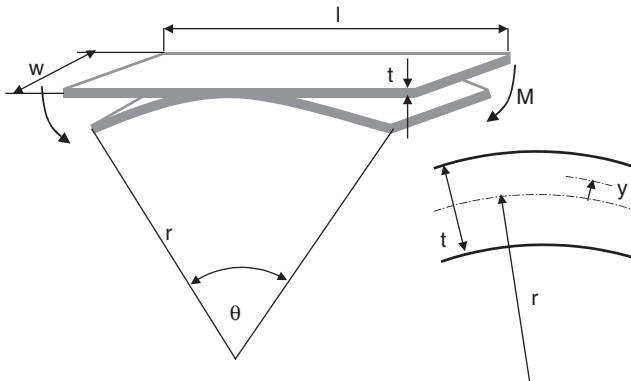


Figure 11.52. Illustration of a simple bending operation.

beverage cans', how Al sheets are processed in order to achieve a good balance between both in order to get  $\Delta R \sim 0$  and to minimize earing.

### 11.7.6 Bending and folding

**11.7.6.1 Stress and strain.** Bending is a relatively simple forming operation, which can be achieved in various ways. A schematic illustration of a bended sheet is shown in Figure 11.52. During bending, the convex part of the sheet (the upper part in Figure 11.52) is in tension and the concave (lower) part in compression. The strain is zero at the neutral axis and maximum at the outer surface. The strain

distribution over the thickness is linear, as illustrated in Figure 11.53. At a distance  $y$  from the neutral axis  $\varepsilon = y/r$  with  $r$  the bend radius and at the surface  $\varepsilon^{\max} = t/2r$ . The strain state during bending of a sheet (with  $w \gg t$ ) is approximately plane strain with  $\varepsilon_l = -\varepsilon_t$  and  $\varepsilon_w = 0$ . The stress state is biaxial with at the surface  $\sigma_l = (2/\sqrt{3})\sigma_f$  with  $\sigma_f$  the flow stress in a simple tensile test, and for isotropic materials,  $\sigma_w = (\sigma_l/2)$  and  $\sigma_t = 0$ .  $S = (2/\sqrt{3})\sigma_f$  is the so-called ‘plane strain flow stress’. For anisotropic material it can be calculated from:

$$S = \sigma_f \left[ \frac{\bar{R} + 1}{(2\bar{R} + 1)^{0.5}} \right] \quad (11.47)$$

When the width of the sheet is not at least 8–10 times larger than the thickness, the stress ratio  $\sigma_w/\sigma_l$  decreases as shown in Figure 11.54.

For practical applications, it is important to know how far a sheet can be bent before cracks appear at the surface. The minimal bend radius is usually expressed as function of the sheet thickness, for example,  $r_{\min} = 3t$ .

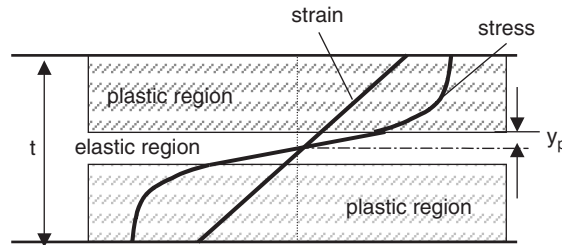


Figure 11.53. Stress and strain distribution over the sheet thickness.

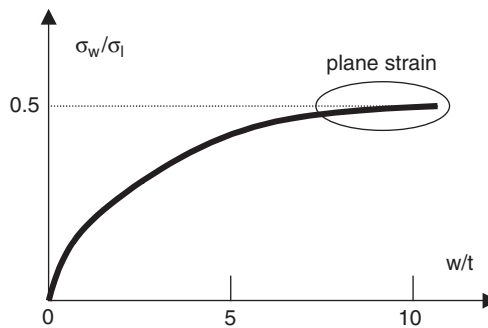


Figure 11.54. Ratio of  $\sigma_w/\sigma_l$  as function of the width over thickness ratio, the bending limit.

It is difficult to calculate an accurate bending limit. An approximate value can be estimated from the reduction in area (RA) in a uniaxial tensile test:

$$\varepsilon_{\max} = \frac{t}{2r} \leq \frac{RA}{(1-RA)} \quad (11.48)$$

According to Eq. (11.48), a small bend radius can be reached for ductile materials with a large RA value; for most materials, this means a low yield strength. This rule of the thumb must however be used with some caution because microstructural effects, especially a morphological texture, can have a big influence on the bendability. Some data about bendability can be found in ASM [1985]. The bending limit predicted by (11.48) can only be reached when the length of the bended zone is sufficiently large. When the length of the bended zone ( $l = r\theta$ ) is too small (Figure 11.55a), the maximum strain in the outer surface will not be reached because the whole length is taken by a transition zone between bended and unbended parts. Only when  $l$  increases by increasing  $r$  or increasing  $\theta$ , a zone with constant maximum strain in the outer region will be present.

**11.7.6.2 Spring back and residual stress.** Spring back is a dimensional change that occurs after plastic forming and unloading, and is a consequence of the recovery

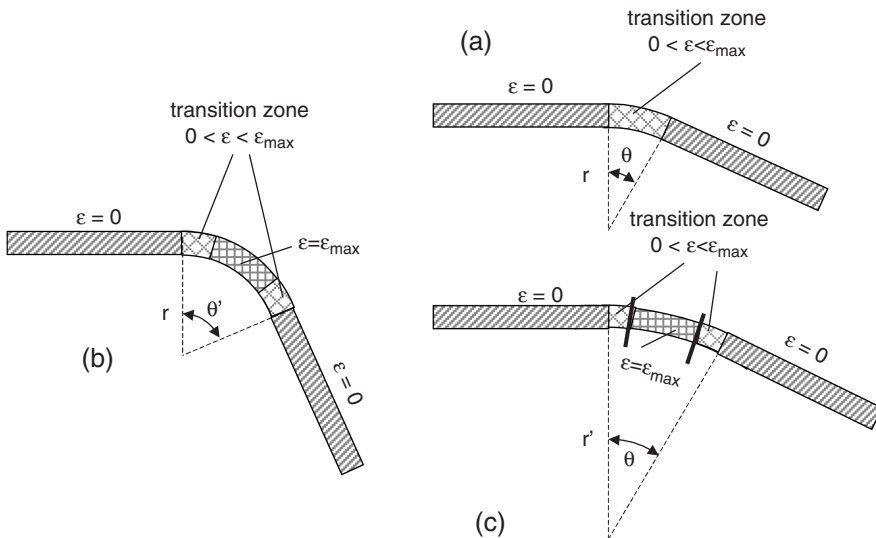


**Figure 11.55.** Effect of bending ( $r/t$ ) on the strain along the circumference.

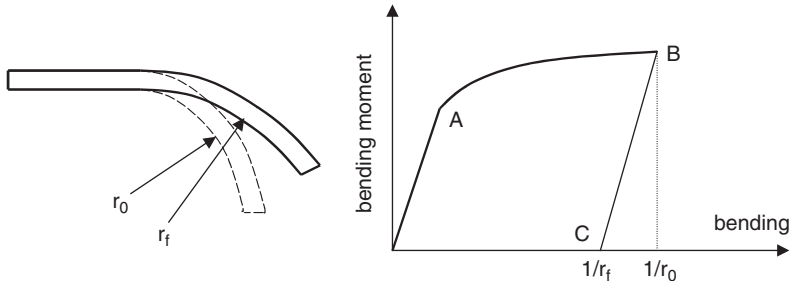


**Figure 11.56.** Spring back as a consequence of the recovery of the elastic part of the deformation. A: end of the elastic deformation ( $\sigma = \sigma_p$ ); B: end of the plastic deformation; C: recovery of elastic deformation.

of the elastic part of the deformation (Figure 11.56). For an ideal plastic material it was shown by Hosford and Caddell [1983] that  $\Delta\varepsilon = -3yS/tE'$ , with  $E'$  the Young's modulus in plane strain [ $E' = E/(1-\nu^2)$  with  $\nu$  the coefficient of Poisson],  $t$  the sheet thickness and  $y$  the distance to the neutral fibre. Figure 11.56 then shows that:

$$\frac{1}{r_0} - \frac{1}{r_f} = \frac{3S}{tE'} \quad (11.49)$$

with  $S$  the plane strain flow stress given by Eq. (11.47).

In practice, it remains a difficult task to predict the spring back accurately. Formula (11.49) can be used as a first estimate and shows which parameters will have an influence on spring back. It appears that spring back will increase with increasing flow stress, increasing strain hardening coefficient, decreasing Young's modulus and decreasing sheet thickness.

After bending and subsequent relaxation of the elastic stress, an internal stress remains inside the sheet. For an elastic-ideal plastic material (Figure 11.57a), it can be shown (Hosford and Caddell [1983]) that the elastic relaxation can be estimated from  $\Delta\sigma = -(3y/t)S$ . Superposition of the total stress during bending and elastic relaxation leads to an internal stress profile shown in Figure 11.57c. It means that after unloading a compressive stress ( $-0.5S$ ) is present at the outer (convex) surface and a tensile stress ( $0.5S$ ) remains at the inner surface.

### 11.7.7 Other techniques

**11.7.7.1 Spinning.** In a conventional spinning process (Figure 11.58a), a circular blank is pushed against a mandrel and rotated. With a rigid tool (often in the form of rollers), the blank is forced against the mandrel. Spinning is a useful cold forming technique for shaping relatively simple axisymmetric parts.

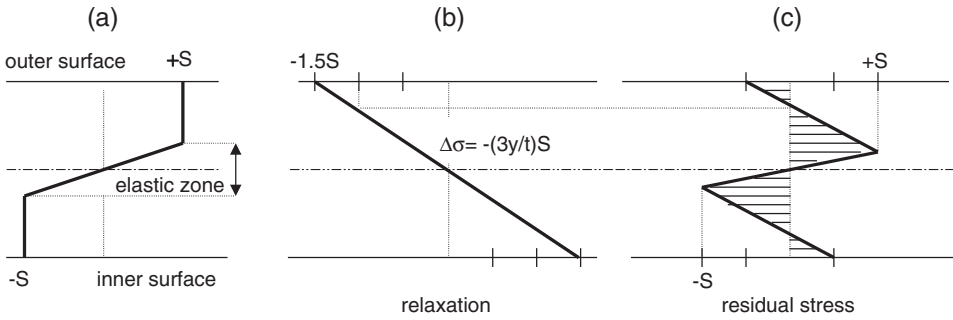


**Figure 11.57.** Bending stress (a), elastic relaxation (b) and residual stress (c) through the sheet thickness.

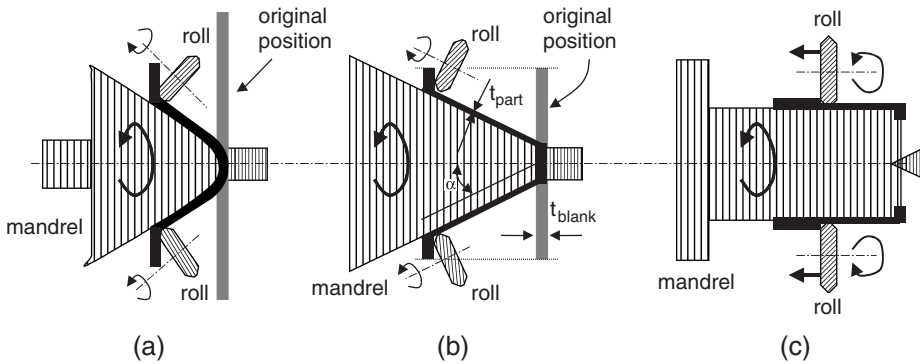


**Figure 11.58.** (a) Conventional spinning; (b) shear spinning; and (c) tube spinning.

Shear spinning is a variant of conventional spinning in which each element of the blank maintains its distance from the axis of rotation. A direct consequence is a reduction of the part's thickness (Figure 11.58b):  $t_{part} = t_{blank} \sin \alpha$ . For many materials, the maximum reduction in wall thickness is around 80%. Some materials with low ductility can be spun at elevated temperature.

In tube spinning (Figure 11.58c), the wall thickness of a cylindrical part is reduced by spinning on a cylindrical mandrel. This operation can be carried out internally or externally. The technique of spinning has recently been reviewed by Wong *et al.* [2003].

**11.7.7.2 Incremental forming.** In incremental forming a rigid, ball-shaped tool is used to gradually deform (emboss) a flat sheet to form a complex 3D metal part (Figure 11.59, left). Although some variants of incremental forming exist for many

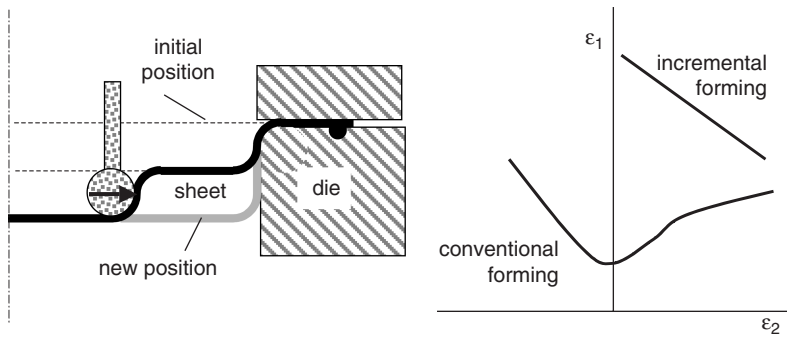


**Figure 11.59.** Schematic of incremental forming (left) and illustration of the increased formability (right).

years (e.g. spinning), new forms of this technique have been developed recently. This technology is well suited for small batch production of sheet metal components. The FLD in incremental forming seems to deviate considerably from that in conventional forming (Figure 11.59, right) (Kim [2002b]).

**11.7.7.3 High strain rate forming.** High strain rate forming of metals has been studied for many years, but up to now has not found widespread applications. The basic idea is to create a shock wave in a fluid, which drives a sheet into the die cavity. Various methods to create the shock wave have been considered, e.g. the detonation of explosives or the discharge of capacitor banks. Most metals seem to have a better ductility at very high strain rates than at conventional strain rates. This effect, which is not fully understood, is sometimes called ‘hyperplasticity’.

In explosive forming, the metal sheet is clamped over a die and placed into a fluid (Figure 11.60a). The air in the die cavity is evacuated and an explosive charge is detonated. The shock wave generated in the fluid drives the sheet into the die cavity. The process is versatile and workpieces of large size can be formed.

In electrohydraulic forming, an electric arc discharge is generated between two electrodes, which are submerged in oil or water. The fluid around the electric arc is rapidly vapourized, creating a shock wave. This system is not fundamentally different from explosive forming; only the energy source is different.

In electromagnetic forming (or magnetic pulse forming), the energy stored in a capacitor bank is discharged into a coil, which is placed near or over the workpiece. An example of a possible configuration is shown in Figure 11.60b. The current pulse causes a high magnetic field around the coil. This magnetic field will induce eddy currents in the workpiece and this generates a second magnetic field, which causes a mutual repulsion between the coil and the workpiece. This repulsive force causes the deformation of the workpiece.

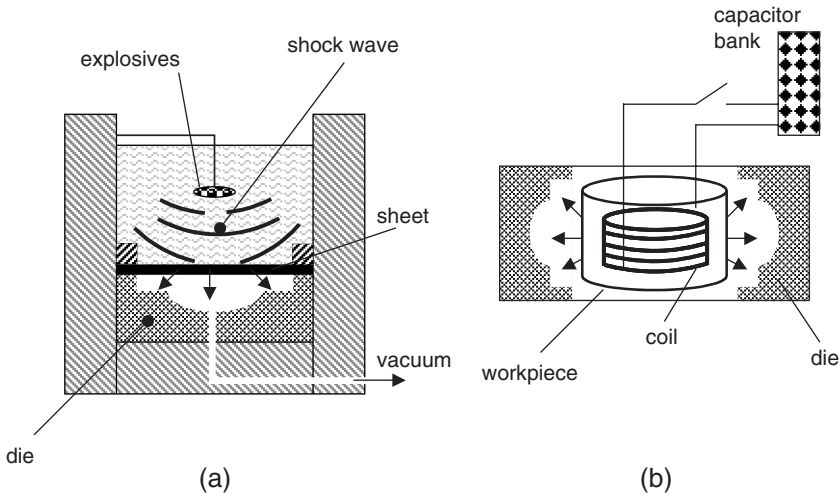


Figure 11.60. (a) Explosive forming and (b) electromagnetic forming.

**11.7.7.4 Peen forming.** Peen forming is a dieless process performed at room temperature. It is used to produce a curvature on sheet metals by shot peening. During shot peening, the surface of a workpiece is impacted by small, round balls from steel or cast iron, called ‘shots’. Every piece or shot acts as a tiny peening hammer, producing a residual compressive stress. In many cases, shot peening is used as a surface treatment to improve corrosion resistance and/or fatigue strength of the material. When one side of a panel is shot peened, the compressive stresses tend to expand the surface layer and cause a convex curvature of the sheet on the peened side. The process is ideal for forming large panel shapes, where the bend radii are reasonably large and without abrupt changes in contour.

## LITERATURE

Pearce R., “Sheet Metal Forming”, Adam Hilger, Bristol (1991).

## 11.8. HYDROFORMING

### 11.8.1 Introduction

‘Hydroforming’ (or ‘fluid forming’) is a relatively new technique with an increasing number of applications in the automotive and aircraft industry. The principle is rather simple: a sheet or tube is pressed into a die cavity by fluid pressure. In most cases, the fluid is separated from the material by a flexible membrane. In some

cases, the die itself can move, to assist the deformation. The production rate of hydroforming is smaller than in conventional press forming, but hydroforming has the advantage that more complex parts can be formed in one pass. Sheet hydroforming is well suited for prototyping or for low-volume production, which is often required in the aerospace industry. A closer control over the sheet thickness is possible and less springback is noticed. In the automotive industry, hydroforming is used for shaping alloys with lower formability (e.g. aluminium alloys and high-strength steels).

### 11.8.2 Sheet hydroforming

An illustration of sheet hydroforming is shown in Figure 11.61. The two principal deformation modes are stretch forming (the pressure of the blank holder is high and the flange material is not allowed to flow into the die cavity) and deep drawing (the flange material is allowed to flow into the die cavity). Most practical hydroform operations start with stretching. When the internal pressure increases, the tensile force on the flange increases and at a certain point the material under the blank holder is pulled inwards and the deformation becomes a combination of deep drawing and stretching, as shown in Figure 11.62. When the internal pressure is too high, two failure modes are possible. For a relatively low blank-holder force, the sealing between die and blank holder starts leaking. For high blank-holder forces, the sheet or part will burst open. Sheet hydroforming can also be used to produce hollow parts, as illustrated in Figure 11.63.

### 11.8.3 Tube hydroforming

Hydroforming can also be used to deform tubes. An example of a fabrication route is shown in Figure 11.64. A tube, in some cases pre-bend, is placed in a die. The

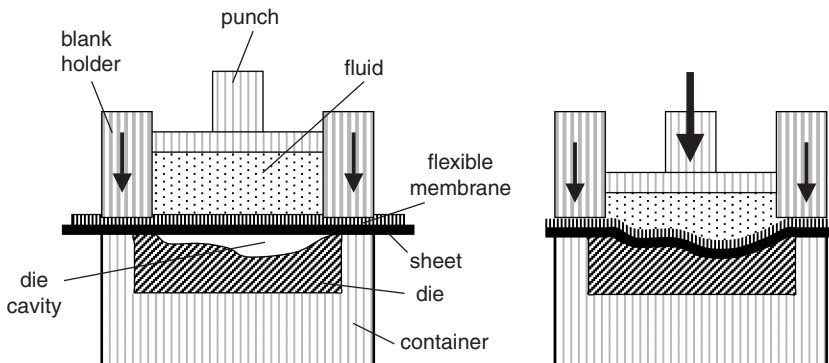
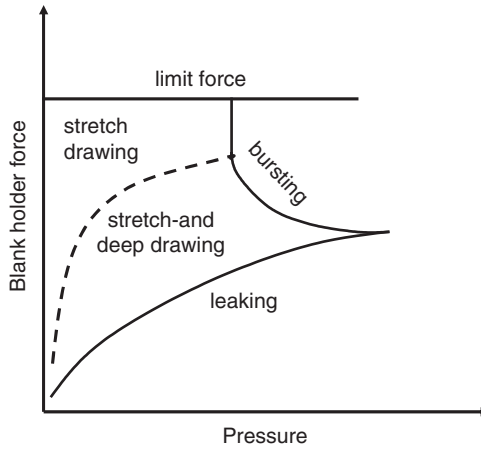
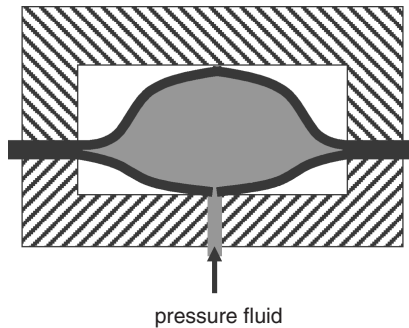


Figure 11.61. Schematic illustration of sheet hydroforming.



**Figure 11.62.** Influence of blank holder force and internal pressure on the strain mode and failure mechanism during hydroforming. After Novotny and Hein [2001].



**Figure 11.63.** Sheet hydroforming, for the production of hollow parts.

die is sealed off on both ends and the tube is put under internal pressure. This pressure may range from 2000 to 10 000 bar, although 3000 bar will do for many applications (Koç and Altan [2001]). An axial displacement of the seals assists the material flow into the cavities of the die. A good synchronization between the pressure built-up and the axial feeding is required. During tube hydroforming, some typical defects can occur. ‘Bursting’ occurs when the pressure in the tube rises too fast and not enough extra material can flow into the die. It is also the typical failure mode at high blank-holder forces. A too fast ‘axial feeding’ of material, will however lead to buckling or wrinkling of the tube.

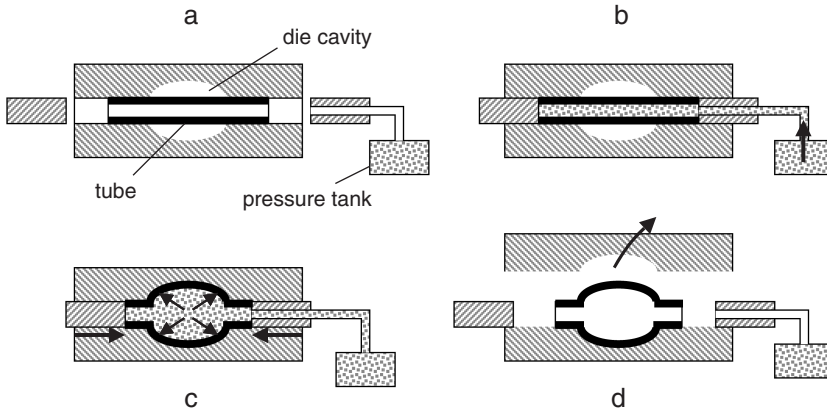


**Figure 11.64.** ‘Tube hydroforming’: (a) positioning of the tube in the die; (b) sealing off the tube and filling with fluid; (c) pressurizing combined with axial feeding; (d) opening of the die.

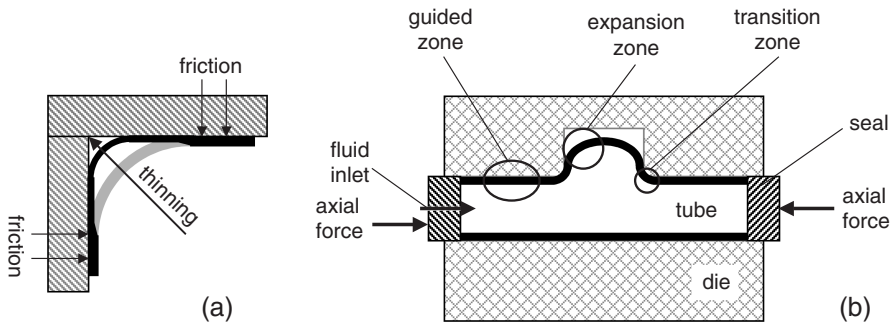


**Figure 11.65.** Illustration of the three friction zones in tube hydroforming. After Ahmetoglu and Altan [2000].

### 11.8.4 Important parameters

**11.8.4.1 Friction and lubrication.** Friction and lubrication are very important, especially in parts where a substantial axial feeding is required. A lubricant reduces tool wear, axial force and the risk of buckling. It prevents sticking of the material to the die as well as galling. Another critical situation is depicted in Figure 11.65a. The tube touches the wall in two contact regions. When friction between tube wall and die is high, the zone in between the contact points will thin down and eventually will burst.

In most hydroforming processes, three ‘friction zones’ can be found (Figure 11.65b): the ‘guided’ zone, the ‘transition’ zone and the ‘expansion’ zone (Ahmetoglu and Altan [2000]). Each of these zones has his own friction characteristics. In the

guided zone, the material does not deform, but it is pushed towards the deformation zone by the cylinders generating the axial force. The major part of the deformation takes place in the transition zone and the so-called ‘calibration’ (fitting the material into the die) takes place in the expansion zone, mostly by local stretching.

Friction itself depends on many parameters like the type of the lubricant, the material of the tube and the surface conditions of the die. A suitable lubricant must be chosen in function of the internal pressure, the contact speed and the contact length. Various types of lubricants are available: solid lubricants like graphite or  $\text{MoS}_2$ , waxes, oils and emulsions.

**11.8.4.2 Material parameters.** The  $\bar{R}$ -value or normal anisotropy of a sheet has an important influence on the deformation during hydroforming. As discussed above, the deformation starts with a biaxial stretching of the sheet because the blank holder withholds the sheet to move inwards. When a certain internal pressure is reached, the axial force overcomes the pressure of the blank holder and the material is pulled inward. At that moment, a deep drawing component is added to the deformation. Since the stretchability of a material is limited, it is important that this deep-drawing component, which feeds material into the die, occurs in an early stage of the process. It has been shown (Novotny and Hein [2001]) that for a material with large  $\bar{R}$ -value, the stress in the sheet raises faster with increasing internal pressure than for a material with a lower  $\bar{R}$ -value (Figure 11.66). This means that for higher  $\bar{R}$ -value, deep drawing starts at a lower internal pressure; and hence, the

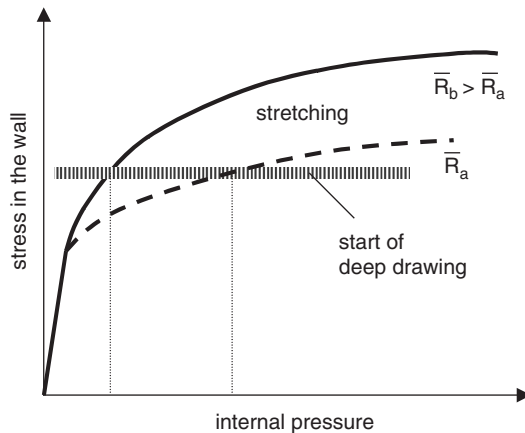


**Figure 11.66.** Influence of the  $\bar{R}$ -value on the relation between internal pressure and the start of the deep drawing component during sheet hydroforming.

risk that the sealing of the die will leak, or that the material will burst before fresh material starts moving into the die, is lower.

The anisotropy is also an important parameter in tube hydroforming. Experiments and simulations have shown that a high  $\bar{R}$ -value is beneficial for the deformation (Carleer *et al.* [2000], Manabe and Amino [2002]). A high strain-hardening coefficient is also beneficial because (like in biaxial stretching), the deformation is more homogeneously distributed over the tube wall and local necking is delayed.

## LITERATURE

K. Siegert (ed.), “Hydroforming of Tubes, Extrusions and Sheet Metals”, vol. 1, Stuttgart University, Institut for Metal Forming Technology, Stuttgart, Germany (1999).

Ibid vol 2 (2001). Ibid vol 3 (2003).

## 11.9. HIPPING

### 11.9.1 Introduction

Hot isostatic pressing (HIP/hipping) involves the simultaneous application of heat and high pressure. A furnace is enclosed in a high-pressure vessel and the workpieces are heated while an inert gas (usually argon) applies a uniform pressure. The technique was invented at the Battelle Memorial Institute in 1955 for the diffusion bonding of dissimilar materials (a method was needed to bond zirconium to a zirconium–uranium alloy (Boyer [1992])), but other applications, usually related to the removal of pores, came gradually into focus. At this time, hipping is mainly used for the densification of high-performance castings, the consolidation of metal powders and for cladding. The temperature used in a hipping cycle is between 0.5 and 0.7 times the melting temperature and the gas pressure is between 20 and 400 MPa, and typically around 100 MPa. This is comparable with the pressure at 10 000 m below sea level. A schematic view of an HIP installation is presented in Figure 11.67. The pressure is obtained partly by pumping-in gas with a compressor, partly by heating this gas.

### 11.9.2 Densification mechanisms

The main purpose of hipping is the densification of a porous product (casting, powder compact, etc.). Several mechanisms can contribute to this densification. When a pressure is applied, some elastic deformation of the component will first occur, followed by plastic yielding at the contact points, e.g. between powder particles (Figure 11.68). Once these contact points can bear the internal forces

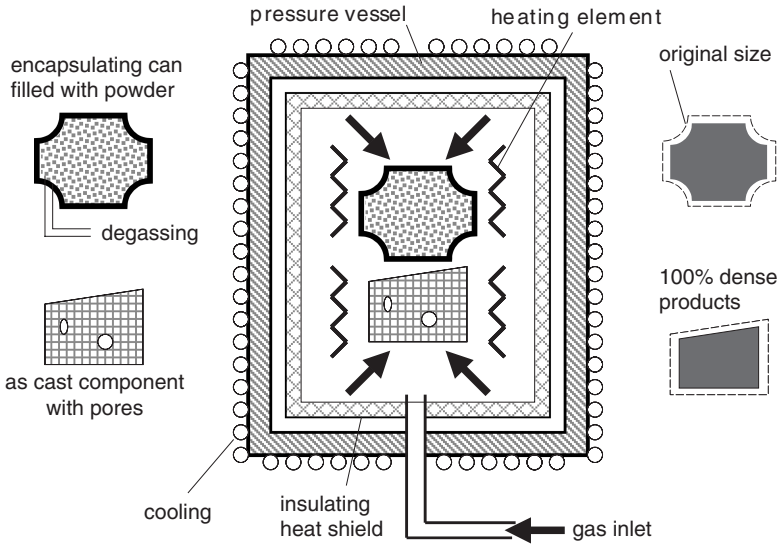


Figure 11.67. Schematic view of an HIP installation.

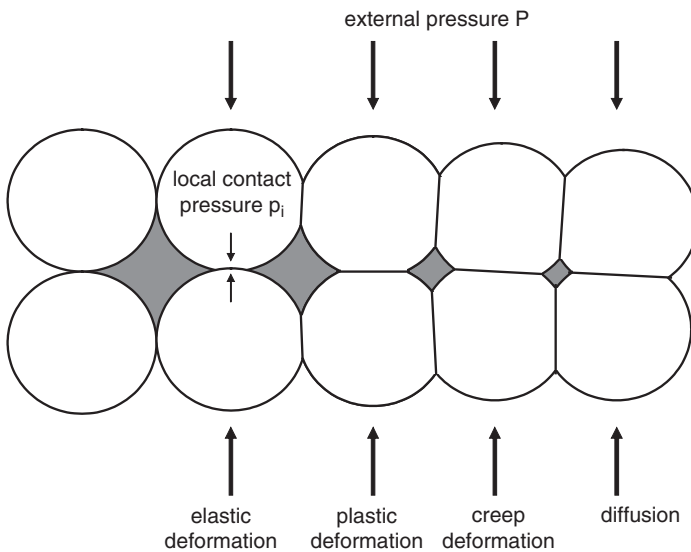
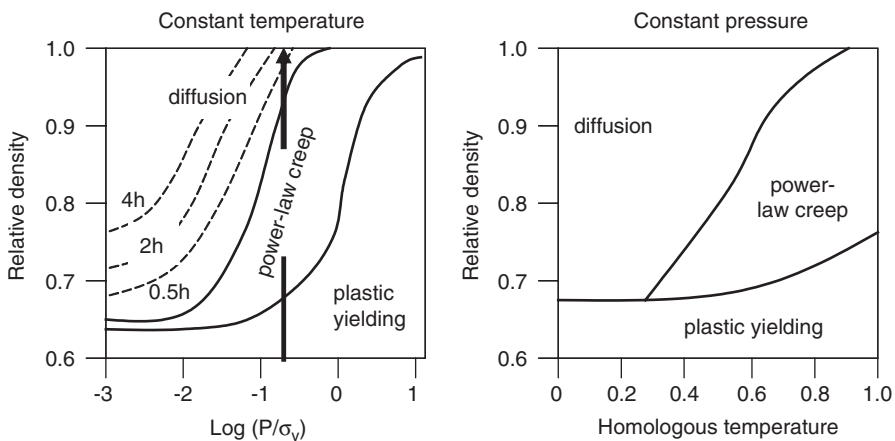


Figure 11.68. Schematic overview of some densification mechanisms occurring during HIPing.

caused by the external pressure, further densification will occur by time-dependent processes such as power-law creep or by diffusion.

An elegant way of visualizing the pressure and temperature dependence of these densification processes was proposed by Arzt *et al.* [1983]. They constructed ‘hot-isostatic pressing diagrams’ (also called ‘HIP-maps’ or ‘densification maps’). These maps show the dominant densification mechanism as a function of external applied pressure and temperature. A schematic representation is shown in Figure 11.69. At a given external pressure  $P$  and temperature  $T$ , the relative density gradually increases (the pore size decreases) with time. When the HIPping process starts, there is first some elastic deformation (not shown in Figure 11.69), immediately followed by plastic yielding. Perhaps, it is surprising that plastic yielding occurs for  $P < \sigma_y(T)$ , but one has to take into account that  $P$  represents the externally applied pressure. Owing to the small contact areas at the beginning of the HIPping cycle, the local contact pressures,  $p_i$  can be much higher than the yield stress of the material. During plastic deformation, the local contact areas increase and the local contact pressures decrease.

When the local contact areas are large enough to bear the local forces, yielding stops and the size of the contact areas continue to grow by power-law creep. This will lead to 100% density only at high external pressure. For low to moderate pressures, the final closure of the pores will occur by diffusion. For some materials, total densification may not be possible and in that case the HIP-map will show a region of ‘no densification’.



**Figure 11.69.** Hot-isostatic pressure maps (density/pressure and density/temperature).  
After Arzt *et al.* [1983].

Many HIP-maps contain lines of ‘constant time’. For example, the HIP-map on the left-hand side of Figure 11.69, shows that for the external pressure indicated by the arrow, 100% density will be reached in about 1 h. This densification process will occur by plastic yielding, followed by power-law creep and the final closure of pores will occur by diffusion.<sup>7</sup> As an alternative for the ‘pressure–density’ maps, a ‘temperature–density’ map, as shown in the right-hand side of Figure 11.69, can be used.

### ***11.9.3 Hipping equipment***

The combination of high temperature and high pressure puts severe demands on the construction of a hipping installation. Especially, the pressure vessel must be designed with great care. The most important requirements are a high tensile strength, a high fatigue resistance and good fracture toughness. There are mainly two types of pressure vessels: forged monolithic vessels made from ductile low-alloy steel and wire wound vessels. The top and bottom closure of the vessel are critical parts of a hipping unit. Some vessels are closed with an external ‘joke-type’ system. The pressure in the vessel is transmitted to the joke by the end closures. Monolithic vessels have a traditional threaded closure, but with rounded threads for a better distribution of the stresses. For safety reasons, hipping units are located in concrete pits.

Most commercial hipping installations have a furnace inside the vessel, with thermal barriers to protect the vessel (Figure 11.67). The gas which is used to exert the pressure (partly by mechanical pumping, partly by heating) is usually high-purity argon. Impurities such as hydrogen, oxygen and nitrogen, even in very small concentrations, cause surface degradation in certain alloys. In nickel-base alloys, for example, nitrogen forms brittle carbonitrides and oxygen forms intergranular oxides (Eridon [1988]). Sometimes additives are required, e.g. for carburized steel, the gas should contain carbon to prevent decarburization. For encapsulated materials, like powders and for aluminium castings cheaper nitrogen gas can be used. The most common materials used to encapsulate powders are mild steel, stainless steel and nickel. Most envelopes are made by spinning, hydroforming and superplastic forming or by conventional sheet-forming techniques. For materials which have to be hipped at very high temperature (1500–2000°C), glass envelopes can be produced by glass blowing. At the hipping temperature, glass is soft enough to be deformed.

<sup>7</sup> It is recommended to look at the ‘deformation mechanism map’ shown in Figure 6.1. This map shows that for decreasing load the dominant deformation mechanism can indeed change from plastic deformation (called: dislocation glide) to creep and diffusion.

**Table 11.16.** Properties of an as-cast, hiped and wrought alloy steel (*Source:* Data from Atkinson [1991]).

	YS (MPa)	UTS (MPa)	Elongation to failure (%)	Toughness to fracture (MNm <sup>-3/2</sup> )
Cast	988	1350	8.9	105
Hipped	1142	1460	13.3	122
Wrought	1155	1480	14.7	124

### 11.9.4 Typical applications

Hipping enables the production of materials of various shapes and sizes. About 50% of the applications are related to the densification of castings, one-third to powder metal products and about 10% to cladding. Hipped products are used in the aerospace, automotive, medical, chemical and petroleum industries.

**11.9.4.1 Densification of castings.** In a casting process, internal porosities may be generated because of shrinkage during solidification or because of entrapped gas. Removal of these pores will improve mechanical properties, e.g. strength, toughness, fatigue and creep resistance. In many cases, the properties of the hiped product are nearly as good as those of a wrought component. Table 11.16 shows an example for an alloy steel.

Materials used for hipping are often titanium alloys and nickel-based alloys. Typical applications are structural castings for jet engines, vanes for divers engines and turbine blades. Lower cost castings from steels and aluminium alloys are an increasing market. Many new applications for the pharmaceutical industry, food processing and vacuum applications require polished, pore-free surfaces at competitive prices.

**11.9.4.2 Densification of powder metal products.** With conventional sintering techniques, it is very difficult to obtain fully dense products. Extended sintering times can lead to unacceptable grain growth, which degrades the properties of the components. However, some products, e.g. wire drawing dies, require zero porosity. In such cases, hipping can transform pre-sintered components into near 100% dense products. Classical examples are the elimination of residual porosity of pre-sintered hard metals (cemented carbides) or hipping of pre-sintered ceramics like Al<sub>2</sub>O<sub>3</sub>, Si<sub>3</sub>N<sub>4</sub> and Si–Al–O–N compounds (Atkinson and Rickinson [1991]).

Hipping can also consolidate fine powders into near 100% dense products. In that case, the powders must first be encapsulated into a container which is degassed and sealed. Typical examples of hiped powder metallurgical parts are

nickel-base superalloys, high-speed tool steels and ceramic powders. Casting of these alloys is problematic, but the production and consolidation of powders offers an attractive alternative. Nickel-base superalloys, for example, undergo severe segregation during classical ingot casting. Production of powders by atomization eliminates macrosegregation and reduces microsegregation. After HIPping a homogeneous product with fine grain size and excellent mechanical properties is obtained. The shrinkage of the product should in principle be isotropic because the pressure exerted by the gas is the same in all directions. However, in practice, some factors like a non-uniform filling of the container may generate slight distortions. In some cases, the shape of a rectangular bar turns into a dog bone because the corners of the container are stronger than the side walls.

**11.9.4.3 Cladding.** Another application of HIPping is to join dissimilar materials that are difficult to join by traditional methods. Owing to the surface roughness, real contact between two surfaces that are pressed together will only occur at some local contact points. At high temperature, local plastic deformation will increase the contact area and subsequently diffusion of atoms from one material into the other will form the bond between them. Remaining porosity will be removed in the same way as illustrated in Figure 11.68 for powder compacts.

## LITERATURE

- Atkinson H.V. and Davies S. Metall. Mater. Trans. A, 31 (2000), 2981.  
Conway J.J. and Rizzo F.J., "Hot Isostatic Pressing of Metal Powders", vol. 7, ASM-Handbook (1998).  
Draney C., Froes F.H. and Hebeison J., Mat. Tech. and Adv. Perf. Mat., 19.2 (2004), p. 140

## 11.10. SUPERPLASTIC FORMING

### 11.10.1 Technology

In Chapter 6, the superplastic behaviour and the underlying deformation mechanisms (grain boundary sliding + accommodation mechanism) of certain materials have been discussed. It was shown that superplasticity occurs in fine-grained materials, deformed at high temperature and low strain rate. In the present paragraph, the technology of superplastic forming will be introduced. In most cases, superplastic forming is carried out with one of the following techniques: blow forming/vacuum forming, thermo-forming or superplastic forming combined with

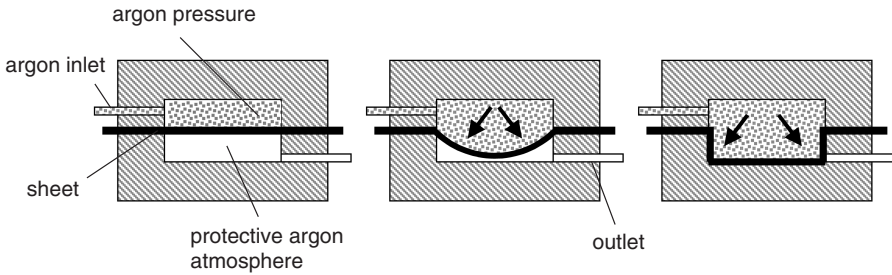


**Figure 11.70.** Illustration of the blow-forming technique for superplastic forming.

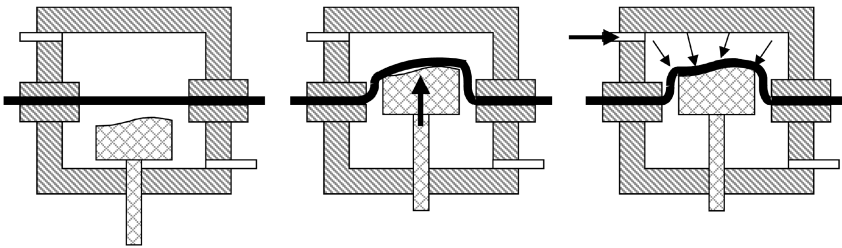


**Figure 11.71.** Illustration of a possible set-up for the thermo-forming technique.

diffusion bonding. Forging and extrusion can also be used to shape superplastic materials.

*Blow forming and vacuum forming* are related techniques. In blow forming, a gas (mostly argon) is used to create a pressure difference over the (warm) superplastic sheet (Figure 11.70). The sheet is stretched and forced to adopt the shape of the die. The outer side of the sheet is held in a fixed position and does not draw-in as would be the case in deep drawing. In some cases, a ‘back pressure’ is used to prevent cavitation. In vacuum forming, the pressure difference over the sheet is generated by vacuum in one of the die chambers. In this case, the pressure difference is limited to 1 atmosphere.

*Thermo-forming* is a typical forming technique for plastics. In this technique, a moving die is used in conjunction with a gas pressure. Several configurations are possible, e.g. a male die is used to stretch-form the superplastic sheet. After that, a gas pressure is used to force the sheet against the die (Figure 11.71). One of the most important advantages of superplastic forming is that complex shapes can be produced in one piece and most often in one pass. The absence of welds, rivets, etc. diminish the risk for fatigue damage and corrosion. An additional advantage is that little or no residual stresses are present. The low forces acting during superplastic forming reduce the tooling cost. A disadvantage of superplastic forming is

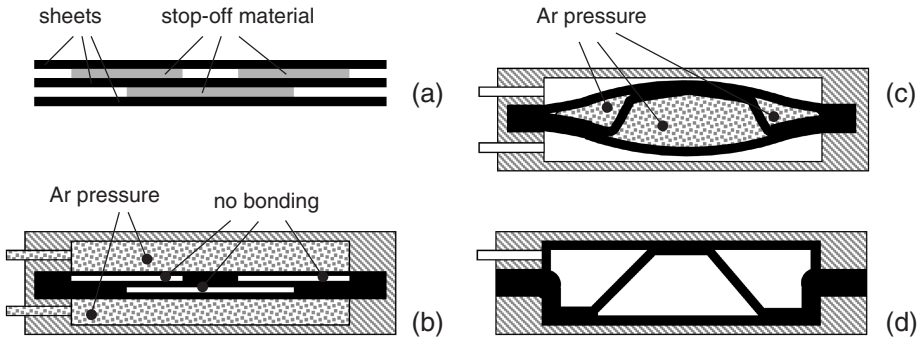


**Figure 11.72.** Combination of superplastic forming with diffusion bonding.

of course the low production rate, because of the limitations in maximum allowed strain rate.

The low production rate is turned into an advantage when superplastic forming is combined with *diffusion bonding* (the ‘SPD/DB’ process). Two or more sheets of superplastic material are stacked together but make direct contact with each other only at some well-chosen locations (Figure 11.72a). At the other contact areas, a diffusion barrier (a so-called ‘stop-off’ material) is used. In a first step, the sheets are heated and bonded together at the chosen locations by diffusion bonding. This bonding process is ‘assisted’ by an external gas pressure (Figure 11.72b). In a subsequent step, the small clefts at the stop-off material are expanded by an internal gas pressure (Figure 11.72c). The outer sheets are forced into the die cavities and the final shape is being formed (Figure 11.72d). The stop-off material depends on the material of the sheets. For titanium alloys, yttrium or boron nitride have successfully been used. The SPD/DB technique is well established for titanium alloys and has many industrial applications, for example, in the aircraft industry. For aluminium alloys, diffusion bonding is less evident because of the surface oxide film and solutions have been sought by introducing interlayers in the form of claddings, coatings or foils.

### 11.10.2 Thinning

Owing to the large deformation during superplastic forming, significant thinning of the sheet is unavoidable. In many cases, this thinning will not be uniform throughout the sheet. In order to deliver products with the required dimensions, this thinning behaviour must be understood and taken into account in the design and production of superplastic parts. Let us consider the case of blow forming (Figure 11.70). In the first stage of the deformation, free bulging of the sheet occurs. In this geometry there is a stress-state gradient from pole to edge, with an

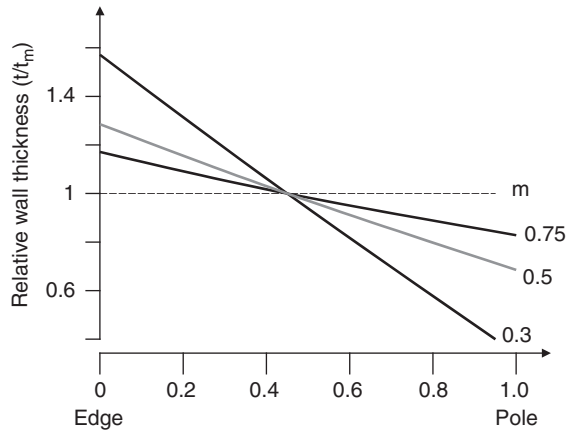


**Figure 11.73.** Relative wall thickness between edge and pole of a hemisphere, for different values of the strain rate sensitivity coefficient  $m$  ( $t$ : actual wall thickness;  $t_m$ : mean wall thickness). After Cornfield and Johnson [1970].

equi-biaxial stress at the pole and a plane strain stress state at the edge. It can be calculated and experimentally verified that this will lead to more thinning at the pole than at the edge. The difference in thickness will be larger when the strain rate coefficient  $m$  is smaller. This is illustrated in Figure 11.73.

Once the hemisphere makes contact with the die, an even more severe problem may occur. Because of friction between the sheet and the die, the corners of the die will be filled by excessive local stretching and significant local thinning of the sheet. This problem resembles a similar problem occurring during hydroforming and is illustrated in Figure 11.65.

Thinning control is often an important issue in superplastic forming. Some possible methods to reduce thickness differences are (Hamilton [1989]):

- Processing the superplastic material to obtain high  $m$ -values.
- Using adequate lubrication to avoid excessive local thinning in the die corners.
- Applying pressure in a controlled and profiled manner (pressure profiling) in order to maintain the strain rate at a level corresponding to a high  $m$ -value.
- Using microstructural gradients (e.g. grain-size gradients) (Cheong *et al.* [2003]).

### 11.10.3 Cavitation

The nucleation, growth and interlinkage of intergranular voids during superplastic forming has been observed in many alloys. This process, called ‘cavitation’, can be responsible for a degradation of the service properties of the superplastic part

or for a premature fracture of the material during superplastic forming. For this reason, it is important to understand and control or inhibit cavitation.

*The nucleation of cavities* (Suéry [1985], Ridley [1989])

Cavities may pre-exist in many alloys due to the TMP carried out to get superplastic material. But there is also a strong suspicion that cavities nucleate continuously at grain boundaries due to insufficient accommodation of grain boundary sliding. The main nucleation points seem to be tripelpoints and hard particles at the boundaries. When the deformation rate remains below a critical value  $\varepsilon_c^\circ$ , the formation of cavities is prevented by diffusive stress relaxation. An expression for the critical strain rate has been proposed by Stowell [1983]:

$$\varepsilon_c^\circ = 11.5 \left[ \frac{\sigma \Omega}{x d^2 D} \right] \left[ \frac{\delta D_{gb}}{kT} \right] \quad (11.50)$$

with  $\sigma$  the external stress,  $\Omega$  the atomic volume,  $d$  the radius of a particle,  $D$  the grain size,  $x$  the fraction of deformation by grain boundary sliding,  $\delta$  the grain boundary width,  $D_{gb}$  the grain boundary diffusion coefficient and  $T$  the temperature. This formula shows that nucleation of cavities increases when larger particles are present and when the grain size becomes larger.

*The growth of cavities* (Suéry [1985], Mukherjee [1992])

A cavity located on a grain boundary can grow by a diffusion-controlled growth mechanism or by plasticity-controlled growth or by a combination of both mechanisms. The first mechanism seems only relevant at very low strain rates and for small cavities. At strain rates typical for superplastic forming, the growth is controlled by plastic deformation of the surrounding region. The growth of cavities can be described by the relation Suery [1985]:

$$\frac{dV}{dt} = kV\varepsilon^\circ \quad (11.51)$$

with  $V$  the cavity volume,  $\varepsilon^\circ$  the strain rate and  $k$  a parameter. The growth rate is proportional to the volume of the cavity and hence an exponential increase of  $V$  with strain can be anticipated. It has been shown by Cocks and Ashby [1982] that  $k$  decreases as the strain rate sensitivity  $m$  increases.

*Cavity interlinkage and fracture*

Individual cavities grow during deformation. At a given moment, two expanding cavities will meet and the two cavities with volume  $V_1$  and  $V_2$  will merge into one cavity with volume  $V_3 = V_1 + V_2$ . This cavity interlinkage will cause an unexpected

shift towards higher values of the cavity size distribution. Attempts to model this process of cavity coalescence have been published (Stowel [1984], Pilling [1985], Nicolaou [1999, 2000]), but the exact mechanism and precise criteria to link coalescence with premature failure seems to be lacking.

*Cavitation control by hydrostatic pressure*

One of the most effective methods to reduce the occurrence of cavitation is to apply a hydrostatic pressure during superplastic forming. For example, during blow forming (Figure 11.70), argon pressure is applied on both sides of the sheet. Of course a pressure difference is maintained to force the sheet into the die. This hydrostatic pressure not only decreases the growth of the cavities, but also reduces the nucleation rate of new cavities. A critical stage in the formation of a new cavity is the growth of the cavity to a critical size, which is stable against shrinkage due to surface tension (Suéry [1985]). The critical radius  $r_c$  for a cavity subjected to a tensile stress  $\sigma$  is given by the expression  $r_c = 2\gamma/\sigma$ , with  $\gamma$  the surface tension. When a hydrostatic pressure  $p$  is superimposed, the critical radius is larger, and can be calculated from:

$$r_c(p) = \frac{2\gamma}{(\sigma - p)} \quad (11.52)$$

This formula shows that the nucleation of stable new cavities can considerably be suppressed by hydrostatic pressure.

**LITERATURE**

- Mukherjee A.K., ‘Superplasticity in metals, ceramics and intermetallics’, in “Materials Science and Technology”, R.W. Cahn, P. Haasen, E.J. Kramer and H.Mughrabi (eds), vol. 6: ‘Plastic Deformation and Fracture of Materials’, Wiley, Weinheim, Germany (1992).
- Nieh T.G., Wadsworth J. and Sherby O.D., “Superplasticity in Metals and Ceramics”, Cambridge University Press, Cambridge, UK (1997).
- “Superplasticity”, AGARD lecture series No 168, Agard (ISBN 92-835-0525-5) (1989).
- “Superplasticity”, Proceedings of the International Conference Grenoble 1985, B. Baudelet and M. Suéry (eds), CNRS, Paris (1985).